FACULTY OF ENGINEERING AND ARCHITECTURE

Development of acrylate-endcapped urethane-based POSS/PLA scaffolds towards breast reconstruction

Karen De Man
Student number: 01602451

Supervisors: Prof. dr. Sandra Van Vlierberghe, Prof. Ruslan Dmitriev
Counsellor: Ir. Coralie Gréant

Master's dissertation submitted in order to obtain the academic degree of
Master of Science in Biomedical Engineering

Academic year 2020-2021

GHENT UNIVERSITY

VUB VRIJE UNIVERSITEIT BRUSSEL

FACULTY OF ENGINEERING AND ARCHITECTURE

Development of acrylate-endcapped urethane-based POSS/PLA scaffolds towards breast reconstruction

Karen De Man
Student number: 01602451

Supervisors: Prof. dr. Sandra Van Vlierberghe, Prof. Ruslan Dmitriev
Counsellor: Ir. Coralie Gréant

Master's dissertation submitted in order to obtain the academic degree of
Master of Science in Biomedical Engineering

Academic year 2020-2021

GHENT UNIVERSITY

VUB VRIJE UNIVERSITEIT BRUSSEL

Acknowledgments

This master thesis was the biggest, most challenging and educative project in my academic career. I'm very grateful for everyone that supported or helped me throughout this thesis.

First of all, I'd like to thank Professor Van Vlierberghe for giving me the opportunity to perform my master thesis in her research group. Thank you for giving advice and answering questions during the follow-up meetings.

I would like to give special thanks to my supervisor Coralie Gréant to introduce me in the research field of AUPs and to teach me a lot. This master dissertation would definitely not be possible without you. Even on Sunday evenings, you listened to my ideas, questions, thoughts, etc. You were there every step of the way to encourage me when things were not going as planned or to celebrate good results. Next to being a supervisor, you were also making sure that your master students had a great time in the lab by chatting, having coffee breaks, cheering after good results, etc. I really appreciate everything you did for me and good luck with the remainder of your PhD.

I would also like to thank Ameya R Narkar from Syracuse University for shipping the TPUs, helping me with questions and providing information about POSS and TPUs.

Next, I would like to thank Valérie and Bo for the great times in the lab. Special thanks to Valérie for the support, the uncountable number of hours in the lab together and the resulting friendship. I really enjoyed working with both of you in the lab.

Also many thanks to Lana Van Damme for performing the cell assays and helping with our endless questions. Also a big thank you to Evelien Vermoesen and Lobke De Vos for performing the GPC measurements and Anna Szabo and Laurens Parmentier to teach me how to work with the light microscope, DLP printer and rheometer. Also a big thank you to the whole PBM group, I couldn't wish for a better research group to end up.

Last but not least, many thanks to my friends and family to support me through this year. Thank you for listening to my complaints during hard times and to be happy for me when things turned out fine. Special thanks for my parents to support me through my whole academic career and for always believing in me.

Karen De Man, June 2021

Permission of use on loan

"The author gives permission to make this master dissertation available for consultation and to copy parts of this master dissertation for personal use.
In all cases of other use, the copyright terms have to be respected, in particular with regard to the obligation to state explicitly the source when quoting results from this master dissertation."

Karen De Man, June 2021

Development of acrylate-endcapped urethane-based POSS/PLA scaffolds towards breast reconstruction

Karen De Man

Supervisors: Prof. Ruslan Dmitriev, Prof. dr. Sandra Van Vlierberghe
Counsellor: Ir. Coralie Gréant

Master's dissertation submitted in order to obtain the academic degree of
Master of Science in Biomedical Engineering

Faculty of Engineering and Architecture
Ghent University

Academic year 2020-2021

Abstract

For women with breast cancer, breast reconstruction can be applied after mastectomy to restore their femininity and to increase their well-being. Unfortunately, current reconstructions have shortcomings like calcifications and capsular contraction. Adipose tissue engineering can offer a solution for these drawbacks and aims to restore damaged body tissues by regenerating tissues. Eventually, the objective is to reconstruct the breast without any residual human-foreign material.
In this master thesis, different materials (thermoplastic polyurethane (TPU), poly(D,L-lactic acid) (PDLLA) and copolymers of PDLLA and poly-ε-caprolactone (PCL)) were synthesised as starting materials. They were functionalised into acrylate-endcapped urethane-based polymers (AUPs) which have the ability to crosslink under UV-light, called photopolymerisation. This chemically crosslinked material can be deformed after heating above glass transition temperature into a smaller shape for minimally invasive implantation in the patient's breast. A shape memory effect (SME) is triggered by the body temperature after implantation and restores the original, chemically crosslinked shape. In order to obtain this SME, the AUP needs to have a glass transition temperature right below body temperature. TPU-based AUPs combine the advantages of an amorphous, organic and a semi-crystalline, inorganic component such as biodegradability and thermal stability. However, the glass transition temperature of these materials is too high to obtain a shape memory behaviour below body temperature. The same applies for PDLLA-based AUPs. One can decrease this thermal property by copolymerisation with PCL.
Due to the crosslinking capacity of photocurable AUP resins, a scaffold was created via digital light processing (DLP). To this end, a resin consisting of AUP, photoinitiator (TPO-L), photoblocker (tartrazine) and solvent (1-methyl-2-pyrrolidinone (NMP)) was developed. In order to achieve appropriate crosslinking, the acrylate density was increased by using triacrylate end groups and by decreasing the polymer molar mass. The gel fraction and swelling ratio of crosslinked discs confirmed that the acrylate density was increased using these two ways. Indirect cell tests demonstrated the biocompatibility of these materials. The obtained AUP-based scaffolds show great potential for minimally invasive breast reconstruction purposes.

Keywords: breast reconstruction, polylactic acid, shape memory effect, photopolymerisation, DLP printing

Development of acrylate-endcapped urethane-based POSS/PLA scaffolds towards breast reconstruction

Karen De Man

Supervisors: Prof. Ruslan Dmitriev, Prof. dr. Sandra Van Vlierberghe
Counsellor: Ir. Coralie Gréant

Abstract — **Breast reconstruction is the next step after mastectomy for many women with breast cancer. The conventional techniques using breast implants and tissue flaps still have many shortcomings such as capsular contraction and dislocation. Adipose tissue engineering can offer a solution as damaged tissues will be replaced by regenerated tissues by combining a biodegradable scaffold, cells and regulating signals of bioactive molecules. The objective of this master dissertation is to develop a scaffold for minimally invasive breast reconstruction. To this end, acrylate-endcapped urethane-based polymers with PDLLA, PDLLA/PCL and TPU as starting materials are used. The ability of these polymers to crosslink under UV-light, which is called photopolymerisation, enables to create a scaffold via digital light processing. By synthesising acrylate-endcapped urethane-based polymers with a glass transition temperature between 30 and 35°C, the body temperature of the patient will trigger a shape memory effect. This effect ensures that a small-scaled scaffold will enlarge towards its fixed shape after implantation due to the body temperature of the patient. In this way, the surgeon can minimise the incision. Different characteristics of this material were examined like biocompatibility and gel fraction.**

Keywords — **breast reconstruction, polylactic acid, DLP printing, photopolymerisation, shape memory effect**

I. Introduction

Breast cancer is a common disease that strikes approximately 2.1 million women every year. For many of these women, the surgical removal of their breast, which is called a mastectomy, is the required treatment option. Due to this removal, many patients feel disfigured and mutilated which causes a decrease in their well-being and quality of life. Therefore, patients often opt for a successive breast reconstruction.[1][2]

Nowadays, breast reconstructions can be classified in two ways. A reconstructive surgery can be done immediately after the mastectomy or during a second reconstructive surgery later on. Furthermore, there are two different types of reconstruction: autologous tissue-based reconstructions and implant-based reconstructions. Nowadays, silicone implants are frequently used during implant-based reconstructions. This type is preferred over the autologous tissue-based reconstruction because of the superior cost-effectiveness. However, implants also have shortcomings like capsular contraction, dislocation, calcifications and so on. Autologous tissue-based reconstructions on the contrary give a more natural and softer breast, but the recovery of the surgery will take longer as the patient is her own donor. To conclude, there is no optimal solution yet for breast reconstructions.[3][4]

In this work, adipose tissue engineering was used as it combines the implantation of a scaffold and the regeneration of autologous tissue. The goal of adipose tissue engineering is to restore damaged body tissues by autologous tissue regeneration. Therefore, three components are used; a biodegradable scaffold, cells and microenvironment for the cells to guarantee tissue formation. This work will focus on the biodegradable scaffold. The latter gives mechanical and structural support and contains pores to ensure migration and growth of the cells within the centre of the scaffold. Due to the biodegradable characteristic of the scaffold, the tissue can regenerate while the scaffold degrades. Ideally, the degradation of the scaffold and regeneration of tissues proceed at a similar rate.[5][6]

In order to be minimally invasive, the scaffold needs to consist of shape memory polymers (SMP). In this work, only thermoresponsive SMPs will be discussed. The permanent state of the scaffold is first fixed by chemical crosslinks to create the ability to return to this shape after deformation. Subsequently, the scaffold is heated to give the polymers more mobility. In this way, the scaffold can be deformed into its temporary small shape. Cooling is needed to temporarily fix the deformed state. Once the scaffold is implanted in the breast of the patient, the shape memory effect is triggered by the body temperature which is above the glass transition temperature. This results in an increased mobility and allows the scaffold to go back to its permanent state. By implanting the scaffold in its temporarily small shape, the surgeon can minimise the incision.[7]

II. Materials and methods

A. Materials

1) Polylactic acid

Poly(D,L-lactic acid) (PDLLA) is a frequently produced biodegradable aliphatic polyester and has been FDA approved for different biomedical applications like sutures and bone fixation due to the moderate glass transition temperature (50-60°C) and degradation into non-toxic products.[8] Ring opening polymerisation (ROP) of PDLLA results in more controlled molar masses and lower dispersities compared to polycondensation and was therefore preferred as synthesis technique. This chain-growth polymerisation is often initiated by alcohols. Three different PDLLA polymers were synthesised with different molar masses; PLA6, PLA11*, PLA13. The numbers for PLA6, PLA11* and PLA13 refer to the molar mass of the polymer obtained via proton nuclear magnetic resonance (H-NMR) spectroscopy, 5.6, 10.7 and

12.6 kg/mol respectively. Due to the relatively high dispersity (Đ) of PLA11* (1.45) (compared to 1.21 and 1.28 for PLA6 and PLA13, respectively) with a molar mass of 2.5 kg/mol according to the gel permeation chromatography (GPC) measurement, the molar mass of the chains is broadly distributed. The general molar mass is probably higher than 2.5 kg/mol as H-NMR spectroscopy resulted in a molar mass of 10.7 ± 3.6 kg/mol. This polymer is called PLA11* due to the large variability in molar mass of the chains.[8]

2) Copolymer of polylactic acid and poly-ε-caprolactone

The glass transition temperature of pure PDLLA (50-60°C) is too high compared to the desired range of 30-35°C.[8] Therefore, a copolymer with poly-ε-caprolactone (PCL) (T_g = -60°C) was created to lower the glass transition temperature. PCL is a biocompatible, biodegradable and FDA-approved polyester. The synthesis of inexpensive poly-ε-caprolactone in this work occurred via ring opening polymerisation. Multiple copolymers, with a molar mass of 10 kg/mol and a weight percentage PCL of eight, were synthesised under different conditions during this master dissertation.[9]

3) Thermoplastic polyurethane

Thermoplastic polyurethanes (TPUs) are frequently used polymers in implants, coatings and so on. These polymers consist of hard and soft segments which leads to a microphase separated morphology. TPUs were synthesised in two steps. First the soft segment, in this master thesis PDLLA, is polymerised into a diol by bulk polymerisation. This soft segment controls the degradation of the thermoplastic polyurethane. Next, the diol is converted into a TPU by adding diisocyanate (hexamethylene diisocyanate) and chain extender (1,2-propanediolisobutyl polyhedral oligomeric silsesquioxane (POSS)) to introduce a semi-crystalline hard block (see Figure 1). The main advantage of this thermoplastic polyurethane is that it can combine the advantages of both PDLLA (amorphous, organic component) and POSS (semi-crystalline, inorganic component). In this way, the TPU is biocompatible, biodegradable and flexible due to the PDLLA chains and the thermal stability and rigidity of the TPU increases by the addition of POSS containing monomers. Three different TPUs were shipped to Ghent from Syracuse University with PDLLA chains of 5.7 kg/mol (TPU1), 7.8 kg/mol (TPU2) and 8.1 kg/mol (TPU3). These molar masses were determined via H-NMR spectroscopy.[10]

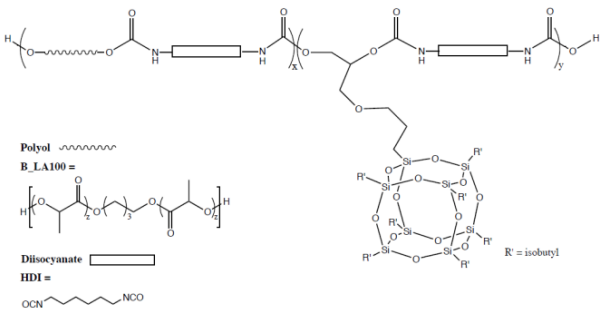

Figure 1: Chemical structure of the thermoplastic polyurethane used in this work [11]

4) Acrylate-endcapped urethane-based polymer

Previously mentioned polymers were functionalised into acrylate-endcapped urethane-based polymers (AUPs). These materials have the ability to crosslink upon exposure to UV-light in the presence of a photoinitiator. AUPs constituted acrylate end groups, spacers, diisocyanates and a polymer backbone, as illustrated in Figure 2. When the photoinitiator is exposed to UV-light, radicals are formed that initiate free radical polymerisation of the acrylate groups. A flexible spacer is introduced between the acrylates and the polymer backbone to give the acrylate groups more mobility which enables them to crosslink in solid state. The backbone polymer is attached to the spacer by using isophorone diisocyanate (IPDI). The functional end groups of the diisocyanate (-NCO) react with the hydroxyl functionalities of the polymer backbone, forming urethane bonds. Finally, the backbone itself is the core of the material and defines most of the properties such as the glass transition temperature, the degradation temperature and the mechanical properties.[12]

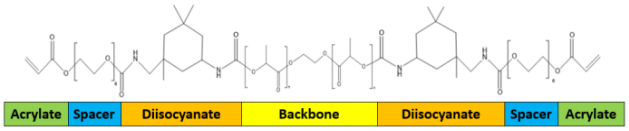

Figure 2: Chemical structure of acrylate-endcapped urethane-based polylactic acid with bisomer PEA6 [12]

Bisomer oligo(ethylene glycol) (6) acrylate (PEA6) was used for AUPs with only one acrylate at each chain-end, while ethoxylated and propoxylated pentaerythritol triacrylate (EPPETA) resulted in AUPs with three acrylates at each chain-end (Figure 3).

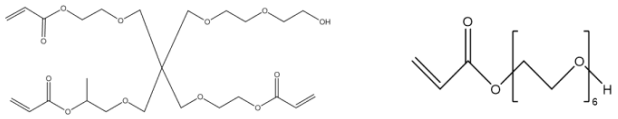

Figure 3: Chemical structure of EPPETA (left) and bisomer PEA6 (right)

B. *Digital light processing*

Digital light processing (DLP) was used as 3D printing technique to process the AUPs into scaffolds. This technique uses photopolymerisation to create a 3D structure, by selectively solidifying a liquid photosensitive polymer with UV-light in the presence of a photoinitiator (PI) and photoblocker (PB). The latter was added to prevent overcuring and to improve the resolution of the scaffold by absorbing the excess of UV-light. The DLP printer used during this project is called *LumenX* from the company *Cellink* with a wavelength of 405 nm (with 19.51 mW/cm^2 for 50% intensity).

III. RESULTS AND DISCUSSION

A. Synthesis of AUPs with appropriate glass transition temperatures

1) Synthesis of AUPs

AUPs with PDLLA as starting material (PLA6, PLA11* and PLA13) were synthesised in a glovebox to avoid that components in the air, such as water, can act as initiators. 40 g lactide (0.278 mol; monomer), 224.38 µl purified ethylene glycol (4.02 mmol; initiator), 1.63 g tin 2-ethylhexanoate (4.02 mmol; catalyst) and 135 ml dry toluene (solvent) were added to a Schlenk flask in the glovebox followed by three freeze-pump-thaw cycles to target 40 g of polymer with a molar mass of 10 kg/mol. The reaction was stirred for 24 hours at 100°C under argon atmosphere. PDLLA was functionalised into both diacrylate and hexaacrylate AUPs. To this end, 40 g PDLLA (4.02 mmol) was dissolved in dry toluene or chloroform for two-step syntheses. This step was not needed during one-step syntheses. The temperature of the solution was increased to 75°C and the mixture was stirred and kept under argon atmosphere. A double excess single acrylate endcap agent (9.35 g, 16.4 mmol) or triacrylate endcap agent (12.62 g, 16.4 mmol) was added to an amber vial together with 1 ml of dry toluene. Bismuth neodecanoate (15.8 mg (2.18 µmol) for single acrylate endcap agent and 14.8 mg (2.04 µmol) for triacrylate endcap agent; catalyst) was added to the vial and the mixture was injected into the Schlenk flask. After reacting for 24 hours at 75°C, the synthesised AUPs was precipitated twice in a 10-fold excess cold methanol and dried in a vacuum oven.

Secondly, different copolymers of PDLLA and PCL were synthesised by adding 36.8 g lactide (0.255 mol), 3.11 ml ε-caprolactone (0.028 mol) and 135 ml dry toluene to a Schlenk flask in the glovebox to target 40 g of copolymer with a molar mass of 10 kg/mol and 8 weight percentage of PCL. After performing three freeze-pump-thaw cycles, 225.28 µl initiator (4.04 mmol; ethylene glycol) and 1.64 g catalyst (4.04 mmol; tin 2-ethylhexanoate) were added to the mixture and the reaction was stirred for 24 hours at 100°C under argon atmosphere. Afterwards, these copolymers were functionalised in AUPs in a similar way as PDLLA.

Upscaling of the polymerisations was not possible due to the crucial role of the glovebox as well as the freeze-pump-thaw cycles. Going from a two-step synthesis (precipitation of the polymer before functionalising it into AUP) to a one-step synthesis (only a final precipitation of the AUP) did result in AUPs with similar characteristics and higher yields. Consequently, one-step syntheses were preferred as synthesis method.

The thermoplastic polyurethanes synthesised by Syracuse University were functionalised into both diacrylate and hexaacrylate AUPs in a similar way as the functionalisation of PDLLA-based AUPs. Precipitations were performed in hexane instead of methanol as this non-solvent was used for the precipitation of TPU. However, H-NMR spectra showed that there were still impurities left after precipitation in hexane. Therefore, methanol was used for the following precipitations which resulted in less impurities but also lower yields. The yield obtained after two precipitations in hexane was 86% while one precipitation in hexane and one in methanol resulted in a yield of 42%. The molar ratio of POSS/PDLLA was aimed to be around three.

2) Structural characteristics

The structural characteristics of the polymers were determined via H-NMR spectroscopy. The molar ratio of thermoplastic polyurethanes was aimed to be around three. However, the actual molar ratios were 0.97, 1.44 and 1.54 for TPU1, TPU2 and TPU3 respectively. These lower ratios can be explained by the lower molar masses of PDLLA. This molar mass was targeted to be 12 kg/mol. However, only molar masses of 5.7 (TPU1), 7.8 (TPU2) and 8.1 (TPU3) kg/mol were obtained which resulted in more PDLLA chains for the same amount of PDLLA. The weight percentages of the hard segment (HDI and POSS) did not vary across the different materials (≈19%).

For all copolymers, a molar mass of 10 kg/mol and 8 wt% PCL was targeted to obtain glass transition temperatures in the desired range. However, the obtained ratio of PCL to PDLLA was lower than the target of 8 wt% for all copolymer batches (between 1.4 and 6.24 wt% PCL). Lactides were found to be more reactive than ε-caprolactone due to a better coordination ability.

3) Thermal characteristics

Ideally, the synthesised AUPs should have a glass transition temperature between 30°C and 35°C to trigger a shape memory effect after implantation of the scaffold into the patient's breast.

A semi-crystalline behaviour was obtained for the thermoplastic polyurethanes due to the incorporation of POSS monomers. This behaviour resulted in melt and crystallisation peaks around 125°C and 120°C, respectively, as shown in the DSC thermogram of TPU1 (Figure 4). The glass transition temperature of TPU1 appeared to be in the desired range. Unfortunately, this material consisted of impurities, such as monomer POSS, leading to this low glass transition temperature. As expected, TPU2 and TPU3 had higher glass transition temperatures of respectively 49°C and 46°C as these are precipitated twice in hexane instead of once. These temperatures did not change significantly after functionalising the TPUs into AUPs.

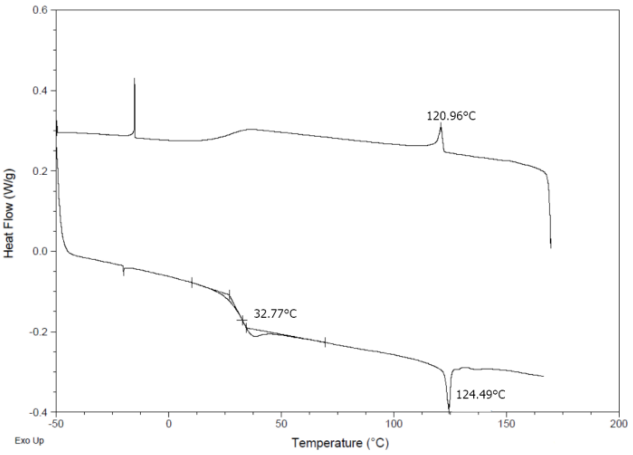

Figure 4: DSC thermogram of TPU1

AUPs with PDLLA as starting materials had glass transition temperatures between 35°C and 42°C. These temperatures are closer to the desired range than the glass transition temperatures of TPU-based AUPs. Since the transition temperatures were still too high, copolymers with PCL were created. The addition of PCL resulted in lower transition temperatures (between 24°C and 34°C) compared to TPU-based AUPs (p-value: 0.005) and PDLLA-based AUPs (p-value: 0.0016).

Thermal degradation of the TPUs started around 225°C, while after conversion into AUPs, the onset degradation temperature increased to 240°C. This increase in degradation temperature was also found for PDLLA (from 205°C to 220°C). TPU-based AUPs turned out to have significantly higher degradation temperatures than PDLLA-based (p-value < 0.0001) and PDLLA/PCL-based AUPs (p-value < 0.0001).

B. Manufacturing of a scaffold

DLP printing was used to process the obtained AUPs into a porous scaffold. To this end, photosensitive resins were developed.

1) Components of the resin

The resins contained four components: AUP, photoinitiator, photoblocker and a solvent. TPO-L is often described in literature as a good photoinitiator for digital light processing. The UV-VIS spectrum, depicted in Figure 5, shows that TPO-L is active around 405 nm, the operating wavelength of the DLP printer.

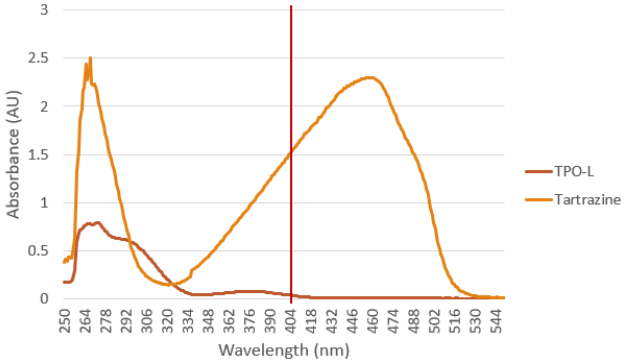

Figure 5: UV-VIS spectra of TPO-L (photoinitiator, 0.01 g/ml$_{NMP}$) and tartrazine (photoblocker, 1E-04 g/ml$_{NMP}$)

Tartrazine is used in the food industry as colour dye and is thus a biocompatible photoblocker with a low cytotoxicity. For this reason and due to having an active range around 405 nm (see Figure 5), tartrazine was chosen as photoblocker. The three components were dissolved in 1-methyl-2-pyrrolidinone (NMP). This solvent was selected due to its high boiling point (202°C) to ensure minimal evaporation during the printing process.

The acrylate density of the AUPs appeared to be important to obtain sufficient crosslinking after exposing the resin to UV-light. This density, and thus also the crosslinking capacity, can be increased in two ways: by decreasing the molar mass or by increasing the number of acrylates at the chain-ends.

2) Optimisation of the resin

The resins need to have a viscosity below 3 Pa.s to obtain a homogeneously spread resin layer in the printing vat.[13][14] The viscosity of the resin depends on its AUP concentration and was determined by means of rheology measurements.

Figure 6 shows the viscosity of TPU2 with 2 acrylates (TPU2AUP(1)) and 6 acrylates (TPU2AUP(3)) for different concentrations. It turned out that TPU-based AUPs have a shear thinning behaviour which is explained by the formation of microdomains of POSS. This shear thinning behaviour was less visible for resins with 30 wt% AUP due to the low amount of POSS clusters.[15]

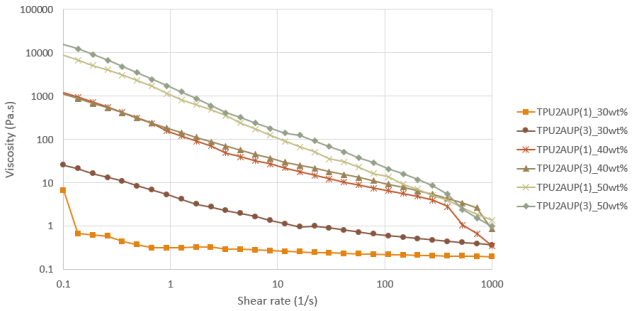

Figure 6: Viscosity as a function of shear rate for TPU2AUP(1) and TPU2AUP(3) at different concentrations

As one would expect, the viscosity increases with increasing AUP concentration. In order to have a good fluidity for DLP printing, resins of TPU-based AUPs with 30 wt% were used.

The optimal resin concentration for PDLLA-based AUPs was determined by examining PLA11*AUP(3). The mean viscosities of this material for different concentrations can be found in Table 1. According to the threshold for DLP printing, 60 wt% would offer the adequate viscosity. However, by inspecting the resins of 60 wt% visually, one could conclude that the resin did not have sufficient flow in order to refill the printing area. The low viscosity might be the result of an inhomogeneous resin of 60 wt% AUP, for which a too liquid part was used for rheology measurements. Therefore, a concentration of 50 wt% was chosen. Additionally, this lower weight percentage provided sufficiently low viscosities for all PDLLA-based AUPs with higher molar masses (like PLA13).

Table 1: Viscosity (Pa.s) for different concentrations of PLA11*AUP(3)

wt% AUP	Viscosity (Pa.s)
50	0.12 ± 0.0016
60	0.61 ± 0.011
70	10.2 ± 2.97

In addition, the optimal amount of photoinitiator needed to be determined. This was done by photorheology measurements. Different resins with 70 wt% TPU1AUP(1) and 2, 10, 20 and 50 mol% TPO-L (with respect to the number of acrylates) were investigated. Figure 7 shows the storage moduli of the different resins as a function of time upon UV-exposure. This allowed to study the crosslinking speed of the different resins. The point at which the modulus has reached approximately 97% of the total increase, was

determined. For 50 mol% TPO-L, this point was already reached after ten seconds, while resins with 2, 10 and 20 mol% needed 68, 40 and 25 seconds respectively. 2 mol% TPO-L might have been insufficient to have adequate crosslinking which resulted in a lower modulus than 10 mol% TPO-L. Additionally, the excessive amount of photoinitiator for 20 and 50 mol% TPO-L resulted in more and faster termination reactions due to the presence of a high amount of radicals leading to a lower storage modulus. The photoinitiator concentration must be high enough to obtain efficient crosslinking. For successful DLP printing, photocrosslinking needs to occur within seconds. On the other hand, high concentrations of photoinitiator are cytotoxic as they form radicals upon exposure to UV-light, which can cause apoptosis of cells. For this reason, a trade-off needs to be made. The optimal amount of TPO-L was chosen to be 10 mol%.

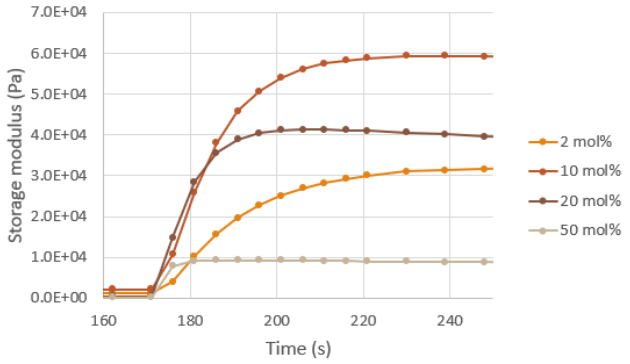

Figure 7: Storage moduli of resins constituting 70 wt% TPU1AUP(1) and different amounts of photoinitiator (2, 10, 20 and 50 mol%) as a function of time upon UV-exposure

In order to compare different materials (for example during cell assays), the amount of initiator was redefined as a fixed concentration in the resin. In literature, concentrations TPO-L in a resin for DLP printing were found to be between one and two percent. For this project, a weight percentage of 1.5 was chosen as this corresponds to a minimal mol% of 7.7 for PLA6AUP(3), the material with the highest acrylate density, which is around 10 mol%. Photorheology measurements confirmed that resins with 1.5 wt% TPO-L and 50 wt% PLA6AUP(3) were photocrosslinkable.[16][17]

Resins with different molar ratios of photoblocker versus photoinitiator (PB/PI) were printed with an intensity of 19.51 mW/cm^2 and exposure time of 20 seconds to determine the optimal amount of photoblocker. Increasing the amount of photoblocker resulted in a better resolution. However, this increase led to partially formed scaffolds (for PB/PI of 0.135 and 0.15). For this reason, a molar ratio PB/PI of 0.125 was chosen.

3) Optimisation of printing conditions

Once the optimal resin condition was found, the ideal conditions for DLP printing were investigated. To this end, the material with the greatest potential for DLP printing was used. PLA6AUP(3) has the best crosslinking capacity due to its high acrylate density because of its low molar mass and the use of EPPETA instead of bisomer PEA6.

At last, the intensity and exposure time were adapted to obtain a higher resolution and sufficient and fast crosslinking. Figure 8 shows that an exposure time of 20 seconds and intensity of 19.51 mW/cm^2 resulted in overcuring as the struts were not well delineated. Decreasing the exposure time to five seconds and increasing the intensity resulted in better resolutions. However, further optimisation is needed as there are still no clear pores in the scaffold.

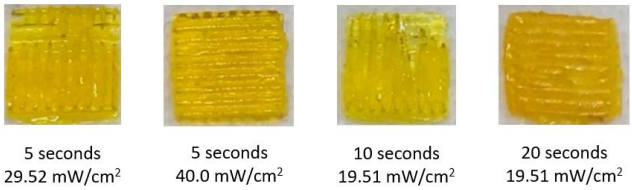

Figure 8: DLP printed scaffolds (1 cm^2 and 2 mm height) PLA6AUP(3) with different intensities and exposure time for a molar ratio PB/PI of 0.125

4) Characterisation of the scaffolds

Different characteristics of the crosslinked materials were investigated considering that these materials will be used for breast reconstruction purposes after optimalisation. The gel fraction was determined for different materials to get an idea of the highest crosslinking density. As expected, PLA6AUP(3) resulted in the highest gel fraction due to the high acrylate density.

The swelling of a scaffold, when it comes in contact with body fluids, was mimicked by immersing crosslinked discs in Dulbecco's phosphate buffered saline (DPBS). This characteristic is reported as the swelling ratio and seemed to be lowest for PLA6AUP(3) (swelling ratio of 0.17).

Furthermore, the effect of (cytotoxic) leachables, after 24 hours immersion of the material in an ethanol solution, on the viability and proliferation of cells was investigated by live/dead staining and MTS assays. The investigated materials were biocompatible as they all resulted in a cell viability above 88%. Figure 9 illustrates that TPU3AUP(3) has a significantly lower metabolic activity than PDLLA-based AUPs. This decrease is the result of leachables. In general, it seems that all materials are biocompatible according to indirect cell assays and ISO standard 10993.

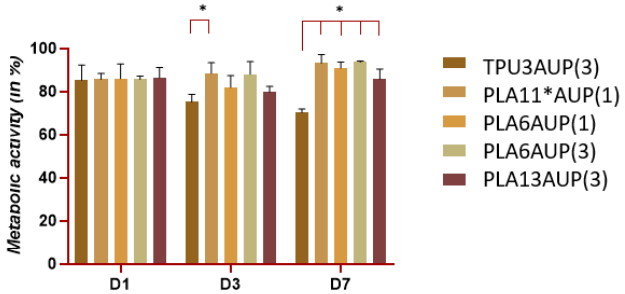

Figure 9: Cell viability obtained via MTS assays

IV. Conclusion and Future Work

In this paper, the development of a porous scaffold with shape memory effect slightly below body temperature was developed for the purpose of minimally invasive breast reconstruction. TPU-based AUPs show great potential as

materials to construct scaffolds due to the many advantages by combining amorphous, organic PDLLA with semi-crystalline, inorganic POSS. However, the glass transition temperature of this polymer is too high to trigger a change in size upon implantation in the body. The same applies for PDLLA-based AUPs. This work showed that the addition of PCL lowers the glass transition temperature. In this way, polymers with a glass transition temperature slightly below body temperature were obtained, which is needed for the shape memory effect. TGA measurements indicated that the addition of POSS and the conversion of polymers into AUPs enhanced the thermal stability.

AUPs were used in resins for DLP printing together with TPO-L (photoinitiator), tartrazine (photoblocker) and NMP (solvent). Resins containing hexaacrylate AUPs with low molar masses, turned out to have good crosslinking capacities. The AUP concentration for TPU-based and PDLLA-based AUPs were 30 wt% and 50 wt% respectively to obtain a homogenously spread resin layer in the printing vat during digital light processing. Photorheology measurements showed that approximately 10 mol% TPO-L was optimal to initiate the radical photopolymerisation. The optimal amount of photoblocker appeared to be around 0.125 molar ratio of photoblocker versus photoinitiator as higher amounts resulted in incomplete crosslinking. Scaffolds with poor resolutions were developed with digital light processing. Further optimisations are needed to obtain porous scaffolds.

For the actual application, one should keep in mind that the scaffold will swell in the aqueous environment of the body. The swelling must be limited to prevent additional pressure on the surrounding tissues. A first indication of this swelling was obtained by measuring the swelling ratio. Additionally, the amount of leaching components needs to be minimised. This was quantified by the gel fraction. Next, cell assays have proven the biocompatibility of the materials and the shape memory behaviour was demonstrated by heating, deforming, cooling and reheating of a scaffold.

This master dissertation includes the initial work for the development of a scaffold for minimally invasive breast reconstruction. An important aspect of the scaffold that was not yet tested during this project, consists of the mechanical properties. Additionally, further quantitative studies on shape memory cycles should be conducted. Testing the biodegradability is also essential for the purpose of tissue regeneration and the biocompatibility needs to be examined further by direct cell assays. To conclude, there is still a lot of research that needs to be conducted before these scaffolds can move to small animal experiments.

REFERENCES

[1] A. Loreti *et al.*, "Immediate Breast Reconstruction after mastectomy with polyurethane implants versus textured implants: A retrospective study with focus on capsular contracture," *Breast*, vol. 54, pp. 127–132, Dec. 2020.

[2] L. R. Mundy, K. Homa, A. F. Klassen, A. L. Pusic, and C. L. Kerrigan, "Breast cancer and reconstruction: Normative data for interpreting the BREAST-Q," *Plast. Reconstr. Surg.*, vol. 139, no. 5, pp. 1046–1055, May 2017.

[3] M. M. Howard-McNatt, "Patients opting for breast reconstruction following mastectomy: An analysis of uptake rates and benefit," *Breast Cancer: Targets and Therapy*, vol. 5, no. 1. Dove Press, pp. 9–15, 26-Feb-2013.

[4] M. Charalambous, R. Daoud, and I. Karat, "Technological advances in breast implants," in *Advances in Medical and Surgical Engineering*, Elsevier, 2020, pp. 141–147.

[5] N. Sarvazyan, "Tissue Engineering: Principles, Protocols, and Practical Exercises Learning Materials in Biosciences[1] N. Sarvazyan, 'Tissue Engineering: Principles, Protocols, and Practical Exercises Learning Materials in Biosciences,' 2020.," 2020.

[6] M. Cheng *et al.*, "Breast tissue engineering," in *Comprehensive Biomaterials II*, Elsevier, 2017, pp. 435–454.

[7] S. M. Hasan, L. D. Nash, and D. J. Maitland, "Porous Shape Memory Polymers: Design and Applications," *J. Polym. Sci., Part B Polym. Phys*, vol. 54, pp. 1300–1318, 2016.

[8] O. M. Sanusi, A. Benelfellah, D. N. Bikiaris, and N. Aït Hocine, "Effect of rigid nanoparticles and preparation techniques on the performances of poly(lactic acid) nanocomposites: A review," *Polymers for Advanced Technologies*. John Wiley and Sons Ltd, p. pat.5104, 02-Oct-2020.

[9] T. P. Gumede, A. S. Luyt, and A. J. Müller, "Review on PCL, PBS, AND PCL/PBS blends containing carbon nanotubes," *Express Polymer Letters*, vol. 12, no. 6. BME-PT and GTE, pp. 505–529, 01-Jun-2018.

[10] S. Wendels and L. Avérous, "Biobased polyurethanes for biomedical applications," *Bioactive Materials*, vol. 6, no. 4. KeAi Communications Co., pp. 1083–1106, 01-Apr-2021.

[11] Q. Guo, P. T. Knight, and P. T. Mather, "Tailored drug release from biodegradable stent coatings based on hybrid polyurethanes," *J. Control. Release*, vol. 137, no. 3, pp. 224–233, Aug. 2009.

[12] A. Houben *et al.*, "Flexible oligomer spacers as the key to solid-state photopolymerization of hydrogel precursors," *Mater. Today Chem.*, vol. 4, pp. 84–89, Jun. 2017.

[13] D. A. Komissarenko, P. S. Sokolov, A. D. Evstigneeva, I. A. Shmeleva, and A. E. Dosovitsky, "Rheological and curing behavior of acrylate-based suspensions for the DLP 3D printing of complex zirconia parts," *Materials (Basel).*, vol. 11, no. 12, Nov. 2018.

[14] M. Krkobabić, D. Medarević, N. Pešić, D. Vasiljević, B. Ivković, and S. Ibrić, "Digital light processing (DLP) 3D printing of atomoxetine hydrochloride tablets using photoreactive suspensions," *Pharmaceutics*, vol. 12, no. 9, pp. 1–17, Sep. 2020.

[15] Z. Qin *et al.*, "Injectable shear-thinning hydrogels with enhanced strength and temperature stability based on polyhedral oligomeric silsesquioxane end-group aggregation," *Polym. Chem.*, vol. 8, no. 10, pp. 1607–1610, Mar. 2017.

[16] E. Skliutas *et al.*, "A Bio-Based Resin for a Multi-Scale Optical 3D Printing," *Sci. Rep.*, vol. 10, no. 1, pp. 1–9, Dec. 2020.

[17] T. Femmer, "Rapid Prototyping of Membranes and Membrane Devices," 2015.

Contents

List of Figures **xii**

List of Tables **xiv**

1 Introduction **1**
1.1 Global impact of breast cancer and breast resection . . . 1
1.2 Increasing importance of breast reconstruction . . . 1
1.3 Current options for breast reconstruction . . . 2
1.3.1 Immediate versus delayed reconstruction . . . 2
1.3.2 Implant-based versus autologous tissue-based reconstruction . . . 4
1.4 Anatomy of the breast . . . 7
1.5 Adipose tissue engineering . . . 8
1.5.1 Cells and cell environment . . . 9
1.5.2 Biomaterials . . . 11
1.6 Materials used . . . 14
1.6.1 Shape memory polymers . . . 15
1.6.2 Starting materials to create photocrosslinkable SMPs . . . 18
1.6.3 Acrylate-endcapped urethane-based polymer . . . 23
1.7 Hypotheses and objectives of the master thesis . . . 24

2 Materials and methods **26**
2.1 Materials . . . 26
2.2 Methods - Synthesis of materials . . . 26
2.2.1 Preparation of components . . . 26
2.2.2 Starting materials . . . 27
2.2.3 Synthesis of acrylate-endcapped urethane-based materials . . . 29
2.3 Methods - Characterisation of materials . . . 30
2.3.1 Thermogravimetric analysis . . . 30
2.3.2 Differential scanning calorimetry . . . 31
2.3.3 Proton nuclear magnetic resonance spectroscopy . . . 31
2.3.4 Gel permeation chromatography . . . 31
2.3.5 Fourier transform infrared spectroscopy . . . 32
2.3.6 Rheology and photorheology . . . 32
2.3.7 UV-VIS spectroscopy . . . 32
2.3.8 Gel fraction and swelling ratio experiments . . . 32
2.3.9 Cell assays . . . 33
2.3.10 Statistical analysis . . . 34

3 Results and discussion **36**
3.1 AUPs with appropriate glass transition temperatures 36
3.1.1 Synthesis of starting materials 36
3.1.2 Synthesis of acrylate-endcapped urethane-based polymers 43
3.1.3 Thermal properties of polymer backbones and AUPs 48
3.2 Manufacturing of a scaffold 55
3.2.1 Components of the resin 55
3.2.2 Optimisation of the resin 58
3.2.3 Optimisation of the printing conditions 63
3.2.4 Characterisation of the scaffolds 65

4 Conclusion and future work **71**

Bibliography **73**

A Ethical considerations **86**
A.1 Reflection about the potential impact of the study 86
A.2 Scientific integrity 86

B Calculations of characteristics via H-NMR spectra **87**
B.1 Molar masses of starting materials 87
B.1.1 Molar mass of PDLLA 87
B.1.2 Molar mass of PDLLA/PCL 87
B.2 Weight percentage ϵ-caprolactone in PDLLA/PCL 88
B.3 Estimation of OH-concentration 88
B.4 Molar ratio POSS/PDLLA for thermoplastic polyurethanes 89
B.5 Hard segment weight percentage of TPU 89
B.6 Estimation of the degree of substitution 89

C H-NMR spectra **91**

D DSC thermograms **93**

E TGA thermograms **94**

F Photorheology results **96**

List of Figures

1.1 Schematic breast after mastectomy (left), with tissue expander (centre) and with permanent implant (right) [1] . . . 4
1.2 Chemical structure of polydimethylsiloxane [2] . . . 6
1.3 Schematic anatomy of the breast [3] . . . 7
1.4 Cornerstones of tissue engineering [4] . . . 8
1.5 Working principle of digital light processing [5] . . . 13
1.6 Absorption spectra of different photoblockers [6] . . . 14
1.7 Shape memory effect of polymers [7] . . . 15
1.8 Shape memory effect of self-tightening sutures [8] . . . 17
1.9 Stereoisomers of lactic acid [9] . . . 19
1.10 Two ways to produce PLA [10] . . . 20
1.11 1,2-Propanediolisobutyl POSS [11] . . . 21
1.12 Hard and soft segments of thermoplastic polyurethane [12] . . . 22
1.13 Chemical structure of the thermoplastic polyurethane used in this master thesis [13] 23
1.14 Chemical structure of acrylate-endcapped urethane-based polylactic acid with n depending on the target molar mass [14] . . . 23

2.1 Chemical structure of single acrylate endcap agent . . . 29
2.2 Chemical structure of triacrylate endcap agent . . . 30
2.3 Process of MTS and live/dead assays . . . 34

3.1 H-NMR spectrum of PLA11* . . . 37
3.2 H-NMR spectrum of PLA/PCL11 . . . 38
3.3 Molar masses obtained from GPC (brown) and H-NMR spectroscopy (orange) . . . 40
3.4 H-NMR spectrum of PDLLA used in TPU2 . . . 41
3.5 H-NMR spectrum of TPU2 [13] . . . 42
3.6 Synthesis of endcap agent with three acrylates . . . 43
3.7 FT-IR spectra during endcap synthesis with EPPETA at different time points . . . 43
3.8 Reaction of isocyanate with water into amine and CO_2 [15] . . . 45
3.9 H-NMR spectrum of PLA11*AUP(1) . . . 46
3.10 H-NMR spectrum of PLA11*AUP(3) . . . 46
3.11 TGA thermogram of PLA6 . . . 49
3.12 TGA thermogram of PLA6AUP(1) (left) and PLA6AUP(3) (right) . . . 50
3.13 DSC thermogram of TPU1 . . . 51
3.14 TGA thermogram of TPU1 . . . 51
3.15 TGA thermogram of TPU3 . . . 52
3.16 TGA thermogram of TPU3AUP(1) . . . 52
3.17 TGA thermogram of 1,2-propanediolisobutyl POSS . . . 52

3.18 Onset degradation temperature of the obtained polymer backbones and AUPs 54
3.19 Glass transition temperature of the obtained polymer backbones and AUPs 54
3.20 Glass transition temperatures for PLA6- and PLA13-based materials 55
3.21 Absorption spectra of TPO-L (left, 0.01 $g_{(\mathrm{TPO-L})}/ml_{NMP}$) and Irgacure 2959 (right, 1E-05 $g_{(Irgacure2959)}/ml_{NMP}$) 56
3.22 Absorption spectrum of tartrazine (1E-04 $g_{(tartrazine)}/ml_{(NMP)}$) 57
3.23 Viscosity as a function of shear rate for TPU2AUP(1) and TPU2AUP(3) for different wt% AUP 59
3.24 Viscosity as a function of shear rate for PLA11*AUP(3) for different weight percentages 60
3.25 Storage modulus for resins with 70 wt% TPU1AUP(1) and different amounts of photoinitiator (2, 10, 20 and 50 mol%) as a function of time upon UV exposure . . 62
3.26 Storage (orange) and loss (brown) moduli of a resin with 60 wt% PLA11*AUP(1) and 10 mol% TPO-L as a function of time during UV irradiation 63
3.27 DLP printed scaffolds of PLA6AUP(3) (left) and PLA13AUP(3) (right) with an intensity of 19.51 mW/cm^2, exposure time of 20 seconds, 1.5 wt% TPO-L and molar ratio PB/PI of 0.1 64
3.28 DLP printed scaffolds of PLA6AUP(3) with different intensities and exposure times for a molar ratio PB/PI of 0.125 65
3.29 Gel fraction (orange) and degree of substitution (brown) of different AUPs based on PDLLA 66
3.30 Swelling ratio determined by mass (orange) and height (brown) of different AUPs based on PDLLA in DPBS 67
3.31 Cell viability (left) and metabolic activity (right) obtained via live/dead and MTS assays for different materials 68
3.32 Results of live/dead viability assays 69
3.33 Deformed scaffolds before immersion in water 70
3.34 Scaffolds after immersion in cold water (left) and water at body temperature (right) 70

C.1 H-NMR spectrum of TPU1 91
C.2 H-NMR spectrum of TPU3 91
C.3 H-NMR spectrum of TPU2AUP(1) 91
C.4 H-NMR spectrum of TPU2AUP(3) 91
C.5 H-NMR spectrum of PLA6 92

D.1 DSC thermogram of TPU2 93
D.2 DSC thermogram of TPU3 93

E.1 TGA thermograms of bisomer PEA6 (left) and EPPETA (right) 94
E.2 TGA thermogram of IPDI 94
E.3 TGA thermograms of endcap with bisomer PEA6 (left) and EPPETA (right) 95

F.1 Storage (orange) and loss (brown) moduli of a resin with 60 wt% PLA11*AUP(1) and 2 mol% TPO-L in function of time during UV irradiation 96
F.2 Storage (orange) and loss (brown) moduli of a resin with 60 wt% PLA6AUP(3) and 1.5 wt% TPO-L as a function of time during UV irradiation 96
F.3 Storage (orange) and loss (brown) moduli of a resin with 60 wt% PLA13AUP(3) and 1.5 wt% TPO-L as a function of time during UV irradiation 97

List of Tables

1.1 Advantages and disadvantages of immediate and delayed breast reconstruction [16, 17] 4
1.2 Properties of PDLLA [18–22] 19

3.1 Structural characteristics for different types of PDLLA 37
3.2 Polymer characteristics for different environmental factors 39
3.3 Molar masses of PDLLA used in the thermoplastic polyurethanes 41
3.4 Molar ratio POSS/PDLLA and weight percentage hard segment 42
3.5 Polymer characteristics for one-step and two-step syntheses 44
3.6 Characteristics of PDLLA/PCL-based AUPs, synthesised under optimal conditions . 45
3.7 Characteristics of AUPs with PDLLA as starting material 47
3.8 Characteristics of TPU-based AUPs 47
3.9 Thermal properties of PDLLAs and PDLLA-based AUPs 48
3.10 Thermal properties of PDLLA/PCLs and PDLLA/PCL-based AUPs 51
3.11 Thermal properties of TPUs and TPU AUPs 51
3.12 Boiling temperatures of the solvent candidates 56
3.13 Viscosity (Pa.s) for different shear rates of PDLLA/POSS-based AUPs 59
3.14 Viscosity (Pa.s) for different weight percentages PLA11*AUP(3) 61

List of abbreviations

ADM	Acellular Dermal Matrix
ADSC	Adipose-Derived Stem Cells
AFG	Autologous Fat Grafting
ATR	Attenuated Total Reflection
AUP	Acrylate-endcapped Urethane-based Precursor/Polymer
BCS	Breast Conserving Surgery
bFGF	Basic Fibroblast Growth Factor
Ca-AM	Calcein-Acetoxymethylester
CAD	Computer-Aided Design
CL	ϵ-caprolactone
DIEP	Deep Inferior Epigastric artery Perforator
DLP	Digital Light Processing
DMD	Digital Micromirror Device
DMED	Dulbecco's Modified Eagle Medium
DPBS	Dulbecco's Phosphate Buffered Saline
DMT	Dimethyl Terephthalate
DS	Degree of Substitution
DSC	Differential Scanning Calorimetry
EPPETA	Ethoxylated and Propoxylated Pentaerythritol Triacrylate
FCS	Fetal Calf Serum
FDA	Food and Drug Administration
FDM	Fused Deposition Modelling
FT-IR	Fourier Transform Infrared spectroscopy
FPT	Freeze-Pump-Thaw
GB	Glovebox
GFP	Green Fluorescent Protein
HDI	Hexamethylene Diisocyanate
IGF	Insulin-like Growth Factor
IPDI	Isophorone Diisocyanate
iPSC	Induced Pluripotent Stem Cells
LA	Lactide
LDI	Lysine Diisocyanate
MTS	3-(4,5-dimethylthiazol-2-yl)-5-(3-carboxymethoxyphenyl)-2-(4-sulfophenyl)-2H-tetrazolium
NMR	Nuclear Magnetic Resonance
PBS	Phosphate Buffered Saline
PCL	Poly-ϵ-caprolactone
PDA	Polydopamine
PDLA	Poly(D-Lactic Acid)
PDLLA	Poly(D,L-Lactic Acid)
PDMS	Polydimethylsiloxane
PEA	Polyethyleneglycol Acrylate
PEG	Polyethylene Glycol
PI	Propidium Iodide

PLA Polylactic Acid

PLLA Poly(L-Lactic Acid)

PMMA Polymethyl Methacrylate

PMRT Postmastectomy Radiation Therapy

PMS Phenazine Methosulfate

POSS Polyhedral Oligomeric Silsesquioxane

PTZ Phenothiazine

QoL Quality of Life

ROP Ring Opening Polymerisation

SLA Stereolithography

SLS Selective Laser Sintering

SMP Shape Memory Polymer

SSPP Solid-State Photopolymerisation

SVF Stromal Vascular Fraction

TCP Tissue Culture Plate

TE Tissue Engineering

TGA Thermogravimetric Analysis

THF Tetrahydrofuran

TPP Triphenylphosphite

TPU Thermoplastic Polyurethane

UV Ultraviolet

VEGF Vascular Endothelial Growth Factor

2PP Two Photon Polymerisation

1. Introduction

1.1 Global impact of breast cancer and breast resection

Every year, nearly 2.1 million women worldwide get confronted with breast cancer, making it the most common cancer for females. The World Health Organisation estimates that 157.100 European women died of breast cancer in 2020. The high prevalence and death rate have a tremendous impact on many families. [23, 24]
Early-stage (stage I or II) breast cancer is often treated with a breast conserving surgery (BCS). However, in the study of Mundy et al. (2017), still 36% of the patients, diagnosed with early-stage breast cancer, underwent a mastectomy or breast amputation. This percentage is even higher for women with advanced breast cancer. In 58% of these cases, the surgeon performed a mastectomy with the aim to remove the tumor. [25]

After mastectomy, breast reconstruction can be suggested to the patient. Such a reconstruction can be performed during mastectomy or in a later stage, after completing the cancer treatment. Eventually, patients often experience a better psychiatric, social and sexual well-being when opting for a breast reconstruction. That explains why 43% of the patients who lost or will lose a breast, opt for a reconstruction. [25, 26]

1.2 Increasing importance of breast reconstruction

In 1882, William Halsted performed his first radical mastectomy. Although other surgeons already performed mastectomies before 1882, Plesca et al. (2016) claim that Halsted is seen as the pioneer since he was the first one with successful survival rates. During this radical mastectomy the breast, axillary lymph nodes and pectoralis muscle were removed. The operation was invasive and disfigured patients in such a way that the conditions were not optimal for a reconstruction. Halsted considered breast reconstruction as a violation of the local control of the disease. This opinion repulsed other surgeons from the idea of reconstructing a breast. [27–29]
Regardless of the belief of Halsted and many other surgeons, Professor Czerny was able to perform the first successful autogenous breast reconstruction by using a fist-sized lipoma from the flank of the patient in 1895. [30, 31]

It lasted until the 1960s before a less aggressive approach was applied for breast reconstruction. The pectoralis muscle was no longer removed during mastectomy and the contour of the chest wall was better preserved, which resulted in better reconstruction results.
This initiated the modern era of breast reconstruction. In 1963 Cronin and Gerow introduced the silicone gel breast implant. [32] This implant was inserted in the body of the patient during a second surgery after mastectomy. In 1971, a silicone implant was implanted immediately after the

mastectomy in a single surgery for the first time. [30, 33]

During the following decades, the 5-year survival rate for women with breast cancer has strongly increased. From 1975 to 1977, the 5-year survival rate for developed countries was 74.8%, while from 2003 to 2009, the rate increased up to 90.3%. Because of this increase, Miseré et al. (2020) claim that the focus of the therapy has changed from surviving breast cancer to giving the patients a better quality of life after treatment, thereby further increasing the importance of breast reconstructions. [26, 34]

The perception of breast cancer treatment has strongly evolved over the last centuries. In the 19th century, the most important goal of mastectomy surgery was to remove the entire tumor. Surgeons preferred to remove more body tissue than strictly necessary to increase the chance of complete tumor removal. Nowadays, surgeons want to remove all tumor tissue, while saving as much healthy tissue as possible for consecutive reconstruction. [34]

The loss of a breast has a major impact on women and can be a traumatic event. It can affect the psychiatric and social well-being of the patient and cause sexual morbidity. As an example, 30% of patients suffer from anxiety and depression after mastectomy. These women often feel disfigured and have concerns about their sexuality and sex life. [35, 36]

Breast reconstruction can alleviate the negative impact on the patient's life after breast tissue removal. Firstly, it offers a cosmetic advantage, as patients don't feel as mutilated and can wear any form of clothing. [17] Breast reconstruction also leads to potential psychological benefits and increased quality of life. It will improve the body image of patients and their sexual intercourse. Moreover, the anxiety and depression rates of women who underwent a mastectomy decrease after having a reconstructive surgery. These benefits are more pronounced for patients having immediate reconstruction compared to patients with a delayed reconstruction. [33, 36, 37]

1.3 Current options for breast reconstruction

Breast reconstruction surgery can be subdivided into two categories, based on the timing and the type of reconstruction. In terms of timing, the reconstructive surgery can be done during the same procedure as the mastectomy, which is called an immediate reconstruction. When a breast reconstruction during the mastectomy is not the preferred option, a delayed reconstruction can be performed. In this case, the patient will undergo a second operation, after mastectomy, to reconstruct the breast. Furthermore, the type of reconstruction can be split into two main classes, the implant-based and autologous tissue-based reconstruction. The latter uses patient's own tissue to regenerate the breast, while during the implant-based procedure a foreign object is inserted in the patient. [38]

1.3.1 Immediate versus delayed reconstruction

1.3.1.1 Immediate reconstruction

Immediate reconstructions are most suitable for patients with round shaped, less ptotic breasts, when less than 300 gram of tissue needs to be dissected. The greatest advantage of this approach

is that no adjuvant surgery is needed. In addition, there is a shorter period of hospitalisation than for delayed reconstruction surgeries. The third advantage is the maximum preservation of the inframammary fold and skin. In this way, reconstructive surgeons can use unscarred skin flaps of good quality. If patients opt for a delayed reconstruction, less skin will be preserved during the mastectomy to prevent rippling of the skin. Lastly, the psychological well-being of the patient will be superior in case of immediate reconstruction, as mentioned in Section 1.2. Patients will have a better body image and feel less anxious and depressed and more sexually attractive. These women are generally less confronted with the loss of their breast. [17, 36–38]

However, in case of immediate reconstructions patients have less time to make decisions. They need to be informed up front about the longer and more complex surgery and the increased risks and complications after surgery, such as skin necrosis and infection. Finally, if postmastectomy radiation therapy (PMRT) is needed, the esthetic outcome will be less satisfying in case of immediate reconstruction. Additionally, postmastectomy radiation therapy can result in a higher risk of capsular contraction in case of an immediate implant-based reconstruction. Especially after immediate autologous reconstruction PMRT can result in adverse effects, such as the formation of fibrosis within the stroma of adipose tissue, which might lead to fat necrosis. [16, 38–40]

1.3.1.2 Delayed reconstruction

The reconstructive surgery can also be performed weeks, months or years after mastectomy. In this case, the patient has more time to become informed and to make a well-considered decision. It also means that adjuvant treatments don't need to be delayed. This timing is preferred when postmastectomy radiation therapy is necessary. Moreover, the injurious effects of the irradiation or chemotherapy can be removed during the reconstruction. Because of these advantages, the delayed breast reconstruction (with an implant) is the most commonly elected option. [16, 38]

In case of delayed reconstruction, surgeons frequently use a tissue expander which is temporarily placed in the breast under the pectoralis muscle group during the first surgery (mastectomy). At regular times, the surgeon injects a saline solution in the expander in order to stretch the muscles and skin. This creates more space for the upcoming reconstruction. When enough room is created by the tissue expander, it is replaced by the permanent implant during a reconstructive surgery (see Figure 1.1). The use of a tissue expander depends on the status of the skin of the patient and the breast size. From 2005 to 2014, the percentage of reconstructive surgeries with tissue expanders has more than doubled (15.54% in 2005 to 33.3% in 2014). [36, 38, 41–43]

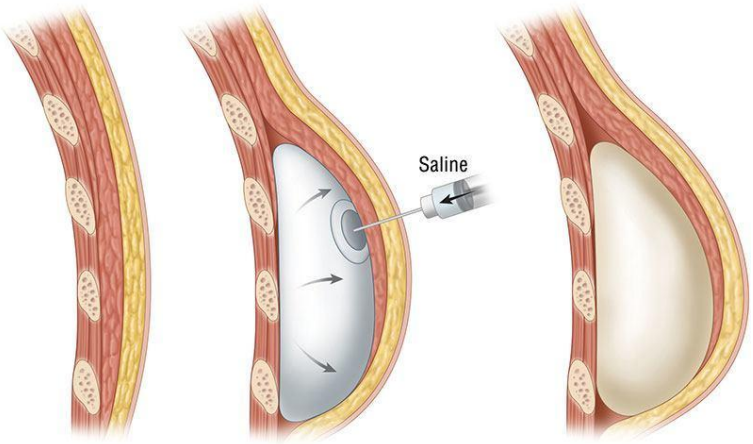

Figure 1.1: Schematic breast after mastectomy (left), with tissue expander (centre) and with permanent implant (right) [1]

Finally, the delayed reconstruction has some disadvantages too. After mastectomy, a second surgery is needed for the reconstruction, which also results in more surgeries and hospitalisation time. When reconstruction is delayed, surgeons rarely perform a skin-sparing mastectomy to prevent excess breast skin to ripple and fold on the chest wall of the patient. Therefore, less breast skin is available during a delayed reconstruction and the esthetic result will be inferior to that of immediate reconstructions. The breast skin that does remain after mastectomy will contract and become less flexible and elastic after months. Finally, the first mastectomy surgery will leave scars that can limit the recreation of the breast. [16, 44, 45]

An overview of the advantages and disadvantages of both reconstruction timings can be found in Table 1.1.

Table 1.1: Advantages and disadvantages of immediate and delayed breast reconstruction [16, 17]

	Immediate	**Delayed**
Advantages	No adjuvant surgery	Time to choose
	Shorter hospitalisation	Remove injurious effects
	Preservation inframammary fold and skin	No postponement of other therapies
	Psychological well-being	
Disadvantages	Less decision time	Second surgery needed
	Higher risk complications	Longer hospitalisation
		Less and inferior breast skin

1.3.2 Implant-based versus autologous tissue-based reconstruction

Another distinction can be made between autologous tissue-based reconstructions, using a patient's own tissue, and implant-based reconstructions, using a saline or silicone breast implant.

After the reconstruction, the patient can opt for an adjunct reconstructive procedure, namely autologous fat grafting (AFG). During this intervention, fat is harvested from a donor site (mostly

the abdomen or thighs) and converted to purified adipocytes and stem cells that are reinjected at the acceptor site (breast). In this way, the shape, size, contour and symmetry of the reconstructed breast(s) are optimized, and the patient can have a better aesthetic outcome. [46, 47]
The latest technique that is already used in the clinic is reversed expansion and lipofilling. Both autologous tissue and an implant are used for this kind of reconstruction. After removal of the mammary gland during mastectomy, an inflated tissue expander is placed in the breast to fill the cavity. After a few months, this expander can be partly deflated and the empty space is filled by lipofilling. This can be repeated multiple times until the tissue expander can be removed and the breast is filled with autologous tissue from lipofilling procedures. In this way, doctors can create a significant volume, with minimized scars and no chronic inflammatory responses. A bottleneck of this technique is that more than half of the injected cells die. Another downside is time. The patient needs several surgeries and the total treatment will last around three years. [38, 46, 47]

1.3.2.1 Autologous tissue-based reconstruction

Flaps, used for autologous tissue-based reconstructions, include skin, fat and blood vessels. The breast mound is reconstructed by relocating a tissue flap on to the chest. The most frequently used technique is the deep inferior epigastric artery perforator (DIEP) flap. This method uses skin and fat coming from the lower abdomen. Moreover, blood vessels are taken to assure vascularisation of the flap. [48]
Lipofilling is also used to reconstruct the breast with autologous tissue, namely fat. Lipofilling can be used as stand-alone technique or combined with a temporary or permanent implant.

Generally, this type of reconstructions gives a more natural, ptotic and softer breast. However, since the patient is her own donor, the surgery will take longer and additional adverse events like scar formation and infections can occur at the donor site. Moreover, the recovery will be longer after an autologous tissue-based surgery than after the insertion of an implant since surgery is performed on two places, the donor and the acceptor site. [17, 36]

The improved quality of life (QoL) is an important advantage of breast reconstruction. Several studies show that women with autologous breast reconstruction are more satisfied than patients with implant-based reconstructions. [36, 49, 50]

1.3.2.2 Implant-based reconstruction

In contrast to the autologous reconstruction, the implant-based one uses a synthetic object to rebuild the breast. In the 1960s the first silicone and saline implants were successfully embedded. Today, these are still used for implant-based reconstructions. Both implants have a silicone shell that is filled with different materials (resp. silicone versus saline). [38, 51]

Silicone is a synthetic material that mainly consists of silicon and oxygen atoms. The physical state of this material can vary from a liquid or a gel to an elastomer or a hard plastic. Polydimethylsiloxane (PDMS) is used for both the shell and the filling of silicone breast implants (Figure 1.2). [2, 52]
The elastomer variant of PDMS is used for the shell of the implant. The synthetic nature of PDMS results in an increased risk of infections and capsular contracture, encapsulating the

implant with connective tissue. This can lead to deformation of the reconstructed breast. To limit capsular contracture, most implants are coated, for example with a polyurethane coating, to minimise the adverse effects. [2, 51–53]

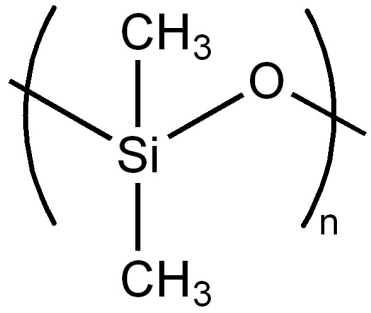

Figure 1.2: Chemical structure of polydimethylsiloxane [2]

As mentioned before, the silicone shell can be filled with either saline solution or silicone, both having their advantages and disadvantages. A silicone-filled implant will feel and appear more natural. However, when the implant is damaged, silicone can leach into and react with the body.
Saline-based implants offer a safer solution. If saline leaks in the body, it will not result in a toxic reaction. Additionally, the deflated silicone shell is first implanted in the patient and then filled with saline which results in a smaller incision. [2, 51, 53]

A technical advancement is the "form stable" silicone implant. The inner part of this kind of implants has a more cohesive consistency due to the increase in crosslinks. When the implant is punctured or sliced, no silicone will leak into the body and the implant preserves its shape. This makes the implant safer and decreases the toxic reactions within the body in case of leakage. [54, 55]

Overall, implant-based reconstructions have their shortcomings. The use of implants can lead to capsular contraction, dislocation of the implant, calcifications, wound dehiscence and rupture/leakage of the implant. Despite the shortcomings, this type of reconstruction remains the most commonly performed type, partly because of the ease and swiftness of the procedure and the cost-effectiveness compared to autologous reconstructions. [56]

Acellular dermal matrices (ADM) overcome some of the drawbacks of implant-based reconstructions. These soft connective tissue grafts can be used during prosthetic breast reconstructions to support the inferolateral side of the implant. Before the use of acellular dermal matrices, immediate implant-based reconstructions were not preferred since they often resulted in infectious complications and patient discomfort. Using ADM results in a more controlled positioning of the implant, facilitation of tissue regeneration and angiogenesis, prevention of capsular contracture and a better aesthetic outcome.
However, according to Smith et al. (2018), the universal acceptance of this technique is still limited despite its advantages. This is due to the concerns about the cost and potential complications to occur during surgery. [55, 57–60]

1.4 Anatomy of the breast

Before digging into the field of adipose tissue engineering, it is crucial to have a thorough understanding of the anatomy and physiology of the breast. Figure 1.3 shows the different structures of the breast, located between the second and sixth rib.

An important part of the parenchyma of the breast is the glandular epithelium. It consists of lobes and ducts and will produce and transport milk. Every lobe is made up of smaller lobules and these lobules end in tiny bulbs that produce the milk. Around 15 to 20 lobes can be found in each female breast. The ducts will lead the produced milk to the nipple by the myoepithelial cells that envelop the epithelial cells of the duct.

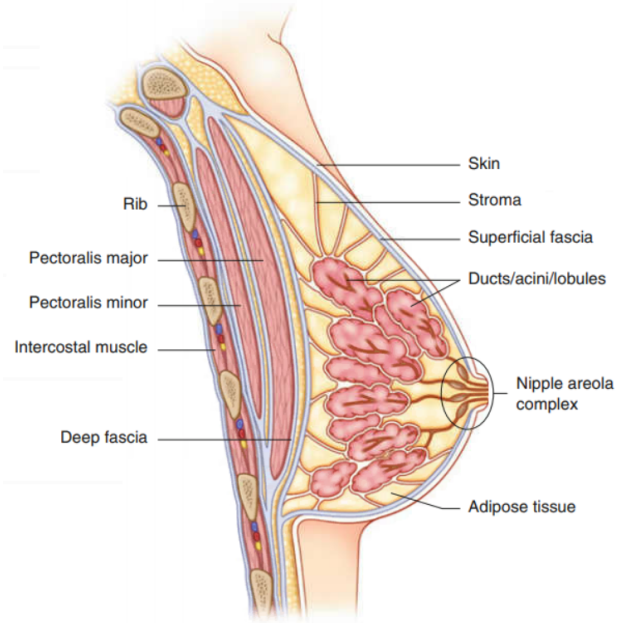

Figure 1.3: Schematic anatomy of the breast [3]

The interconnection of the skin, Cooper's ligaments and the superficial and deep fascia, together with the intersections with the pectoral muscles, result in the supporting system of the soft tissues. The stroma indicated in Figure 1.3 refers to Cooper's ligaments. These are fibrous bands made of connective tissue that end in the dermis.
The remainder of the breast is composed of adipose tissue or fat. This tissue fills up the space between the deep and the superficial fascia and is thereby the dominant tissue in female breasts. Adipose tissue will protect the lobes and ducts and is responsible for the soft texture.

Next to these specific components, the breast also consists of blood vessels, as the vascularisation of tissues is essential for their viability, and lymph nodes, as they play an important role in the immune system. The latter are located under the arm, close to the breast. Lymph nodes store white blood cells and defend the body against infections and diseases. [3, 56, 61–64]

1.5 Adipose tissue engineering

Tissue engineering (TE) is a booming, multidisciplinary field that combines physics, chemistry, biology, engineering and medicine. The goal of TE is to restore damaged body tissues by tissue regeneration. Tissue engineering uses three main components: a scaffold, cells and microenvironment for the cells to guarantee tissue formation (Figure 1.4). These three components will vary for different tissues, as human body parts have different properties. [12, 65]

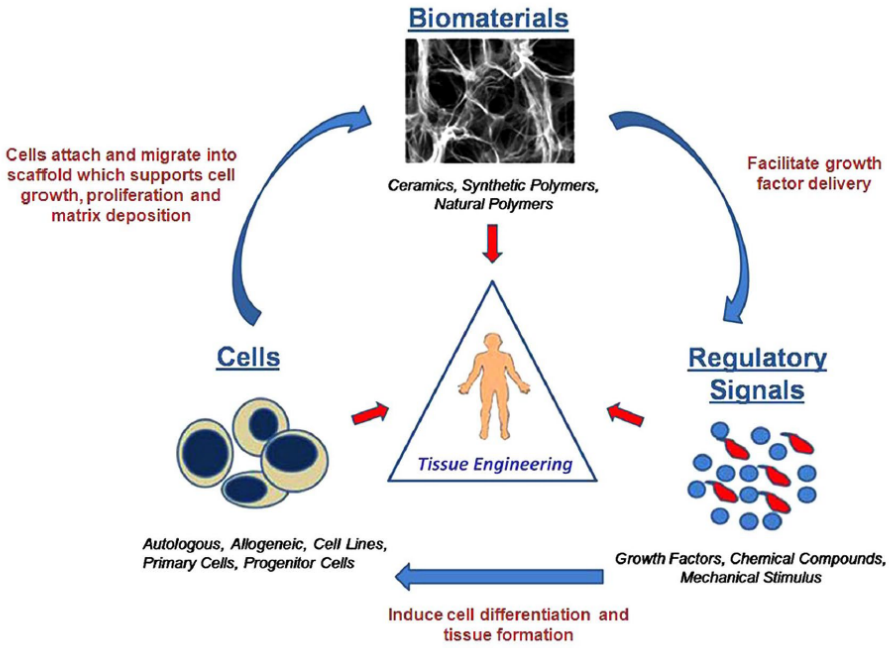

Figure 1.4: Cornerstones of tissue engineering [4]

The scaffold is an important element in tissue engineering. It should mimic the native extracellular matrix and its mechanical and structural properties should ideally be close to those of the native tissue it will replace. Furthermore, a good cellular affinity is required as the interaction between the scaffold and the cells is crucial for cell communication and regulation of cell migration, differentiation and survival. [61, 65, 66]
Scaffolds are often made from natural or synthetic polymers. Natural polymers are generated by biological systems and offer good biocompatibility as well as biological properties similar to the *in vivo* characteristics of the native tissue. On the other hand, synthetic polymers allow adjustment of degradability and mechanical and chemical properties. During this project, synthetic polymers are used as biomaterials for the development of the scaffold to ensure mechanical and structural support. Additionally, a gelatin-derivative is used as a support material to increase cell survival and improve cell retention upon injection. [67]

The porosity of the scaffold is important to ensure migration and growth of cells, to provide room for vascularisation, nutrient transportation and clearance of waste products. 3D printing can produce such a porous scaffold with precisely controlled structures. Deposition-based 3D printing and digital light processing are commonly used 3D printing technologies for tissue engineering. [68]

As explained earlier, the mechanical properties of the scaffold should be similar to those of the native tissue. These properties need to promote adipose tissue growth and protect the regenerating tissue while maintaining flexibility to ensure the patient's comfort. [68]

Most tissue-engineered scaffolds are biodegradable to allow cells to generate their own extracellular matrix. The scaffold must provide structural support until the newly formed tissue can support itself. Therefore, the degradation rate must match the rate of regeneration. Ideally, in the end, no foreign material should be left in the body of the patient, as this avoids long-term foreign body reactions. [68, 69]

The creation of a scaffold for breast reconstruction purposes is the scope of this master dissertation. However, cells are needed for the actual regeneration of the tissue. Stem cells are mostly used in the tissue engineering field because of their proliferation capacity and ability to differentiate into multiple cell types. These cells need a specific environment to proliferate and differentiate into the desired phenotype, being adipocytes in case of breast reconstruction.

1.5.1 Cells and cell environment

In tissue engineering, cells are seeded on or encapsulated in the scaffold to regenerate tissues. Stem cells are frequently used for this purpose, thanks to their high proliferation capacity and possibility to differentiate into different phenotypes. In this way, the phenotype can be defined and controlled by researchers. [70, 71]

1.5.1.1 Sources of stem cells

There are four main sources of stem cells: embryonic tissue, fetal tissue (like fetus, placenta and umbilical cord), adult tissue (like fat, bone marrow, skin and muscle from adult organisms) and genetically reprogrammed stem cells. Stem cells can have different potencies. This is the capacity of cells to differentiate into different cell types. Only embryonic cells from morula are totipotent cells which means that they can differentiate into any cell type. After embryonic development, these cells (fetal cells) become pluripotent since they cannot differentiate into extra-embryonic tissues anymore. Despite the ability of embryonic and fetal cells to differentiate in (almost) every kind of cell, their use in tissue engineering is limited because of ethical and regulatory issues.
Induced pluripotent stem cells (iPSCs) are another class of stem cells that have the ability to differentiate into different cell types. These cells arise from genetically reprogrammed adult somatic cells, mostly fibroblasts or epithelial cells, and are not prone to ethical and legal issues. However, mutational and other adverse effects are the main bottlenecks associated with induced pluripotent stem cells. [56, 70]

Interestingly, adult stem cell sources can overcome the drawbacks of both embryonic/fetal tissues and iPSCs. They are multipotent stem cells, meaning that they can only differentiate into a limited number of cell types. The type of cell in which adult stem cells will differentiate depends on different factors. The composition, architecture, mechanical and physicochemical properties of the scaffold, on which cells will be seeded, will play an important role during differentiation. Additionally, the composition of the culture media and mechanical stimulation can guide adult

stem cells to differentiate into a certain phenotype. The mechanical properties of the environment should mimic the native niche of the desired cell type. Adipogenic cells for example will differentiate better in softer matrices. The composition of the culture media should contain specific growth factors and other biomolecules to guide the differentiation into a specific cell type. [70]

1.5.1.2 Regeneration of adipose tissue

Adipose tissue is the dominant type of tissue present in a female breast. The most common cells in these tissues are non-proliferative, mature adipocytes. These cells do not only mechanically protect inner structures, they are also an energy storage depot and have an endocrine function since they produce specific hormones to maintain energy homeostasis. Adipose tissues need to be highly vascularised as they are metabolically active tissues. The vascular system is important for the supply of nutrients and oxygen, transport of growth factors, hormones, cytokines and waste materials. [56, 72]

As described in the previous section, adult stem cells are the preferred type of cells for (adipose) tissue engineering. Adult bone marrow-derived and adipose-derived stem cells are the two most frequently used mesenchymal stem cells for adipose tissue engineering. They are both multipotent, meaning that they can differentiate in different kinds of cell types. Although bone marrow-derived stem cells are often described in literature for adipose tissue regeneration, the painful procedure of obtaining them limits their clinical application. Therefore, human adipose-derived stem cells (ADSCs) are the preferred source of cells for adipose tissue engineering. Choosing these cells over bone marrow derived-stem cells results in less donor site morbidity and a safer and less invasive way of obtaining them. ADSCs are largely available and easily accessible through liposuction and biopsies. After centrifuging adipose tissue, stem cells can be found in the stromal vascular fraction (SVF). The isolated stem cells are sometimes treated with neoadjuvant chemotherapy to improve oncological safety. Adipose tissue also has a higher stem cell density than bone marrow. Cytokines and growth factors, secreted by adipose-derived stem cells, stimulate the regeneration of cells and vascularisation. [56, 67, 69–72]

The environment of adipose-derived stem cells should mimic the native environment of adipocytes to realise differentiation into fat cells. The native microenvironment is characterised by a certain pH, oxygen level and extracellular composition. In addition, adipogenic stimulants, growth factors, adipokines, inflammatory and thrombosis associated cytokines can also be found in the native niche. One can conclude that the environment of adipocytes is very complex. [67, 69]

Because of the need for oxygen and high metabolic activity of adipocytes, the formation of a vascularised network is important to prevent necrosis and volume loss of adipose tissue. The promotion of vascularisation is a general challenge in tissue engineering. Moreover, upscaling of *in vitro* and small animal models to large animal models and females can cause avascularised zones and eventually cell necrosis as it will be more difficult to get oxygen in the centre of large structures. Therefore, in tissue engineering of adipose tissue specifically, special attention should be given to angiogenesis. Luckily, ADSCs secrete several growth factors like vascular endothelial growth factor (VEGF), basic fibroblast growth factor (bFGF) and insulin-like growth factor (IGF) to stimulate angiogenesis and regeneration. Recently, co-cultures in adipose tissue engineering have been introduced by culture of endothelial cells with adipose stem cells. Adding endothelial

progenitor cells to the medium can also facilitate vascularisation. [56, 67–69]

1.5.2 Biomaterials

The biomaterials used for the scaffold are, next to the cells and their environment, also important and will be the scope of this master thesis. Some important characteristics of a scaffold used for adipose tissue engineering were already summed up above. Below, more details about the desired mechanical and biodegradable properties will be given as these are important in TE.
Eventually, these biomaterials need to be processed in a desired structure. 3D printing is a commonly used manufacturing technique for biomedical applications. Digital light processing (DLP) will be used as 3D printing technique in this project and will be explained in Section 1.5.2.2.

1.5.2.1 Scaffold requirements for adipose tissue engineering

In adipose tissue engineering, the properties of the scaffold should promote the regeneration of adipose tissue. The mechanical properties and biodegradability of the scaffold can influence this regeneration. The creation of a scaffold will be the purpose of this master dissertation.

Ideally, the scaffold should mimic native adipose tissue, also in terms of mechanical properties. Several studies have shown that the Young's modulus of healthy adipose tissue lies between one and four kPa. [73, 74] Therefore, many researchers choose this range as target for the Young's modulus of their scaffold. This modulus has shown to promote the proliferation and differentiation of adipose-derived stem cells into adipocytes. If the scaffold is too rigid, scar tissue is formed in the surrounding tissues, which feels uncomfortable for the patient. On the contrary, if the scaffold is too soft, there is a risk that the structure will collapse. Additionally, the scaffold must be rigid enough to protect the cells from adverse impacts. These properties must remain until the tissue can support itself.
The scaffold created during this master thesis will not mimic the extracellular matrix but will support and protect the gelatin-derivative, containing the cells, and will therefore have a higher Young's modulus. The extracellular matrix will be mimicked by the gelatin-derivative. [68, 69, 73, 75]

Biodegradable scaffolds are often used in tissue engineering to avoid long-term foreign body reactions like capsular contracture in case of implant-based breast reconstruction. In this case, fibrous tissue is formed around the implant which can cause deformity and pain. By degrading the scaffold, no foreign material will ultimately stay in the patient's body. The degradation time of the scaffold should be synchronized with the tissue regeneration time to make room for and to support the regeneration of tissue until the tissue can support itself (between six and twelve months for adipose tissue). Next to the degradation rate, the degradation products should also be considered. These breakdown products should not be toxic and result in controlled inflammatory reactions. [68, 76]
Polymers are mostly degraded by chain scissions resulting in oligomers and monomers. The two main mechanisms of degradation are hydrolysis and enzymatic hydrolysis, as in the body, the scaffold will be in contact with water and enzymes. The first can trigger the formation of chain scission and the latter acts as a catalyst during these scissions.
The degradation via hydrolysis can occur by two mechanisms, bulk and surface degradation. During surface degradation, mainly the outer part of the scaffold is degraded, while during bulk degradation, the scaffold volume remains constant for a longer time period. Polyesters like PLA

undergo bulk degradation. Water hydrolyses the ester groups, resulting in degradation of the scaffold. The degradation time depends on the stereochemistry of PLA. PLLA has a degradation time exceeding 24 months, while PDLLA already degrades between three and six months, both depending on the dimension of the scaffold. As the regeneration of adipose tissue takes between six and twelve months, the degradation time of PDLLA is too short to support the regenerating tissue. Therefore, copolymers of PDLLA are often used in adipose tissue engineering. [77, 78]

Different factors can influence the rate of degradation, but the most important one is the composition of the material. The more sensitive the polymer bonds are for water, the faster the material will degrade. Additionally, the molar mass, end group functionalities, type of monomers and monomer ratio influence the rate. For example, while PDLLA is an amorphous polymer, PLLA is semi-crystalline and will therefore degrade slower. Next to the composition, the environment of the polymer, like pH and enzymes, can influence the degradation rate. Additionally, the ratio of surface area to volume and physical loadings will also affect the decomposition rate of the scaffold. Finally, surface treatments like plasma treatments can change the degradation rate by changing the hydrophilicity of the polymer. [76, 77]

1.5.2.2 3D printing

In tissue engineering, cells are combined with biomaterials which are first manufactured in the desired structure. An often used manufacturing technique for biomedical applications is 3D printing. 3D printing is a process in which a three-dimensional structure is built layer-by-layer using 3D software (CAD) to give instructions to the 3D printer. This relatively new technique of manufacturing has great benefits and is therefore widely used in different fields. The 3D printing technique was introduced in industry a few decades ago. However, only in the last decade, additive manufacturing has been used in biomedical applications. [5, 79–81]

Many new possibilities were created with the arrival of 3D printing. It has, for example, a big impact on personalized medicine. Based on scans of the patient (MRI or CT), 3D-printed personalized implants can be made. Moreover, the fabrication of complex structures with good precision is possible due to rapid prototyping. Control of the architecture is essential for cell seeding and attachment to serve applications in the tissue engineering field. For these reasons, 3D printing is gaining a lot of popularity in biomedical applications and will play an important role in the future of tissue engineering. [5, 80, 81]

Different 3D printing techniques can be used for biomedical applications, for example 3D printing based on material extrusion (e.g. Fused Deposition Modelling, FDM), photopolymerisation (e.g. Digital Light Processing, DLP or stereolithography, SLA or Two Photon Polymerisation, 2PP), powder bed fusion (e.g. Selective Laser Sintering, SLS) and material jetting. Of all these techniques, deposition-based 3D printing is often used in the biomedical field. [5]
Fused deposition modelling (FDM) is an example of such a commonly used deposition-based technique. By heating and extruding thermoplastic polymers through a nozzle onto a platform, a 3D printed structure can be formed layer-by-layer. This method guarantees good efficiency and low costs for both the operation and implementation. [5, 80]
However, the use of laser-based 3D printing, such as DLP, is increasing and is therefore used in this master thesis as 3D printing technique. [81]

Digital Light Processing

Digital light processing (DLP) uses vat photopolymerisation to create a 3D structure, by selectively solidifying a liquid photosensitive polymer with UV-light in the presence of a photoinitiator and photoblocker. The technique is similar to stereolithography (SLA), however, the difference is that DLP can solidify a whole layer at once while SLA does this point-by-point. In this way, DLP is a faster printing technique than SLA. [81–83]

DLP-devices use a photopolymer resin, a lifting platform and an imaging system for the manufacturing of 3D structures (see Figure 1.5). Light is projected onto the resin via a dynamic mask, often called digital micromirror device (DMD). This device contains controllable micron-sized mirrors that can control the path of the light towards the resin or away from it. If the light is projected on the sample by a specific mirror, the polymer will solidify in a specific plane. For every layer, the DMD will decide for every pixel if it is solidified or not by controlling the pathway of the light. After one layer, the lifting platform will move along the Z-axis and a new, fresh layer of resin can be exposed to UV-light. [5, 83–86]

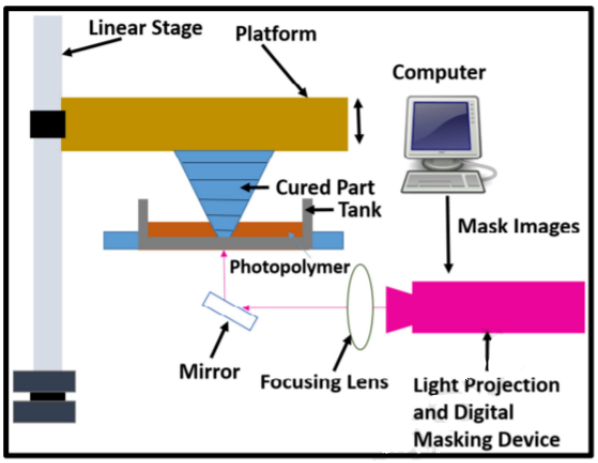

Figure 1.5: Working principle of digital light processing [5]

Compared to FDM, digital light processing has a good resolution. According to literature, the resolution for DLP ranges between 6 and 30 μm, while FDM has a resolution around 100 μm. [83, 87, 88] Furthermore, DLP is a relatively fast printing technique and the complexity of the scaffold that needs to be printed will not change the printing speed. The printing speed of FDM (50-150 mm/hr) is higher than the speed of printing with SLA (around 25 mm/hr), DLP printing will be faster than SLA since it can illuminate a whole layer at once. [89–91] *LumenX* from company *CELLINK* was used as DLP printer during this master dissertation. [5, 81, 92]

The viscosity of the resin needs to be controlled during digital light processing. The photosensitive resins should have a viscosity below three Pa.s to guarantee the proper operation of the DLP-device. One of the biggest disadvantages for biomedical applications is the need for a photoinitiator. Photoinitiators, needed for the initiation of the polymerisation, can be toxic and therefore need to be chemically incorporated in the construct or removed afterwards. [81, 83, 85, 93, 94]

During DLP printing, not only the layer that needs to polymerised is exposed to UV-light, previously printed layers are also exposed by excess light. This causes overcuring and a decrease in resolution, more specifically in the z-direction. To avoid this, photoblocker can be added to the resin, to absorb the excess UV-light and restrict the penetration depth, leading to minimal overcuring and improved resolution. [95] Yang et al. (2020) investigated different photoblockers and their absorption spectra (see Figure 1.6). [6]

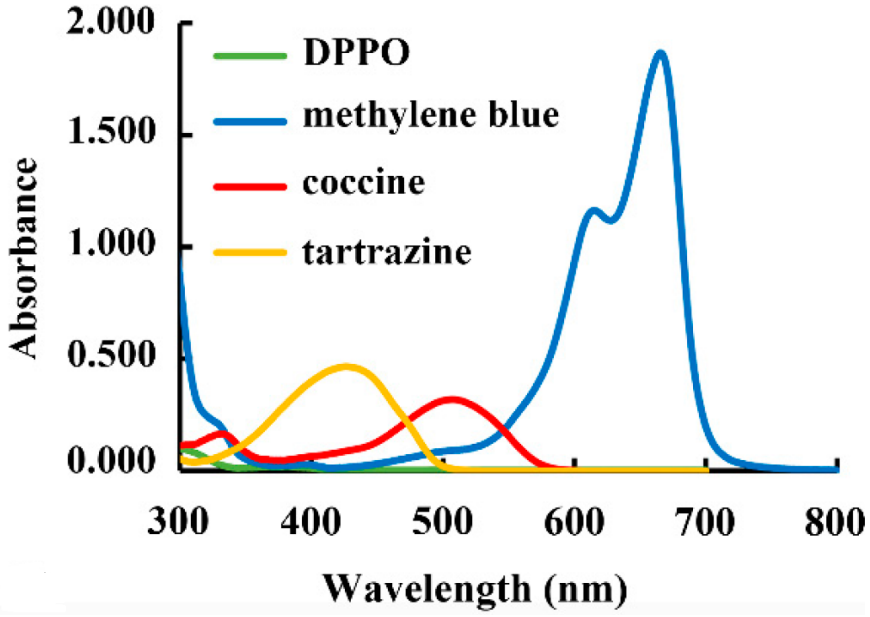

Figure 1.6: Absorption spectra of different photoblockers [6]

Currently, many researchers have published on the successful use of DLP printing for biomedical applications, showing the potential of DLP in tissue engineering. As an example, the study by Saed et al. (2020) showed that hard tissue scaffolds of poly(L-lactic acid) can be successfully formed with digital light processing. [81]

To conclude, 3D printing is gaining popularity as an advanced processing tool in biomedical applications with many advantages like the ability to create more complex, personalised structures.
Extrusion-based printing is the most commonly used 3D printing technique for biomedical structures. In the future, the use of digital light processing is expected to increase due to the good resolution and speed compared to other 3D printing techniques. [5, 80, 81]

1.6 Materials used

The purpose of this master thesis is to develop a biodegradable scaffold with shape memory properties for breast reconstruction purposes. Shape memory polymers can change from a temporary state into a permanent state after being triggered by for example an increase in temperature. By compressing the scaffold into a temporary reduced size, the scaffold can be implanted in the body through a smaller incision. When implanted, the body temperature will act as a trigger to transform the scaffold to the more expanded, permanent shape.

Thermoplastic polyurethanes (TPUs) are often used for biomedical applications as they have interesting properties, like flexibility and toughness, by combining hard and soft segments. The polyester (polylactic acid) is used as soft segment since these materials are biodegradable, biocompatible and easy to synthesise by polycondensation or ring opening polymerisation. Polyhedral oligomeric silsesquioxanes (POSS) can incorporate inorganic, rigid nano-sized silicon cages into the polymer and are therefore used as hard segments. They ameliorate the thermal stability and rigidity of the thermoplastic polyurethane.
Finally, these thermoplastic polyurethanes can be functionalised into acrylate-endcapped urethane-based polymers. These acrylate end groups will allow the formation of a crosslinked 3D network after adding photoinitiator and upon exposure to UV-light.

1.6.1 Shape memory polymers

1.6.1.1 Shape memory effect

Shape memory polymers (SMP) are polymers that can return to a certain shape after being triggered. The most frequently used triggers are temperature and light. Nowadays, ultrasound, electricity, moisture, magnetism and exposure to solvents are also possible ways to bring the polymer from the temporary to the permanent shape. Recently, shape memory polymers, especially thermoresponsive polymers, are finding their way into biomedical applications. Shape memory is not an intrinsic property of a polymer as certain processing steps are required to gain this characteristic. In this master thesis, only thermoresponsive shape memory polymers will be discussed. [96, 97]

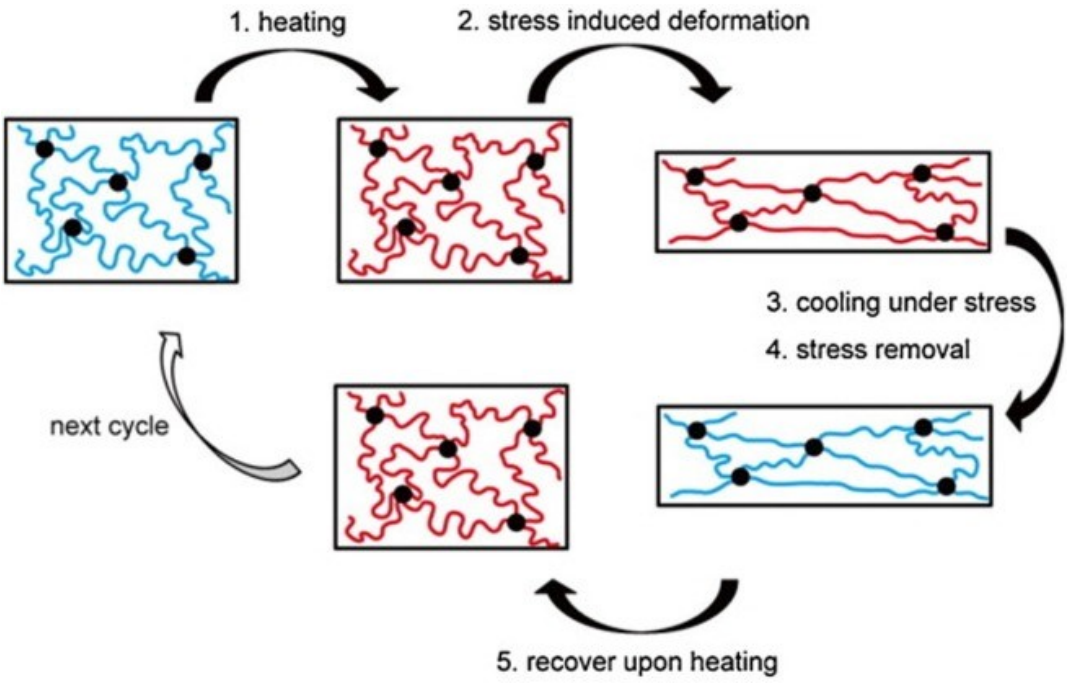

Figure 1.7: Shape memory effect of polymers [7]

SMPs contain so-called soft and hard regions. The latter will fix the permanent shape of the

polymer in order to recover this shape after deformation, while the soft regions will ensure the switch between the temporary and permanent state.
The process begins with fixation of the permanent shape, which is the final shape the polymer needs to return to. The fixation of the hard regions can be done in two ways. Either the polymer is chemically crosslinked and forms a thermoharder or it can be physically crosslinked and forms a thermoplast. Below, these two approaches are described in detail.
By heating the material, the polymer chains become more mobile and the material can be deformed to the temporary state. Due to the new orientation of the polymer chains during deformation, this new state will have a higher energy than the undeformed polymer, as the entropy of the system is decreased. To fix this high energy state, the temperature is lowered under the transition temperature while the polymer is kept in its deformed state. After cooling, the stress to deform the material can be withdrawn. For amorphous polymers, this transition temperature is equal to the glass transition temperature T_g, while for semi-crystalline materials the crystallisation temperature T_{cryst} is used. In this way, the temporary shape is fixed and will not change unless the material is triggered. [7, 96–98]
Once the SMP is programmed in its reversible shape, the polymer can be triggered, for example by heating the material above the transition temperature. The thermal energy given to the material results in a higher mobility of the polymer chains. By increasing the mobility, the stored energy is released and the material will return to the more favourable, permanent shape. The mechanism is depicted in Figure 1.7. [7, 99, 100]

1.6.1.2 Chemically versus physically crosslinked shape memory polymers

Permanent junctions in SMPs can be used to create a three-dimensional structure that will block the polymer in its permanent shape. The junctions give the polymer a memory and will prevent the slippage and creep of the chains during deformation. As mentioned earlier, the formation of this three-dimensional network can be done in two ways by chemical or physical crosslinks. [96, 97]

Chemical reactions that form a covalent network can create a chemically crosslinked permanent shape. These covalent bonds are irreversible so once the materials are crosslinked, the permanent shape is fixed and can't be reshaped afterwards. Chemical crosslinks have some advantages over physical crosslinks. Chemically crosslinked materials are more resistant and have superior shape fixation and recovery over physically crosslinked polymers. This recovery is faster when the crosslink density increases. [8, 96, 101]

The most frequently used chemically crosslinked SMPs use acrylates to form the covalent bonds. They can be crosslinked by a radical mechanism. The study of Yakacki et al. (2007) shows the potential of an acrylated, chemically crosslinked shape memory polymer for cardiovascular stent interventions. Due to the shape memory, the catheter size can be reduced during delivery and the deployment at body temperature is highly controlled. [96, 101]

The permanent state of shape memory polymers can also be fixed by physical crosslinks. Because of a difference in transition temperature between two regions of the polymer, a shape memory effect is obtained. The region with the highest transition temperature will fix the permanent shape using physical crosslinks. The switching between both states will be guaranteed by the other region with the lower transition temperature.
These thermoplastics are reversible and can still be adapted after the formation of a

three-dimensional structure. Some bottlenecks are the inferior stability and mechanical properties compared to chemically crosslinked materials and the trade-off between the shape recovery rate and recovery stress. [8, 96]

For example, Tseng et al. (2013) created a physically crosslinked thermoplastic polyurethane that consists of PDLLA and POSS. As the crystallisation temperature of POSS segments is higher than the glass transition temperature of PDLLA, a shape memory polymer is acquired. The crystallisation of POSS will fix the permanent shape, whereas PDLLA will ensure the transition between the two states. Cells were seeded on this scaffold during the temporary state of the shape memory polymer. After triggering, the shape of the scaffold was recovered. The study showed that the cells remained attached and viable and concluded that this cytocompatible scaffold had great potential to be used for tissue engineering. [99]

1.6.1.3 Biomedical applications of shape memory polymers

Thermoresponsive shape memory polymers are increasingly used in biomedical applications in which they are designed to use the body temperature as trigger. Since large three-dimensional structures can have a reduced temporary shape, materials can be inserted in the patient through a small incision in a less invasive way. In addition, the automatic recovery to the permanent shape, which can be patient-specific, prevents an extra intervention of the surgeon. [96, 98, 100]

SMP sutures are a novel approach for closing incisions (see Figure 1.8). Due to body temperature, the suture will try to recover to the permanent shape. This self-tightening suture can close wounds with the appropriate amount of tension. This is important because if the force is too high, necrotic tissue can be formed and if the force is too low, the scars will be worse. Biodegradable shape memory polyurethanes are often used as self-tightening sutures. Thanks to their biodegradability properties, the sutures do not need to be removed later on. [8, 98, 102, 103]

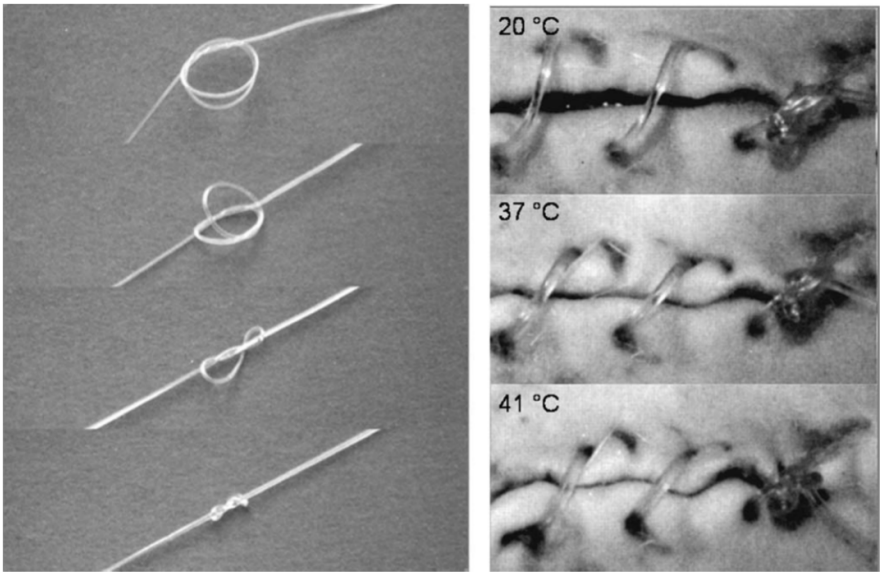

Figure 1.8: Shape memory effect of self-tightening sutures [8]

Shape memory can also be combined with additive manufacturing. In this way, a four-dimensional material can be created. There is no limitation in the timing of this trigger and different 3D printing techniques can be used to manufacture a 3D scaffold with shape memory properties. The study of Hongzhi Wu et al. (2019) shows that it is possible to print such a smart polymer by using digital light processing. However, finding a shape memory photosensitive resin that is suited for DLP is still challenging, according to this study. [102, 104]

Shape memory materials for biomedical applications are not limited to polymers. As an example, shape memory metals are already used in medicine, like stents made from nitinol. However, shape memory polymers have different benefits compared to other shape memory materials, such as a lower processing cost, tunable properties, lower densities and superior biocompatibility and biodegradability. [8, 98, 102]

1.6.1.4 Influence of shape memory effect on cells

The viability of cells is essential for tissue regeneration. Therefore, the effect of shape memory recovery on cells was studied by Neuss et al. (2009). They investigated the effect of a shape memory PCL-dimethacrylate network on the viability of cells. The results showed that the cells were subjected to shear forces. The activation of the shape memory effect resulted in the disconnection of cell monolayers, the reduction of the number of cells and apoptosis of some cells. However, no necrotic cells were found after recovery of the shape. The authors concluded that there was no inflammation after activation due to the absence of necrotic cells.
As shear forces are not uniformly distributed over a scaffold, unaffected confluent cell monolayers were found at certain places on the scaffold, while in other regions cells underwent apoptosis. These shear forces, thus also the number of apoptotic cells, can be reduced by applying an extension below 100%. Additionally, the authors believed that the geometry of the scaffold influences the cells, although this was not proven during the study. [100, 105]

To conclude, cells can be affected by shape memory activation. This effect depends on different parameters like pore interconnectivity, recovery rate, extension of the material, geometry and so on. Therefore, it is hard to predict the influence of shape memory on seeded cells. [106]

1.6.2 Starting materials to create photocrosslinkable SMPs

1.6.2.1 Polylactic acid

Polylactic acid is the most frequently produced biodegradable aliphatic polyester due to its low price, excellent biocompatibility and biodegradability. Lactic acid can be made from 100% renewable resources by hydrolysis and fermentation of carbohydrates gathered from sources like sugar canes and corn starches, which makes lactic acid commercially interesting. Different medical applications that have been approved by FDA, including the use of PLA for sutures, as bone fixation material, in drug delivery and so on. Moreover, PLA is even used in packaging industries as environmentally friendly substitute for non-degradable plastics because of its good mechanical properties. [107–111]
However, it is not ideal for many advanced medical products as it has a low thermal stability, low toughness, poor impact strength and poor dielectric properties. [111–113]

Two stereoisomers of lactic acid exist, since it has a chiral centre, i.e. D-lactic acid and L-lactic acid (Figure 1.9). Homopolymers can be formed from one of both stereoisomers. These are called poly(D-lactic acid) (PDLA) and poly(L-lactic acid) (PLLA) and are both semi-crystalline. Additionally, a racemic polymer can be formed with the two enantiomers resulting in amorphous poly(D,L-lactic acid) (PDLLA). The latter will be used in the current master thesis as the moderate glass transition temperature of PDLLA (Tg = 50-60°C) makes the polyester suitable for applications in the human body. As such, scaffolds in tissue engineering often use polylactic acid. Different properties of PDLLA can be found in Table 1.2. [112, 114]

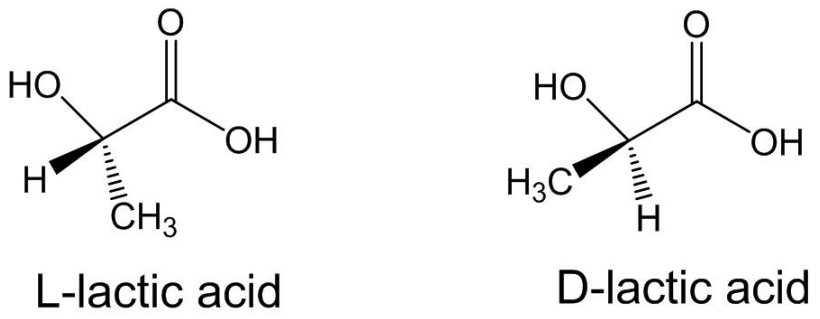

Figure 1.9: Stereoisomers of lactic acid [9]

Table 1.2: Properties of PDLLA [18–22]

	PDLLA
Density	1.25-1.27 g/cm^3
Glass transition temperature	50-60°C
Degradation temperature	270-370°C
Degradation time	3-6 months
Young's modulus	1-3.9 GPa
Tensile strength	27-50 MPa
Elongation at break	2-10%
Dielectric constant	2.7-3.6

Direct polycondensation and ring opening polymerisation (ROP) are the two mainly used techniques to synthesise PDLLA (see Figure 1.10). Direct polycondensation starts from lactic acid. It is not the preferred option for this master thesis, as the resulting polymer has low and uncontrolled molar mass and poor mechanical properties. Water, produced during polycondensation, needs to be removed by an energetically costly distillation. Moreover, longer reaction times are necessary compared to ring opening polymerisation. [109, 114]

Ring opening polymerisation (ROP) of lactides is the most frequently used approach to produce PDLLA. Lactide is a cyclic dimer that is synthesised by the depolymerisation of low molar mass PLA, which is formed during polycondensation of lactic acid. ROP is a chain-growth polymerisation which consists of initiating, propagating and terminating steps. An initiating alcohol (often diol) is necessary to begin the polymerisation reaction. An organometallic catalyst is often used to facilitate the reaction. This type of ring opening polymerisation is called metal-mediated ROP and is the favourite way to synthesise PDLLA.

After coordination of lactide, the ester bond is activated. Subsequently, a hydroxyl group of the initiator can perform a nucleophilic attack on these ester bonds resulting in the anionic opening of the ring. After the initiating step, propagation can begin. Monomers are added to the reactive polymer, in a serial way, to eventually result in PDLLA with a controlled molar mass with low dispersity. The polyaddition can be performed in bulk or in solution. [107, 109, 112, 115]

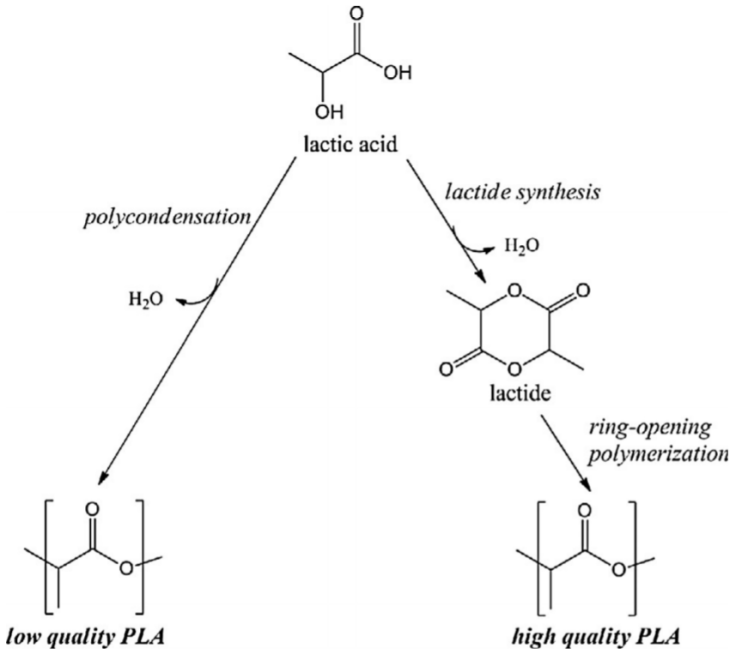

Figure 1.10: Two ways to produce PLA [10]

The most frequently used catalyst for ring opening polymerisation of lactides is tin 2-ethylhexanoate ($SnOct_2$). This catalyst is already approved by FDA as additive for PDLLA in food packaging. Due to this catalyst, a coordination insertion mechanism occurs during the ring opening polymerisation. This mechanism results in fewer transesterification reactions than in case of anionic or cationic catalysts, which leads to lower dispersity. The difficult removal of the catalyst afterwards is a bottleneck for organotin-based catalysts. Therefore, they often remain in the polymer which can cause toxicity and adverse body reactions when used for biomedical applications. [12, 110, 115]

Degradable scaffolds used in tissue engineering applications can only be successful if the scaffold degrades in non-toxic components. PDLLA breaks down via hydrolysis in biocompatible, non-toxic components. Ester linkages are cleaved and this results in the formation of oligomers and eventually lactic acid that can be metabolised naturally by the body. [76, 107, 110, 116]

1.6.2.2 Polyhedral oligomeric silsesquioxane

Polyhedral oligomeric silsesquioxane (POSS) belongs to the family of silsesquioxanes that can be subdivided into two categories, namely non-caged and caged structures. POSS belongs to the latter classification. This silsesquioxane is a small silica particle (1-3 nm) and a highly symmetric molecule. The molecule consists of $(RSiO_{1.5})_n$ with n equal to 4, 6, 8, 10 or 12. The

octafunctional cubic cage (T_8) is the most studied variant and is used in this master dissertation. [111, 113, 117, 118]

As introduced earlier, the cubic cage of polyhedral oligomeric silsesquioxanes consists of silicon and oxygen atoms. Silicon is located at the vertices and oxygen on the edges of the cube. These two molecules form the inorganic rigid nano-sized cage. At the silicon vertices, eight organic functional side groups form a voluminous organic shell. These organic groups will increase compatibility with other organic materials. A lot of different vertex groups exist, which leads to a wide range of hybrid materials that can be formed out of POSS. The nano-sized material and combination of the advantages of the inorganic (thermal stability, rigidity) and organic material (flexibility, biodegradability, processability) lead to remarkable properties. [107, 111, 113, 119, 120]

The synthesis of polyhedral oligomeric silsesquioxanes consists of the controlled hydrolysis and condensation of trifunctional organosilicon monomers (e.g. $RSiX_3$) in a solvent. POSS dissolves in many solvents like THF, toluene, hexane and chloroform and has a melting temperature around 120°C. For the purpose of this project, POSS will be chemically introduced in a polymer by copolymerisation with PDLLA. Grafting and reactive blending are two other possibilities to chemically introduce POSS in the material. Minimally one organic molecule on the vertices should contain at least two reactive hydroxyl groups to successfully integrate POSS. To create linear polymers, no more than two hydroxyl groups should be available. Otherwise an uncontrolled, crosslinked network will be formed. One way to embed the silsesquioxane in the polymer is to use diisocyanate, which reacts with the hydroxyl groups of POSS. The type of POSS used for this project is called 1.2-propanediolisobutyl POSS and is depicted in Figure 1.11. [117, 119–122]

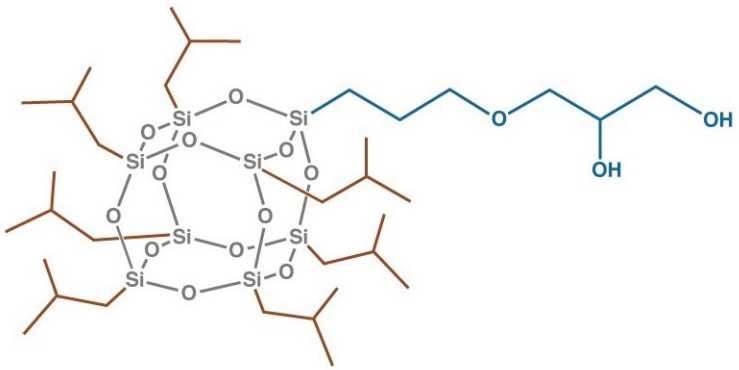

Figure 1.11: 1,2-Propanediolisobutyl POSS [11]

POSS can be used as tissue engineering scaffolds, biological sensors, drug delivery systems and so on. John et al. (2017) studied the possibility of using POSS as drug delivery systems. The 3D structure, nanoscale size, low toxicity and the possibility to be taken up by cells make POSS an excellent candidate for this purpose. It can be strictly designed in contrast to micelles and dendrimeric drug delivery systems. Especially the cubic POSS molecule can form supra-molecular networks, so small molecules like drugs can be entrapped in the crystal lattice. The small molecules are released under physiological conditions, by hydrolysis of the POSS carrier into non-toxic products. [111, 123]

1.6.2.3 Thermoplastic polyurethane

Thermoplastic polyurethanes (TPU) are polymers that are frequently used as implants, drug delivery systems, coatings, adhesives and in many other applications. Porous networks of TPU can be used to mimic biological tissues (such as cartilage, muscle and nerves) and support cell adhesion, proliferation and differentiation after modifications. They consist of hard and soft segments. Due to the thermoplastic behaviour and the absence of chemical crosslinks, the material can be (re)processed after heating. [12, 124]

TPUs are mostly synthesised in two steps. First, the soft segment is polymerised into a diol. This soft segment controls the degradation of the thermoplastic polyurethane. Next, the polymer is transformed into a TPU by adding diisocyanates and chain extenders to introduce the semi-crystalline hard block. The chain extender will increase the modulus, ductility and thermal stability of the polymer. The diisocyanates are used for their high reactivity with alcohols and will bind the soft and hard segments by urethane bonds. Nowadays, non-aromatic diisocyanates such as hexamethylene diisocyanate (HDI) and lysine diisocyanate (LDI) are preferred because they are more compatible with biological compounds. [124–127]

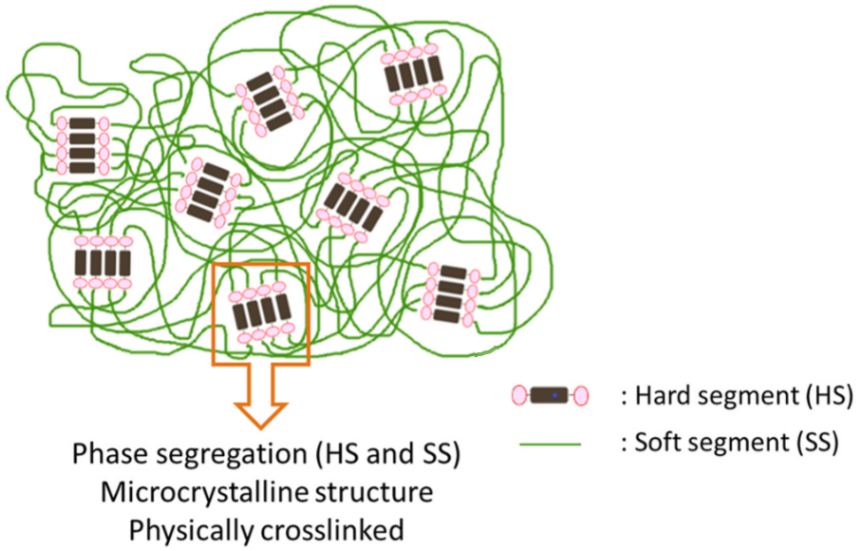

Figure 1.12: Hard and soft segments of thermoplastic polyurethane [12]

Because of the hard and soft segments, linear polyurethanes are multi-segmented polymers that have a microphase separated morphology. Areas of more structured, physically crosslinked, hard domains are dispersed into a continuous soft phase, as can be seen in Figure 1.12. This phase separation results in interesting properties such as flexibility and toughness. [117, 119, 122, 128]

In this project, PDLLA is used as soft segment and the hard segment consists of hexamethylene diisocyanate (HDI) and 1,2-propanediolisobutyl POSS. Urethane bonds between HDI and both PDLLA and POSS are needed to incorporate these two components together in one chain. The chemical structure is depicted in Figure 1.13.

The main advantage of this thermoplastic polyurethane is that it combines the advantages of both

PDLLA (amorphous, organic component) and POSS (semi-crystalline, inorganic component). In this way, the TPU is biocompatible, biodegradable and flexible due to the PDLLA chains and the thermal stability and rigidity of the TPU will increase by the addition of POSS monomers.

The thermoplastic polyurethane is synthesised at Syracuse University. They tried to achieve a TPU with PDLLA chains of 12 kg/mol and a POSS/PDLLA molar ratio of 3, which is correlated with z equal to 84 and y/x equal to three in Figure 1.13.

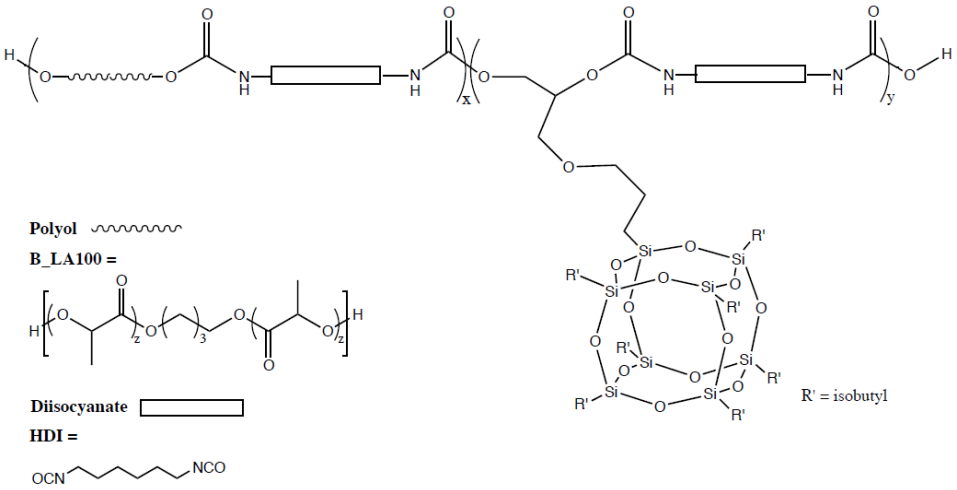

Figure 1.13: Chemical structure of the thermoplastic polyurethane used in this master thesis [13]

1.6.3 Acrylate-endcapped urethane-based polymer

Acrylate-endcapped urethane-based polymers (AUPs) are materials that can crosslink due to UV-light in the presence of a photoinitiator or photosensitiser, called photopolymerisation. Due to the exposure of the UV-light, radicals are formed from the added photoinitiator and free radical polymerisation of the acrylate groups is initiated. [14, 129–131]

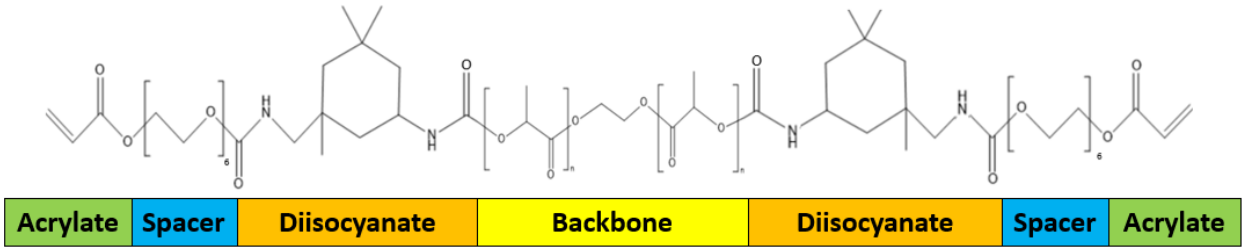

Figure 1.14: Chemical structure of acrylate-endcapped urethane-based polylactic acid with n depending on the target molar mass [14]

AUPs are built out of acrylate end groups, spacers, diisocyanates and a polymer backbone, as can be seen in Figure 1.14. Acrylates are needed to crosslink the polymers. A flexible spacer is introduced between the acrylates and polymer backbone to give the acrylate groups more mobility. Houben et al. (2017) showed that adding a spacer can enable crosslinking in solid-state,

also called solid-state photopolymerisation (SSPP). The AUP doesn't need to be in a liquid state to have enough mobility to crosslink. [14, 131, 132]
The backbone polymer is attached to the spacer by using isophorone diisocyanate. The functional end groups of the diisocyanate (-NCO) will react with the hydroxyl end groups of the polymer backbone and form urethane bonds. Finally, the backbone itself is the core of the material and will define most of the properties such as the glass transition temperature, the degradation temperature and rate and it will have an influence on the mechanical properties, shape memory effect and so on. Any polyol, like polylactic acid used in Figure 1.14, can be used as backbone. Using a diol will result in the formation of a linear chain. [14]

Different researchers have already studied acrylate-endcapped urethane-based polymer precursors for biomedical applications. Pien et al. (2020) showed the potential of using AUP with a poly-ϵ-caprolactone backbone to repair deep flexor tendons. [132]

1.7 Hypotheses and objectives of the master thesis

The overall objective of this master dissertation is to create a biodegradable scaffold for minimal invasive breast reconstruction via DLP printing. This scaffold will consist of linear acrylate-endcapped urethane-based polymer precursor (AUP) which has the ability to crosslink in the presence of UV-light and photoinitiator. Different polymers were examined as starting material, namely a copolymer of poly(D,L-lactic acid) (PDLLA) and polyhedral oligomeric silsesquioxane (POSS), a copolymer of PDLLA and poly-ϵ-caprolactone (PCL) and a homopolymer of PDLLA. Thanks to the mobility created in the soft segment of these materials, the scaffold can be brought into a small temporary shape enabling the surgeon to implant the scaffold in a minimally invasive manner. Upon implantation, the temperature of the patient's body will act as a trigger for the scaffold to expand towards its original, chemically crosslinked, patient-specific shape. To this end, photocrosslinkable materials with a glass transition temperature right below body temperature need to be developed.
For the eventual application, cells will be incorporated in a gelatin-derivative which will be injected in the developed scaffold after implantation for the regeneration of adipose tissues. Therefore, the scaffold needs to have appropriate properties for implantation such as biocompatibility and a low swelling ratio.

Hypotheses:

- An acrylate-endcapped urethane-based polymer can be synthesised with desired thermal characteristics for breast reconstruction purposes.
- A photocurable resin can be developed for digital light processing (DLP) purposes.
- The crosslinking density of resins can be increased by using triacrylate endcap agent and by decreasing the polymer molar mass.
- Resins can be processed into porous, biocompatible scaffolds by means of DLP with shape memory behaviour.

Objectives:

- Synthesise and characterise AUPs with a glass transition temperature between 30 and 35°C starting from different polymer backbones (PDLLA/POSS, PDLLA/PCL and PDLLA).

- Develop a photocurable resin with optimal parameters for DLP printing.
- 3D printing of a resin into a porous, biocompatible and biodegradable scaffold.
- Study the viability and proliferation of cells that are exposed to a culture medium that has been in contact with the scaffold by live/dead staining and MTS assays.

2. Materials and methods

2.1 Materials

Chloroform a.r. (≥99.5%), ethylene glycol a.r. (≥99.5), hexane p. (≥ 99%), methanol p. (≥99%), tetrahydrofuran (THF) (≥99%) and toluene p. (>99%) were all purchased from *Chem-Lab*. 1,4-Dioxane anhydrous (99.8%), 1-methyl-2-pyrrolidinone (NMP, ≥99%), 3.6-dimethyl-1.4-dioxane-2.5-dione (lactide, ≥99%), dimethyl sulfoxide (DMSO, ≥99.9%), dimethyl terephthalate (DMT), dulbecco's phosphate buffered saline (DPBS), magnesium sulfate ($MgSO_4$, ≥99.5%), phenothiazine (PTZ, ≥98%) ethyl lactate and tartrazine (≥85%) were obtained from *Sigma-Aldrich*. Ethyl acetate (EtOAc) and bisomer PEA6 are acquired from *Rijksuniversiteit Ghent* and *GEO* respectively. Triphenyl phosphite (TPP, ≥99%) is purchased from *Honeywell Fluka*. Bismuth neodecanoate, ethoxylated and propoxylated pentaerythritol triacrylate (EPPETA) and ethyl (2,4,6-trimethylbenzoyl) phenyl phosphinate (speedcure TPO-L) were obtained from *Umicore*, *Allnex* and *Lambson* respectively. Deuterated chloroform ($CDCl_3$, 99.80%) was purchased from *Eurisotop*. Chloroform HPCL was acquired from *Biosolve*. Tin 2-ethylhexanoate (Sn(II)Oct, >85.0%) and ϵ-caprolactone (≥99.5%) were obtained from *TCI* and *Merck* respectively. Irgacure 2959 was purchased from *BASF*. Thermoplastic polyurethane (TPU) is synthesised at Syracuse University.

2.2 Methods - Synthesis of materials

This master dissertation will compare different PDLLA-based AUPs. Three different polymers, pure PDLLA, as well as PDLLA/PCL and PDLLA/POSS copolymers, with different molar masses were investigated as starting materials for the creation of both diacrylate and hexaacrylate AUPs to study the influence on glass transition temperature, crosslinking density, gel fraction etc. This section delineates the syntheses that were performed to develop acrylate-endcapped urethane-based polymers.

2.2.1 Preparation of components

Before using D,L-lactide for polymerisation, the monomer needed to be recrystallised for purification. First, ethyl acetate (EtOAc) was dried by stirring the solvent in presence of $MgSO_4$ for 24 hours. Next, it was used to recrystallise D,L-lactide. To this end, 200 g of D,L-lactide was placed in a 2-neck-flask together with the dried ethyl acetate and a stirring bar. Lactide was dissolved in the 2-neck-flask with a reflux set-up at a temperature of 85°C under argon atmosphere. Subsequently, the mixture was cooled down steadily, giving sufficient time to D,L-lactide to properly recrystallise. The crystals were filtered by a Buchner filter and dried for 12

hours on an oil pump.

Monomer ϵ-caprolactone was distilled prior to the polymerisation to remove impurities and water. Therefore, the monomer was heated under vacuum. The vapor was cooled by a condenser and captured in a flask. The first and last 10% of ϵ-caprolactone mixture that dripped in the flask were eliminated. The remainder 80% was considered as pure ϵ-caprolactone and was used during the polymerisation.

Toluene was dried by heating over sodium with benzo-phenone as indicator in a reflux set-up. The removal of water is crucial as it can act as an additional initiator during the polymerisation.

Ethylene glycol was dried by vacuum distillation. Ethylene glycol was added to a 1-neck-flask and placed under vacuum. The temperature was raised while stirring in the presence of a stirring bar until the diol boiled. The first fraction was collected and removed. The remaining ethylene glycol was collected on molecular sieves and stored under argon.

2.2.2 Starting materials

The polymers that are functionalised into acrylate-endcapped urethane-based polymers are referred to as polymer backbone or starting material. They determine most of the material properties such as glass transition temperature. After the polymerisation, these backbones were modified into AUPs to make them chemically crosslinkable, needed for DLP printing. The syntheses of PDLLA, PDLLA/PCL and PDLLA/POSS are described in the following sections.

2.2.2.1 Synthesis of PDLLA

Ring opening polymerisation of lactides was performed to develop poly(D,L-lactic acid). Before conducting the polymerisation, toluene was dried, lactide was recrystallised and ethylene glycol was distilled. Afterwards, the formed crystals were used as monomers, dry toluene as solvent and ethylene glycol as initiator during the solution polymerisation.

Solution polymerisation of PDLLA
The first part of the polymerisation was conducted in the glovebox under argon atmosphere. Recrystallised D,L-lactide (40 g; 0.278 mol) was added to a flame-dried Schlenk flask together with 135 ml dry toluene, 224.38 µl initiator (4.02 mmol; distilled ethylene glycol), 1.63 g catalyst (4.02 mmol; tin 2-ethylhexanoate) and a magnetic stirrer to obtain a molar mass around 10 kg/mol. Next, the schlenk was sealed with a septum and brought outside the glovebox to perform three freeze-pump-thaw cycles. Therefore, the mixture was frozen in liquid nitrogen, put on an oil pump to remove O_2 and other interfering gasses and eventually thawed to start the next cycle. Afterwards, the mixture was heated until 100°C under argon atmosphere to dissolve the monomers and start the solution polymerisation. After 24 hours, the polymerisation reaction was finished. Either the polymer was directly functionalised into AUP (one-step) or first precipitated in a 10-fold excess cold methanol and dried in the vacuum oven (two-step).

Solution polymerisation was chosen as polymerisation technique because the heat, coming from the exothermal reaction, can be dissipated in the solvent. Furthermore, solvents can act as chain transfer agents which results in a better control of the molar mass distribution compared to bulk polymerisation. Additionally, for practical reasons, solution polymerisation is preferred to remove the polymer from the 2-neck-flask. [133–135]

2.2.2.2 Synthesis of PDLLA/PCL

PCL is a biocompatible, biodegradable and FDA-approved polyester. The polymerisation of inexpensive ϵ-caprolactone monomers occurs via a ring opening polymerisation.

The copolymerisation of lactide and ϵ-caprolactone was performed in a similar way as the polymerisation of PDLLA described above. To incorporate a weight percentage of PCL around 8% in the final polymer, 36.80 g of lactide (0.255 mol) was combined with 3.11 ml of distilled ϵ-caprolactone (0.028 mol) to target 40 g of copolymer. Monomer ϵ-caprolactone was also added to the Schlenk flask in the glovebox, after the addition of lactide crystals.
However, in this case 225.28µl initiator (4.04; ethylene glycol) and 1.64 g catalyst (4.04 mmol; tin 2-ethylhexanoate) were added after lactide was dissolved to create a random copolymer. Adding these two components earlier will result in a block copolymer. Creating a block copolymer would result in two glass transition temperatures whereas for statistical copolymers there is only one. Ethylene glycol and tin 2-ethylhexanoate were weighed in the glovebox, but only added to the mixture after the freeze-pump-thaw cycles and once the D,L-lactide crystals were dissolved to create a statistic copolymer.

2.2.2.3 Synthesis of thermoplastic polyurethane

As described in Section 1.6.2.3, thermoplastic polyurethane was synthesised by Syracuse University, USA. The production of TPUs consists of two main processes, the synthesis of PDLLA diol and the synthesis of thermoplastic polyurethane.

Mass polymerisation of PDLLA
At first, PDLLA was generated by mass polymerisation. Therefore, 0.074 ml of 1,4-butanediol (0.84 mmol; initiator) and 0.01 ml of tin 2-ethylhexanoate (0.031 mmol; catalyst) were added to 10 g purified lactide (69.4 mmol) to create PDLLA with a molar mass of 12 kg/mol. Moisture and oxygen were removed by purging extensively with nitrogen gas. The temperature was raised to 140°C and the mixture reacted for 12 hours. Afterwards, the temperature was decreased to room temperature and the PDLLA was dissolved in 30 ml THF. At last, the polymer was precipitated in an excess hexane, air-dried in a fume hood overnight and dried in a vacuum oven.

Conversion of PDLLA into TPU
5 g of synthesised PDLLA was dissolved in 30 ml dry toluene. Distilled HDI (0.271 ml; 1.69 mmol) and 0.01 ml of dibutyltin dilaurate (0.017 mmol; catalyst) were added to this mixture. Moisture and oxygen were removed by purging with nitrogen gas. Subsequently, the reaction temperature was increased to 50°C and the mixture was stirred during 30 minutes. Next, 1.19 g of

1,2-propanediolisobutyl POSS (1.25 mmol), dissolved in 2 ml dry toluene, was added to the reaction. After reacting 12 hours at 90°C, 25 ml THF was added to dilute the solution and the whole precipitated in a 10-fold excess cold hexane. For TPU2 and TPU3 the polymer was dissolved again in chloroform and precipitated in a 10-fold excess cold hexane for a second time. Finally, the polyurethane was dried in a vacuum oven.

2.2.3 Synthesis of acrylate-endcapped urethane-based materials

As mentioned in Section 1.6.3, acrylate-endcapped urethane-based endcap agent is used to functionalise the backbone to enable the creation of a covalent network under UV-light in the presence of a photoinitiator. The production of acrylate-endcapped urethane-based SMPs was performed in two steps: the synthesis of the endcap agent and the functionalisation of the polymer backbone into AUP.

2.2.3.1 Synthesis of single acrylate endcap agent

15 g of isophorone diisocyanate (67.5 mmol; IPDI) and a stirring bar were added to a flame-dried 2-neck-flask, together with 20 mg of both phenothiazine (0.10 mmol; PTZ) and triphenylphosphite (0.064 mmol; TPP) acting as post reaction stabilisers. A 1.1 excess of bisomer PEA6 (24.89 g; 74.1 mmol) relative to IPDI was added to a flame-dried addition funnel, as well as 15 mg of bismuth neodecanoate (0.0207 mmol; catalyst). The 2-neck-flask was connected to the addition funnel and a Liebig condenser. The set-up was put under argon atmosphere in an oil bad at 70°C and was flushed three times with argon to remove moisture and oxygen. When the temperature reached 70°C, the bisomer mixture was added dropwise to the 2-neck-flask. The mixture was covered with aluminum foil to shield the mixture from light. After reacting for two hours, the temperature was raised to 90°C and the reaction continued for 1h15. The final product was transferred in a plastic bottle, put under argon atmosphere and covered from light. The chemical structure of the final construct is depicted in Figure 2.1.

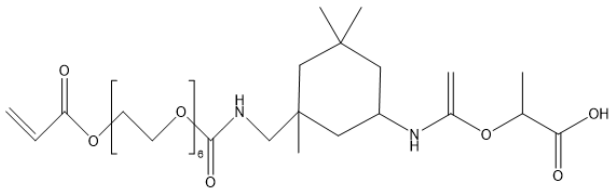

Figure 2.1: Chemical structure of single acrylate endcap agent

2.2.3.2 Synthesis of triacrylate endcap agent

The process of creating a triacrylate endcap agent is similar to the synthesis of one acrylate endcap. For this synthesis 42.7 g ethoxylated and propoxylated pentaerythritol triacrylate (80.3 mmol; EPPETA), see Figure 2.2) was used, instead of bisomer PEA6. The reaction was conducted for 4h30 at 75°C instead of 3h15 with an increase in temperature from 70°C to 90°C after two hours. The structure of the triacrylate endcap agent is illustrated in Figure 2.2.

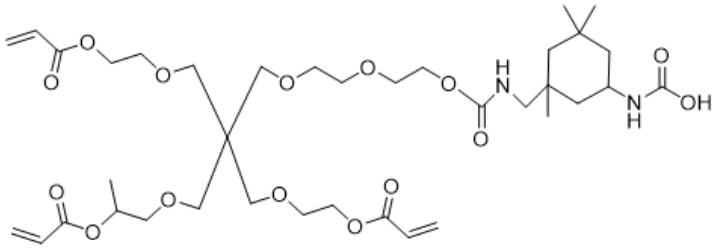

Figure 2.2: Chemical structure of triacrylate endcap agent

2.2.3.3 Formation of acrylate-endcapped urethane-based polymers

The conversion of polymers into AUPs was done in two ways. If the polymer backbone was already precipitated and dried, it was dissolved in an appropriate amount of dry toluene or chloroform in order to start the second part of the synthesis. This is referred to as a two-step AUP synthesis. If the polymer was still dissolved after polymerisation, no extra dissolving step was required. This is called a one-step AUP synthesis. The functionalisation of the polymer backbone into an AUP is the same for TPU, PDLLA and PDLLA/PCL. It is described below for the specific case of PDLLA (two-step).

First, 40 g PDLLA (4.02 mmol) was added to a flame-dried 1-neck-flask together with a stirring bar. Dry toluene was poured into the flask to dissolve PDLLA and the flask was sealed with a septum. The temperature of the solution was increased to 75°C and the mixture was stirred and kept under argon atmosphere by using an argon balloon attached to a needle, punctured through the septum.
A double excess single acrylate endcap agent (9.35 g, 16.4 mmol) or triacrylate endcap agent (12.62 g, 16.4 mmol) was added to an amber vial together with 1 ml of dry toluene. Bismuth neodecanoate (15.8 mg (2.18 µmol) for single acrylate endcap agent and 14.8 mg (2.04 µmol) for triacrylate endcap agent; catalyst) was added to the vial and the mixture was injected into the 1-neck-flask. After reacting for 24 hours at 75°C, the acrylate-endcapped urethane-based polymer was precipitated in a 10-fold excess cold hexane or methanol. The precipitated AUP was then dissolved in chloroform to precipitate the material for a second time in a 10-fold excess cold hexane or methanol to remove impurities. The AUP was dried in the vacuum oven for at least six hours to remove the remaining solvents. During this synthesis, the mixture was shielded from UV-light to avoid early crosslinking reactions.

2.3 Methods - Characterisation of materials

2.3.1 Thermogravimetric analysis

Thermogravimetric analysis (TGA) was used to determine the degradation temperature of the materials by monitoring the weight change under inert atmosphere. During this master thesis a *TA Instruments Q50 device* was used. First, the material (approximately 10 mg) was placed on a tarred platinum pan and the sample was equilibrated at 35°C. Next, the temperature was increased to 600°C at a rate of 10°C/min. Subsequently, the sample was equilibrated at 350°C. The thermograms were analysed by the *Universal Analysis* software package. The onset temperature (T_{onset}), the temperature at 1% weight loss (T_{99}) and temperature at 5% weight loss

(T_{95}) were determined.

2.3.2 Differential scanning calorimetry

Differential scanning calorimetry (DSC) was used to determine the glass transition temperature (T_g), melt temperature (T_m) and crystallisation temperature (T_{cryst}) of the synthesised materials. A *TA Instruments Q2000 device* was used during this project. It measures the heat flow needed to increase the temperature of two pans at a constant rate. Therefore, an aluminum Tzero pan was filled with 5-10 mg material, sealed with an aluminum Tzero lid and compared to an empty reference aluminum Tzero pan. Both pans were first equilibrated at 45°C. Next, the temperature was increased with a constant rate of 10°C/min until 120°C for PDLLA and PDLLA/PCL and 170°C for PDLLA/POSS and kept isothermal for five minutes. In this way, the thermal history of the sample was erased. Subsequently, the temperature was decreased with a rate of 5°C/min to -50°C and kept isothermal again for five minutes. Finally, the sample was heated until 120°C or 170°C, depending on the material, with a heating ramp of 10°C/min. The thermograms were analysed by the *Universal Analysis software package*. Degradation temperatures needed to be determined first in order to not exceed this temperature during DSC measurements.

2.3.3 Proton nuclear magnetic resonance spectroscopy

Proton nuclear magnetic resonance (H-NMR) spectroscopy was used to gain more insight in the structure of the starting materials and AUPs. A small amount of material, in mg-range, was dissolved into deuterated chloroform ($CDCl_3$) and inserted in a NMR tube. A 400 MHz *Bruker Avance II Ultrashield* spectrometer was used at room temperature to determine the H-NMR spectrum. The spectra were analysed by using the *MestReNova* software package. Whittaker Smoother was performed for smoothening the baseline and the chloroform peak at 7.260 ppm was used as reference peak. Dimethyl therephthalate (DMT) was used as standard for quantitative H-NMR spectroscopy.

Different characteristics of the materials such as molar mass, concentration of hydroxyl groups, weight percentage of PCL and degree of substitution were determined by analysing the H-NMR spectra. These calculations are described in Appendix B. The degree of substitution quantifies the number of hydroxyl end groups that was converted into acrylate functionalities.

2.3.4 Gel permeation chromatography

The number average molecular weight (M_N), the weight average molecular weight (M_W) and the dispersity ($Đ$) of the polymers were determined via gel permeation chromatography (GPC). Samples were prepared by dissolving 5-10 mg polymer into 1.5 ml HPLC-grade chloroform (*Biosolve*, HPLC grade). This solution was filtered through a filter with a pore size of 0.45 µm. Polystyrene standards (from *Agilent Technologies* with molar masses between 3 and 67.6 kg/mol) were used for calibration. A Mark-Houwink correction factor of 0.58 was used. [136] A *Waters 1515* isocratic HPLC pump was used together with a *Waters 2414* refractive index detector, *Waters 717plus* Autosampler and a SDV column with a flow rate of 1 ml/min.

2.3.5 Fourier transform infrared spectroscopy

Fourier transform infrared spectroscopy (FT-IR) was used to detect functional groups by measuring the absorbed infrared light as molecules absorb infrared light at specific wavenumbers that are characteristic for the atoms and their bonds. A Frontier FT-IR spectrometer from *PerkinElmer* was used in combination with a MKII Golden Gate set-up with a diamond crystal from *Specac*. The measurements were executed in the Attenuated Total Reflection (ATR) mode. First, a background measurement was performed. Next, the sample was placed on the Golden Gate and a scan was performed between 600 and 4000 cm^{-1}.

2.3.6 Rheology and photorheology

Rheology is the study of the deformation and flow under stress. During this master thesis, a parallel-plate rheometer of *Anton Paar* (Physica MCR 301) was used.
After initialising and setting the zero gap, the polymer resin was placed in the middle of the base plate under a spindle with a diameter of 1.5 cm and a gap setting of 0.3 cm. Two different tests were performed with the rheometer at 22°C.

First, rotational tests were performed to measure the viscosity with increasing shear rate. Therefore, the speed of rotation was increased from 0.1 to 1000 1/s with a logarithmic ramp.

The rheometer was also used in combination with a UV-source to determine the storage (*G'*) and loss (*G"*) moduli during oscillatory tests.
Photorheology measurement were performed at a strain of 0.1% and a frequency of 1Hz. During the measurement, the polymer solution was irradiated by UVA-light (*EXFO Novacure 2100* UV-light source with an intensity of 3500 mW/cm^2 and a wavelength of 365 nm) and a normal force of one newton was applied to keep contact with the material after crosslinking.

2.3.7 UV-VIS spectroscopy

$UVIKON_{XL}$ from *BIO-TEK instruments* with *LabPowerv4* software was used to perform ultraviolet-visible spectrophotometry. One PMMA cuvette was filled with the reference solution (NMP) and another PMMA cuvette with the solution that needed to be examined. The reference cuvette was placed in the $UVIKON_{XL}$ and a baseline was recorded. Next, the cuvette containing the sample was placed in the instrument and an AutoZero measurement was performed at default wavelength 580 nm. As this is done to set the absorption level at zero, the corresponding wavelength may not belong to an absorption peak in the spectrum. Finally, a full wavelength scan was executed. These measurements were done in triplicate.

2.3.8 Gel fraction and swelling ratio experiments

The gel fraction was determined to evaluate the crosslinking effectiveness. First, a photocurable resin was created containing the AUP, TPO-L (1.5 wt%), tartrazine (10 mol% of TPO-L) and THF as a solvent because it dissolves uncrosslinked AUP and it has a low boiling point (66°C) which leads to an easy removal of the solvent and more accurate gel fractions. [137] The boiling point of NMP (202°C) is too high to remove the solvent in the vacuum oven without affecting the crosslinked AUPs which makes it impossible to measure the gel fraction of resins with NMP. The resins with THF were placed between two glass plates, covered with release foil, with a spacer

(height 1 mm). The set-up was crosslinked by placing it 30 minutes under an UVA-lamp (10 mW/cm^2). After crosslinking, three discs of 8 mm were punched out of this sheet and placed in the vacuum oven (at least six hours) to dry. Subsequently, these discs were weighed (m_{dry1}) and placed in a vial with THF. After 24 hours in THF, the parts that were not (fully) crosslinked were dissolved and the discs were dried in the vacuum oven for another 24 hours. Finally, the dry mass (m_{dry2}) was determined of the three discs. The gel fraction (%) was determined by Equation 2.1.

$$Gel\ fraction = \frac{m_{dry2}}{m_{dry1}} * 100(\%) \tag{2.1}$$

The swelling ratio was obtained in a similar way. However, for these experiments, the resin was made with the solvent that is used in the eventual application (NMP). This resin was placed between two glass plates, covered with release foil, with a spacer (height 1 mm). The resin was crosslinked by placing it 30 minutes under an UVA-lamp (10 mW/cm^2). Three discs of 8 mm were punched out of the crosslinked sheet. These discs were washed with acetone to remove the material that was not crosslinked, mimicking similar conditions as the final application. The discs were dried in the vacuum oven for at least six hours. Next, the discs were placed in a vial with Dulbecco's phosphate buffered saline (DPBS) to mimic physiological conditions in order to examine the swelling that will occur in the patient's breast. After 24 hours, the excess of DPBS was removed and the swollen discs were weighed ($m_{swollen}$). The discs were again placed in the vacuum oven to remove the residual DPBS. At last, the masses of the dried discs (m_{dry}) were determined and with this information the swelling ratio was calculated by Equation 2.2. These measurements were done in triplicate. [138, 139]

$$Swelling\,ratio = \frac{m_{swollen} - m_{dry}}{m_{dry}} \tag{2.2}$$

2.3.9 Cell assays

Multiple discs were made in order to test the effect of leaching components on the viability and proliferation of cells. First of all, resins were made with AUP, TPO-L (1.5 wt%), tartrazine (10 mol% of TPO-L) and NMP. This resin was placed between two glass plates, covered with release foil, with a spacer with a height of 1 mm. The resin was crosslinked by placing it 30 minutes under an UVA-lamp (10 mW/cm^2) and nine 8 mm discs were punched out of the crosslinked sheet. These discs were washed with acetone and dried in the vacuum oven for at least six hours.

The discs were sterilised by immersing them 24 hours in a solution with 70% ethanol followed by irradiation under UVC-light for 30 minutes. Next, the sterilised discs of around 10 mg were incubated (37°C; 5% CO2) in 1 ml cell culture medium of Dulbecco's modified eagle medium (DMEM), 10% fetal calf serum (FCS) and 1% penicillin/streptomycin (P/S) during one, three and seven days.

In meantime, a cell culture with DMEM, 10% FCS and 1% (P/S) was used to culture human adipose derived stem cells (ASCs). The medium was replaced every two to three days until the desired amount of cells was reached. Once a cell confluency between 80 and 90% was obtained, the

cells were seeded in the wells of a 96-well plate (approximately 10^4 cells per well in 200 µl culture medium). After 24 hours of cell attachment, the medium was removed and 200 µl of the medium that had been in contact with the discs, was placed in the wells that contained the ASCs. Finally, MTS and live/dead assays were used to examine the ASCs (Figure 2.3).

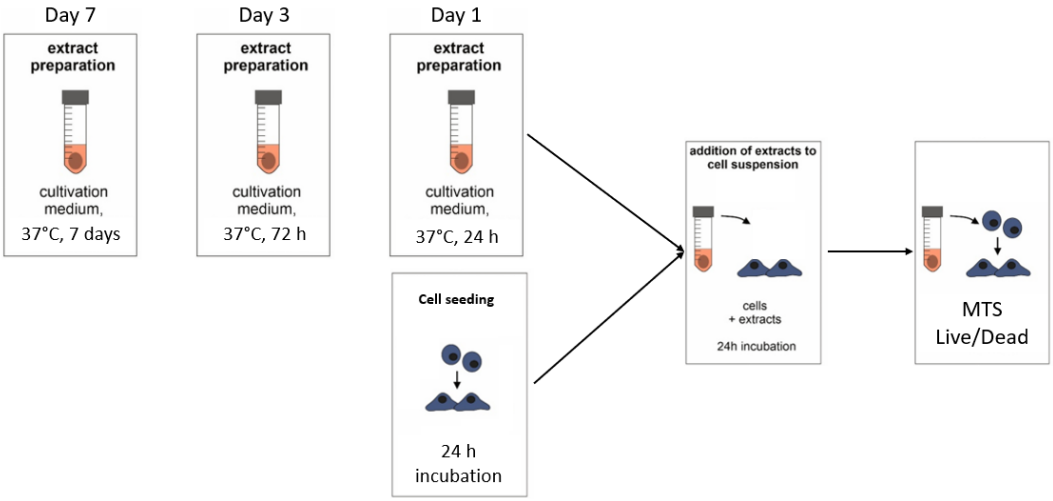

Figure 2.3: Process of MTS and live/dead assays

2.3.9.1 MTS assay

3-(4,5-Dimethylthiazol-2-yl)-5-(3-carboxymethoxyphenyl)-2-(4-sulfophenyl)-2H-tetrazolium (MTS) was used to examine the viability and proliferation of cells. The cells were exposed to a cell culture with 16 v/v% of MTS that was mingled with 0.8 vol% of an electron coupling reagent, namely phenazine methosulfate (PMS). During two hours of incubation (37°C; in the dark), the cells converted MTS into the purple-coloured formazan by enzymatic reduction under incessant shaking. This conversion was an indication of the metabolic activity of the cells. Finally, a spectrophotometer from *BioTek Instruments* (EL800 Universal Micropate Reader) was used with GEN5 software to measure the absorbance of formazan around 490 nm.

2.3.9.2 Live/dead viability assay

Calcein-acetoxymethylester (Ca-AM), together with propidium iodide (PI), was used during live/dead viability assays. Therefore, cells were exposed to a mixture of 0.2 vol% Ca-AM, 0.2 vol% PI and phosphate buffered saline (PBS). After incubation (15 min; in the dark), the cells were separated from the mixture and visualised by using green fluorescent proteins (GFP) and Texas red. To this end, a fluorescence microscope (*Olympus IX 81*) with *Xcellence Pro* software was utilised with a GFP and texas red filter for green living cells and red dead cells respectively.

2.3.10 Statistical analysis

Statistical analysis was performed with a statistical significance of 0.05. One-way ANOVA was used to determine statistical significance between more than two groups. T-tests were used for comparing two groups. Linear regression analysis was applied to determine if there is a statistical

correlation between two continuous variables. Two-way ANOVA was used for the analysis of the biological evaluation.

3. Results and discussion

3.1 AUPs with appropriate glass transition temperatures

This master thesis focuses on three different PDLLA-based materials, namely a PDLLA homopolymer, a PDLLA/PCL copolymer and a copolymer of PDLLA and POSS (TPU). These polymers are functionalised into acrylate-endcapped urethane-based polymers. In this section, the results of the syntheses and the structural characteristics of these materials are discussed followed by their thermal properties.

3.1.1 Synthesis of starting materials

3.1.1.1 Synthesis of PDLLA

Poly(D,L-lactic acid) was synthesised with different molar masses as starting material for AUPs. The objective was to make a polymer batch with a molar mass of 5 kg/mol and a polymer batch of 10 kg/mol. The actual molar masses, measured by H-NMR spectroscopy, were 5.6 kg/mol (PLA6) for a target of 5 kg/mol, 10.7 kg/mol (PLA11*) and 12.6 kg/mol (PLA13) for a target of 10 kg/mol. These values can be found in Table 3.1 together with the molar masses and dispersities obtained via gel permeation chromatography (GPC). In general, ring opening polymerisation (ROP) results in low dispersities and the dispersity increases with increasing molar mass, which is also the case in this master thesis (PLA6 vs PLA13). Li et al. (2017) obtained dispersities between 1.09 and 1.22 for PDLLA chains around 10 kg/mol with $(\mathrm{LTi-O})_2$ as catalyst. The authors claim that using tin-octanoate as catalyst results in a slightly higher dispersity, which is in line with the obtained dispersities. [140, 141] The dispersity of polylactic acid, synthesised via ROP, is significantly lower than for polymers made via polycondensation due to the formation of water during polycondensation. Cação et al. (2019) obtained dispersities between 1.70 and 2.22 for polylactic acid synthesised via polycondensation (with molar masses between 8 and 12 kg/mol). [142]
The molar mass of the chains for PLA11* is broadly distributed due to the relatively high dispersity (1.45) compared to PLA6 and PLA13, with a molar mass of 2.5 kg/mol according to the GPC measurement. The general molar mass is probably higher than 2.5 kg/mol (according to the H-NMR spectrum (10.7 kg/mol)). This polymer is called PLA11* due to the variability in molar mass of the chains.

An example of a H-NMR spectrum of PDLLA (PLA11*) is shown in Figure 3.1. From this spectrum, the molar mass of the polymer can be calculated as described in Appendix B.1.1.

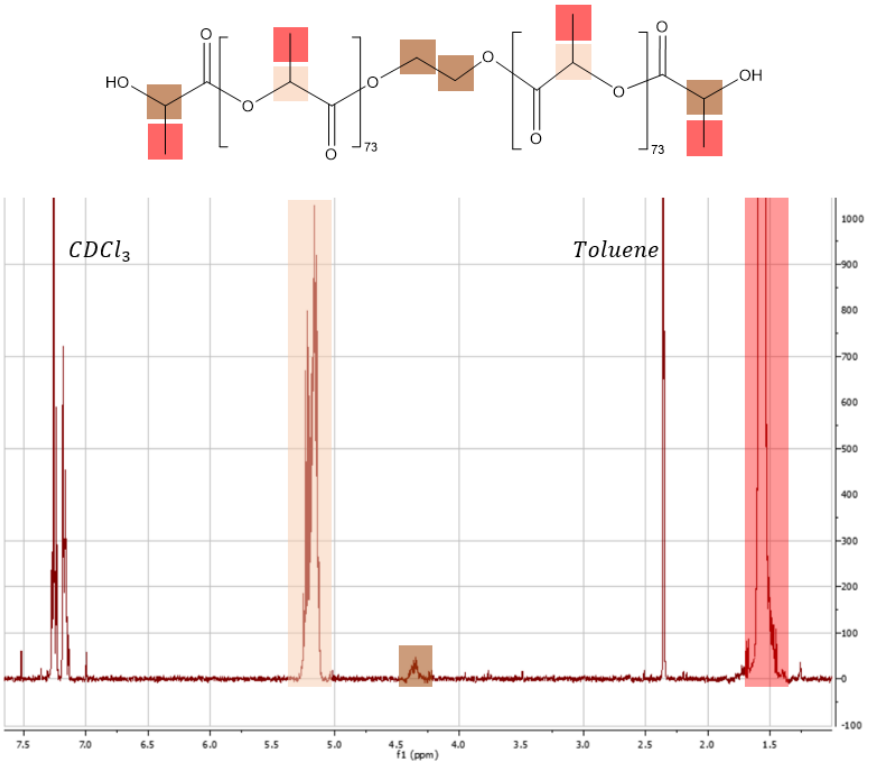

Figure 3.1: H-NMR spectrum of PLA11*

From a H-NMR spectrum with DMT, the hydroxyl concentration can be determined as explained in Appendix B.3. Knowing the number of hydroxyl groups at the end of the chains is useful to determine the amount of endcap agent needed to fully convert the polymer into an AUP. Table 3.1 shows the number of hydroxyl groups per gram polymer (OH-concentration) for the different materials. It can be shown that for higher molar masses (PLA13 compared to PLA6), the hydroxyl concentration decreases as longer chains are formed which results in a decrease in hydroxyl end groups per gram PDLLA. PLA11* has a higher OH-concentration than expected, according to the molar mass obtained via GPC. This is in line with the hypothesis that the sample measured by GPC exhibited a lower molar mass than the overall molar mass of the material batch.

Table 3.1: Structural characteristics for different types of PDLLA

Material	**Molar mass NMR (kg/mol)**	**Molar mass GPC (kg/mol)**	**Đ**	**OH-concentration (mol_{OH}/g_{PDLLA})**
PLA6	5.6 ± 1.0	4.3	1.21	2.98E-04
PLA11*	10.7 ± 3.6	2.5	1.45	1.37E-04
PLA13	12.6 ± 2.6	7.6	1.28	1.76E-04

3.1.1.2 Synthesis of PDLLA/PCL

The research performed during this master thesis about PDLLA/PCL and PDLLA/PCL-based AUPs was a continuation of previously performed research by ir. C. Gréant. The examinations were done in collaboration with ir. C. Gréant and V. Stragier.

The glass transition temperature of a random copolymer can be calculated via the Fox equation (see Equation 3.1). [143] In order to obtain a glass transition temperature between 30°C and 35°C, 12 to 15 wt% ϵ-caprolactone needs to be included in the copolymer according to this equation. However, research of C. Gréant has shown that copolymers with a molar mass around 10 kg/mol and a weight percentage PCL close to eight, have glass transition temperatures within the desired range after functionalisation into AUPs.

$$\frac{1}{T_g} = \sum_i \frac{w_i}{T_{g,i}} \tag{3.1}$$

The H-NMR spectrum of PLA/PCL11 copolymer with a molar mass of 11.4 kg/mol, is illustrated in Figure 3.2. The same peaks that were detected on the H-NMR spectrum of PDLLA are seen in this spectrum (around 5.10 ppm and 4.25 ppm) together with some characteristic signals of PCL. The signals around 4.10 ppm and 2.38 ppm result from PCL in the polymer chain, while the signal at 3.64 is generated by ϵ-caprolactone near the end of the polymer chain.

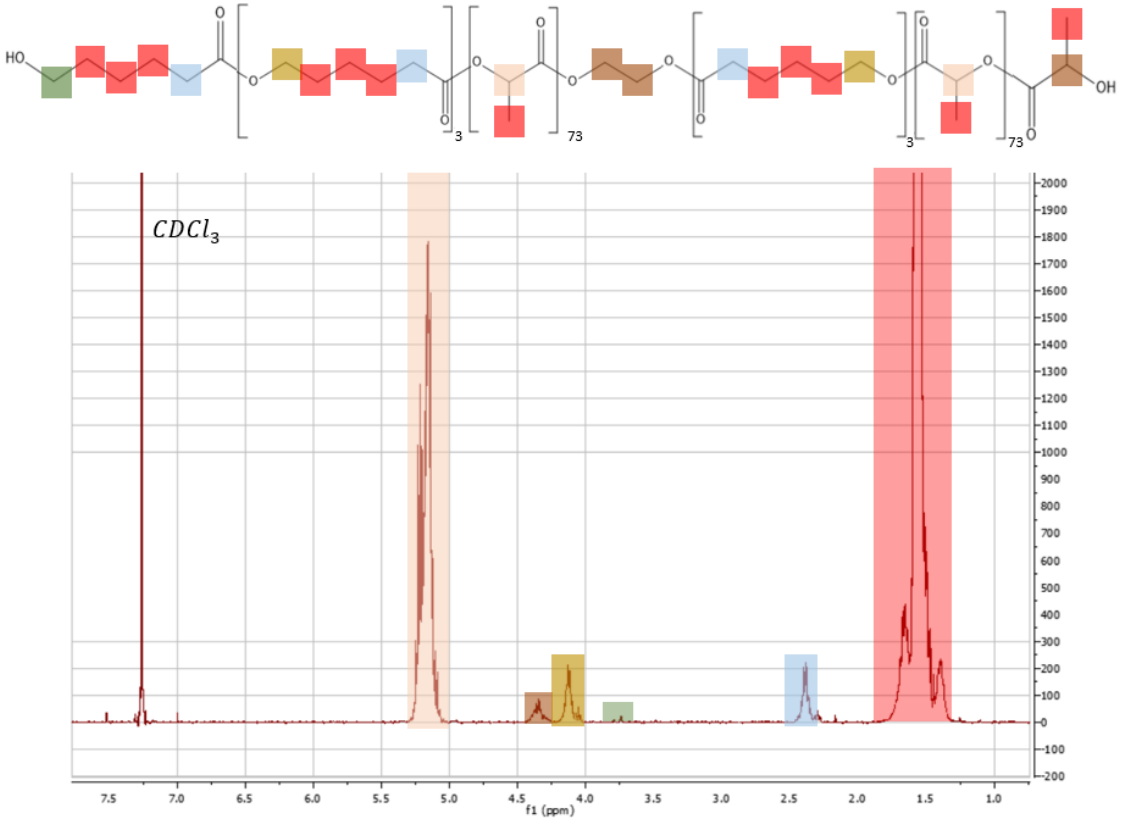

Figure 3.2: H-NMR spectrum of PLA/PCL11

Previous research showed that the maximum amount of polymer that can be created during one synthesis is approximately 40 g. Upscaling of the synthesis was considered to create larger material batches within the same synthesis time. To this end, the possibility to use a big reactor (5L capacity) was examined. In order to use this big reactor, the optimal synthesis method that was described in Sections 2.2.2.2 and 2.2.3, needed some adaptations. The new synthesis had to

be performed under nitrogen atmosphere (atm) instead of argon, it had to take place outside the glovebox (GB) and the three freeze-pump-thaw (FPT) cycles needed to be eliminated in the synthesis procedure. Copolymer PLA/PCL1BR° was synthesised under these "big reactor conditions" (BR) and copolymer PLA/PCL1° was synthesised under argon atmosphere with the inclusion of three freeze-pump-thaw cycles. Both syntheses were performed outside the glovebox (indicated by °). The results of these two copolymer syntheses can be found in Table 3.2.

Table 3.2: Polymer characteristics for different environmental factors

Material	**Atm**	**FPT**	**GB**	**Molar mass NMR (kg/mol)**	**wt_{PCL} (%)**
PLA/PCL1BR°	N_2	No	No	0.77	1.4
PLA/PCL1°	Ar	Yes	No	0.80	1.4
PLA/PCL12	Ar	Yes	Yes	11.6	5.6

One can conclude that the molar masses obtained from the H-NMR spectrum, are very low (0.77 and 0.80 kg/mol) compared to the targeted molar mass of 10 kg/mol. Moreover, the weight percentages of PCL, calculated by H-NMR spectroscopy, are far below the desired 8 wt%. This means that neither PLA/PCL1BR° nor PLA/PCL1° had a successful polymerisation. By comparing these two copolymers with copolymer PLA/PCL12, for which the polymerisation was performed in the glovebox, under argon atmosphere and with three FPT cycles, one can conclude that PLA/PCL12 was successfully synthesised (with a molar mass around 11.6 kg/mol and a weight percentage PCL of 5.6). These results show that the glovebox is crucial for a proper polymerisation as H_2O present in air can act as initiator and therefore lower the molar mass. Consequently, the big reactor cannot be used for copolymerisations of PDLLA/PCL.

3.1.1.3 Comparison between molar masses obtained via GPC and H-NMR spectroscopy

The differences in molar masses determined by GPC measurements and H-NMR spectroscopy were examined. In order to correlate the standard deviation of the molar masses obtained from H-NMR spectroscopy with the dispersity (Đ) of the GPC results, the dispersity is reformulated into a standard deviation by using Equation 3.2 where s represents the standard deviation of the number average molar mass (M_N). [144]

$$s = M_N\sqrt{1 - Đ} \tag{3.2}$$

PDLLA and PDLLA/PCL polymers were targeted to have a molar mass of 10 kg/mol, except for PLA6 that was targeted to have chains of 5 kg/mol. Figure 3.3 shows that the molar masses obtained via GPC measurements were lower compared to molar masses obtained via H-NMR spectroscopy. This might be a result of the difference in hydrodynamic volume of polystyrene (used as standard) and PDLLA and PDLLA/PCL. A Mark-Houwink correction factor of 0.58 was used. [136] However, this correction factor is applied in literature for PDLLA when THF is used as eluent instead of chloroform. Further research is needed to find a more accurate correction factor for both PDLLA and PDLLA/PCL.

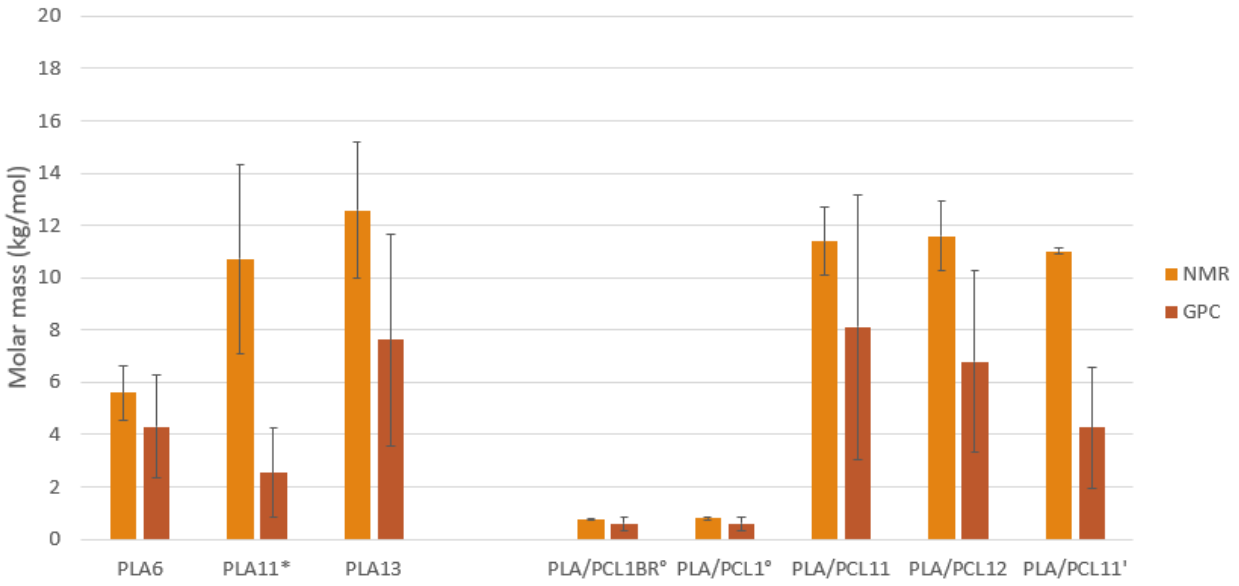

Figure 3.3: Molar masses obtained from GPC (brown) and H-NMR spectroscopy (orange)

3.1.1.4 Synthesis of TPU

Thermoplastic polyurethane is synthesised by Syracuse University. The researchers of Syracuse tried to achieve a TPU with PDLLA chains of 12 kg/mol and a POSS/PDLLA molar ratio of three. Three batches of this TPU (TPU1, TPU2 and TPU3) were shipped to Belgium. The synthesis of TPU backbones was conducted in two steps.

First, PDLLA was synthesised by mass polymerisation. The H-NMR spectrum of PDLLA incorporated in TPU2 can be found in Figure 3.4. From this spectrum, the molar mass of PDLLA was determined. The mean molar masses for the three batches can be found in Table 3.3 together with their standard deviation. These molar masses do not reach the target of 12 kg/mol. The lower molar mass will result in a decrease in glass transition temperature and better crosslinking efficiency. Both are beneficial for the development of DLP printed scaffolds with glass transition temperatures slightly below body temperature.

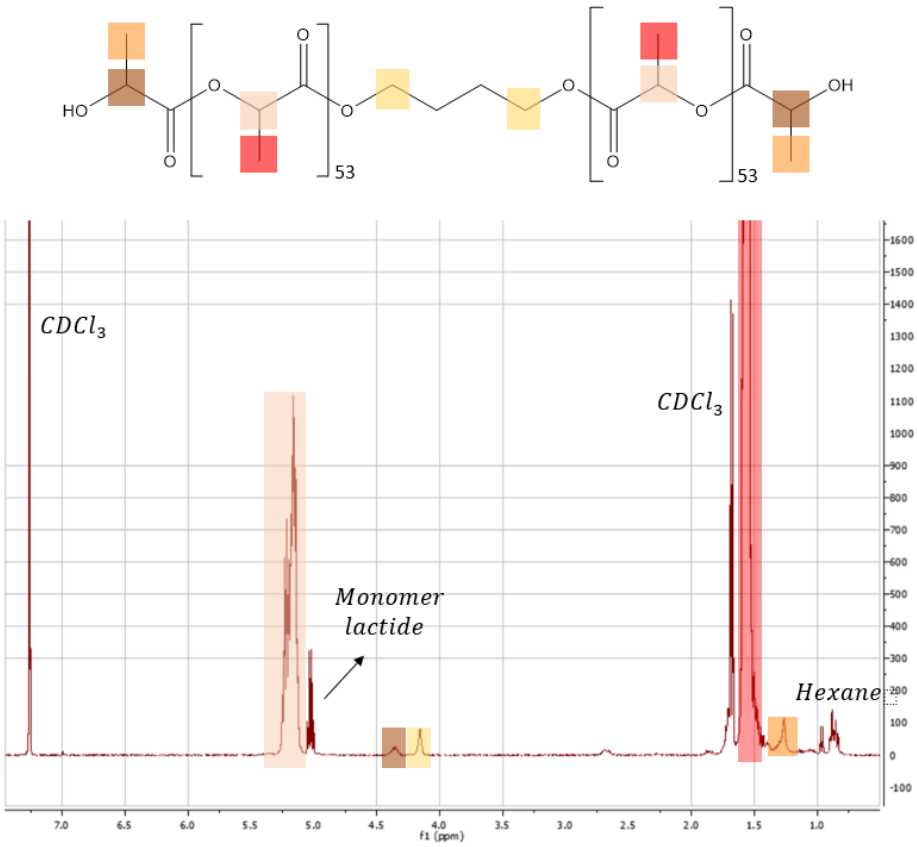

Figure 3.4: H-NMR spectrum of PDLLA used in TPU2

Table 3.3: Molar masses of PDLLA used in the thermoplastic polyurethanes

Material	**Molar mass of PDLLA in TPU (kg/mol)**
TPU1	5.7 ± 0.9
TPU2	7.8 ± 0.5
TPU3	8.1 ± 0.1

Secondly, these PDLLA chains are used during the synthesis of the thermoplastic polyurethanes as described in Section 2.2.2.3. The H-NMR spectrum of TPU2 can be found in Figure 3.5. Figures C.1 and C.2 in Appendix C show the H-NMR spectra of TPU1 and TPU3. The spectrum of TPU1 looks different than the other ones, which indicates the presence of impurities such as monomer POSS (between 2.60 and 2.80 ppm). TPU2 and TPU3 were synthesised by an optimised protocol (two precipitations in hexane instead of one) which resulted in less residual monomers.

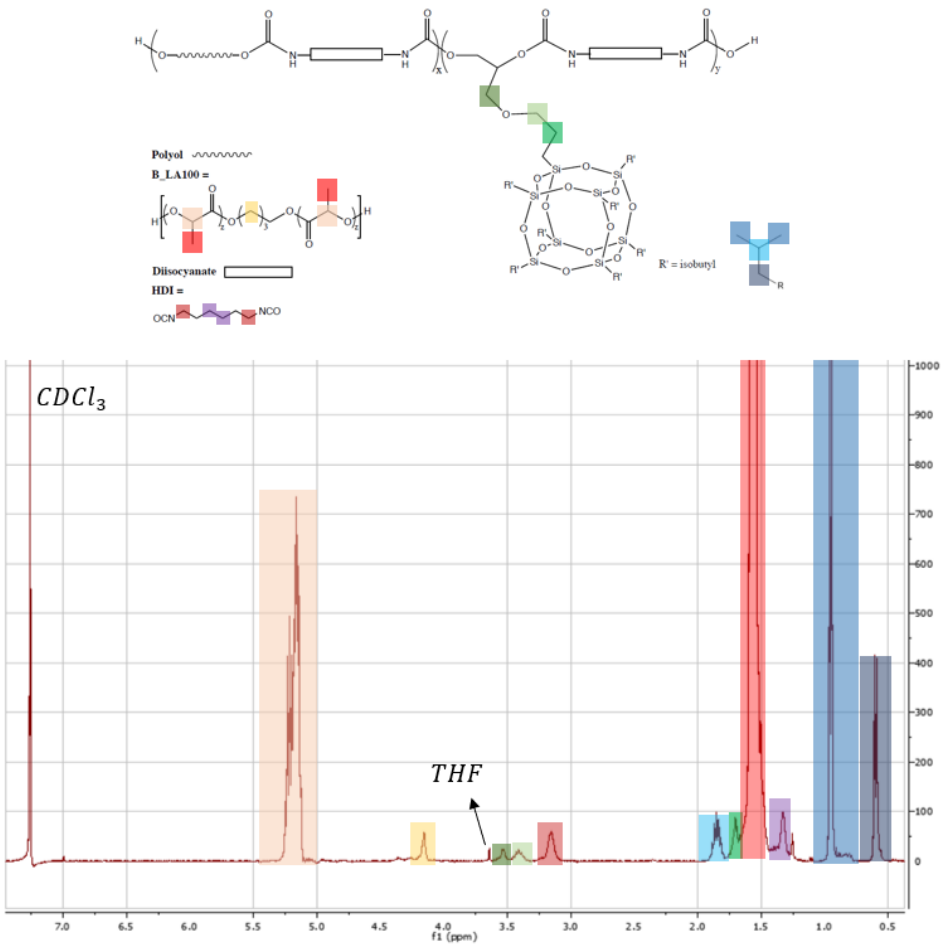

Figure 3.5: H-NMR spectrum of TPU2 [13]

The molar ratio of POSS relative to PDLLA and the weight percentage of the hard segment (mass of HDI and POSS compared to total mass) were determined for the three batches (see Table 3.4). One can conclude that longer PDLLA chains result in higher molar ratios of POSS to PDLLA as there are less PDLLA chains in the final material for the same amount of PDLLA. All molar ratios are below the target of three as the target molar mass of PDLLA (12 kg/mol) was not reached. Additionally, the obtained molar ratios in the research of Knight (2010) were all lower than the targeted ratio indicating the difficult incorporation of POSS. [145] The weight percentages for the hard segment are equal for the different batches and are thus independent of the molar mass of PDLLA and the molar ratio. Unfortunately, the molar masses of total TPU chains could not be determined by H-NMR spectra due to overlap between different signals. Additionally, it was not possible to perform GPC measurements due to the presence of urethane bonds.

Table 3.4: Molar ratio POSS/PDLLA and weight percentage hard segment

Material	**Molar ratio POSS/PDLLA**	**wt_H %**
TPU1	0.97 ± 0.05	19.87 ± 0.64
TPU2	1.44 ± 0.10	18.52 ± 0.96
TPU3	1.54 ± 0.06	19.00 ± 0.59

3.1.2 Synthesis of acrylate-endcapped urethane-based polymers

3.1.2.1 Reaction time of endcap agent with EPPETA

The starting materials were functionalised into both diacrylate AUPs (based on bisomer PEA6) and hexaacrylate AUPs (using EPPETA). As there was no standard operating procedure yet to synthesise endcap agent with EPPETA, FT-IR spectroscopy was performed at different time points during the synthesis to determine the optimal reaction time.

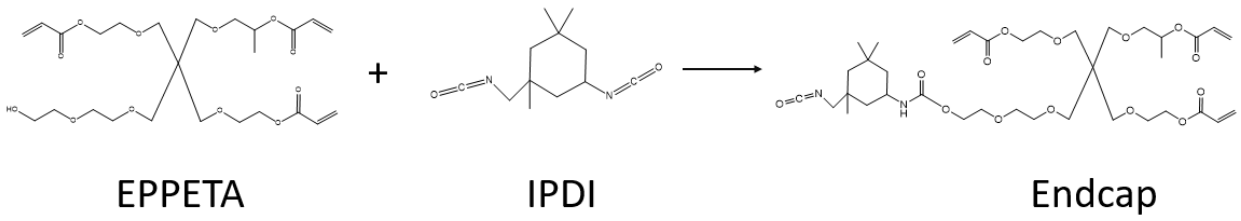

Figure 3.6: Synthesis of endcap agent with three acrylates

During this synthesis, the hydroxyl groups of EPPETA react with the isocyanate groups of IPDI (see Figure 3.6). This means that O-H (3443 cm^{-1}) and N=C=O (3362 cm^{-1}) bonds disappear while N-H (2253 cm^{-1}), and C-O (1150-1250 cm^{-1}) bonds are formed. [146] During the synthesis of the endcap, a FT-IR spectrum was recorded at different times. The first FT-IR spectrum (T0) was recorded at the moment that EPPETA (together with bismuth neodecanoate catalyst) was added to the mixture of IPDI, TPP and PTZ. The next spectra were recorded 0.5h (T1), 1h (T2), 1.5 (T3), 2h (T4), 3h (T5), 4.5h (T6), 6h (T7) and 8h (T8) after the start of the reaction. This allowed to monitor the progress of the reaction (see Figure 3.7).

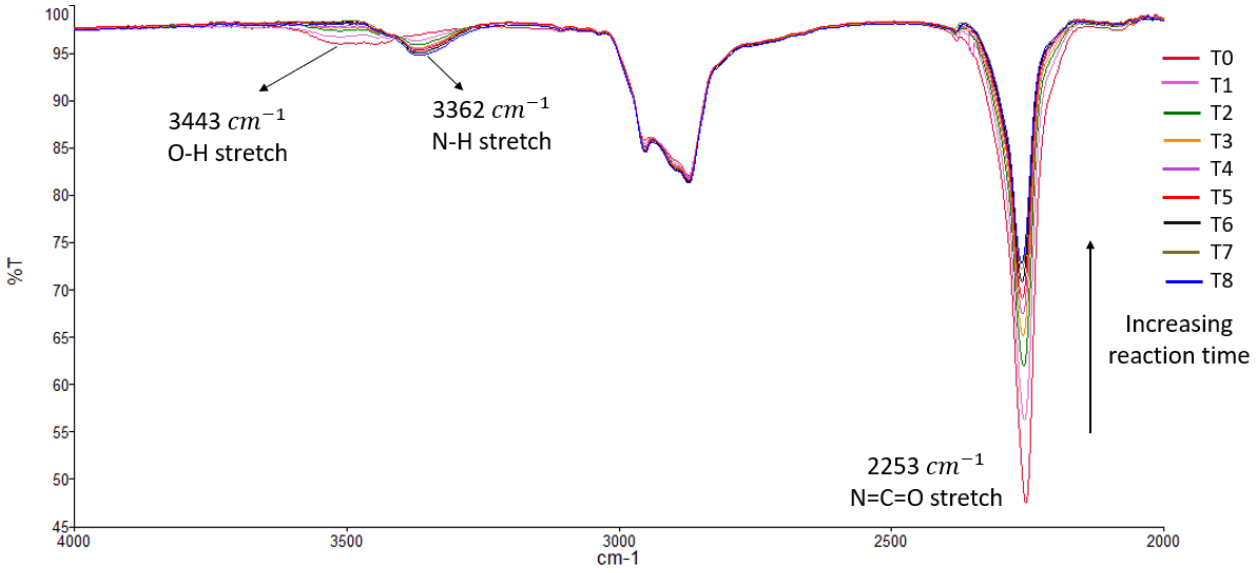

Figure 3.7: FT-IR spectra during endcap synthesis with EPPETA at different time points

Figure 3.7 shows the percentage transmittance (%T) as a function of wavelength (cm^{-1}). The peak corresponding to the N=C=O stretch decreased over time. As expected, the number of

isocyanate groups decreased as they react with hydroxyl groups of EPPETA. During the first reaction hours, this signal decreases tremendously, while this slows down after a few hours. In order to maintain a balance between conversion into endcap agent and time efficiency of the synthesis, a reaction time of 4.5h (T6) was chosen as the conversation rate is reaching a plateau after several hours.
Additionally, the peak at 3443 cm^{-1} (O-H bonds) reduced over time and eventually ceased to exist as hydroxyl groups reacted with IPDI and formed N-H bonds (3362 cm^{-1}).

The reaction time for endcap agent with three acrylates (around 4h30) is longer than for endcap with one acrylate (around 3h). This is due to the bulkier character of EPPETA compared to bisomer PEA6 which caused steric hindrance resulting in lower conversion rates.

3.1.2.2 Synthesis of PDLLA/PCL-based AUPs

The different PDLLA/PCL polymers were functionalised into AUPs. Only endcap with bisomer PEA6 was used for these materials. This means that all AUPs of PDLLA/PCL will have maximum one acrylate functionality at each chain-end. In order to increase the yield of this synthesis, a two-step synthesis (PLA/PCL12_2AUP(1); indicated by _2) was compared to a one-step synthesis (PLA/PCL11_1AUP(1); indicated by _1). Precipitations were performed in methanol. The characteristics of these materials can be found in Table 3.5. Yields were calculated by dividing the mass that was left after the synthesis by the total amount of mass added during the synthesis.

Table 3.5: Polymer characteristics for one-step and two-step syntheses

Material	**One- or two-step**	**Yield (%)**	**Molar mass NMR (kg/mol)**	**wt_{PCL} (%)**
PLA/PCL11_1AUP(1)	One-step	49	11.4	6.2
PLA/PCL12_2AUP(1)	Two-step	40	11.6	5.6

Both materials were successfully polymerised and have a similar molar mass and weight percentage of PCL. The yield differs between the two AUPs. This was expected because due to the extra step/precipitation, more material was lost during the two-step synthesis. As there is no difference in the other characteristics, further syntheses were performed in one-step to obtain higher yields and to reduce the synthesis time.

Characteristics for PDLLA/PCL-based AUPs, synthesised by a one-step synthesis, can be found in Table 3.6. One can conclude that the molar masses are relatively close to the target, except for PLA/PCL4_1AUP(1). We suspect that the dried toluene still contained some water which can cause lower molar masses as water acts as an initiator. The yields are all higher than the one of PLA/PCL12_2AUP(1), synthesised via two-step synthesis.

Table 3.6: Characteristics of PDLLA/PCL-based AUPs, synthesised under optimal conditions

Material	**Molar mass NMR (kg/mol)**	**Yield (%)**	**DS (%)**	**wt_{PCL} (%)**
PLA/PCL11_1AUP(1)	11.4	49	31.9 ± 1.1	6.24
PLA/PCL4_1AUP(1)	3.9	60	16.7 ± 1.5	4.04 ± 0.04
PLA/PCL11_1AUP(1)'	11.0	64	84.2 ± 24.3	5.45

The targeted amount of PCL (8wt%) was never reached. This finding seems to indicate that ϵ-caprolactone is less reactive than lactide. This is in agreement with literature that states that lactides have a higher coordination ability. This ability will result in a higher reactivity due to the coordination insertion mechanism of tin 2-ethylhexanoate described in Section 1.6.2.1. The two ester bonds in lactide rings, compared to one for ϵ-caprolactone, will contribute to this difference in coordination ability. [147, 148]

The degree of substitutions for PLA/PCL11_1AUP(1) and PLA/PCL4_1AUP(1) are low. This can be explained by unwanted reactions of the reactive isocyanate functionalities with components like water during storage of endcap agent in the fridge (see Figure 3.8), making them unusable to react with hydroxyl functionalities of the polymer. For that reason, endcap agent was created right before it needed to be added to the polymer to reduce the amount of side reactions. This was the case for PLA/PCL11_1AUP(1)' (indicated by '). One can conclude that the degree of substitution is significantly higher for PLA/PCL11_1AUP(1)' than the ones of PLA/PCL11_1AUP(1) and PLA/PCL4_1AUP(1). For all TPU-based and PDLLA-based AUPs, the endcap was made right before the functionalisation of the polymer backbone into an AUP.

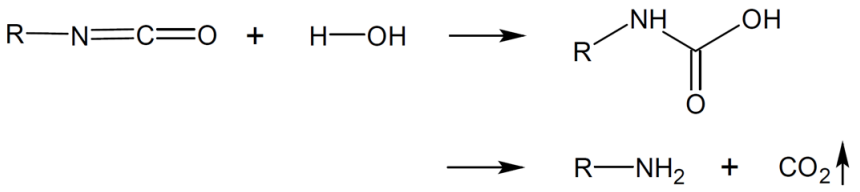

Figure 3.8: Reaction of isocyanate with water into amine and CO_2 [15]

3.1.2.3 Synthesis of PDLLA-based AUPs

The H-NMR spectra of a PDLLA-based diacrylate AUP (PLA11*AUP(1)) and hexaacrylate AUP (PLA11*AUP(3)) are shown in Figure 3.9 and Figure 3.10, respectively. The three green peaks between 5.70 ppm and 6.50 ppm indicate the presence of acrylates.

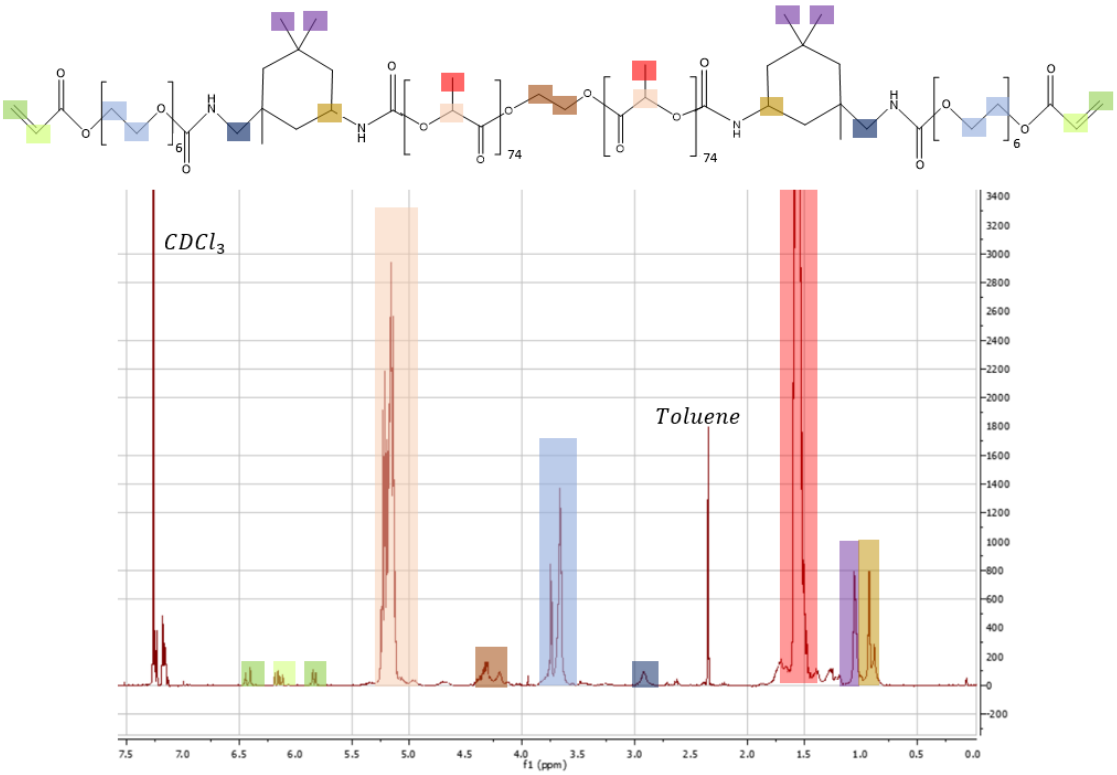

Figure 3.9: H-NMR spectrum of PLA11*AUP(1)

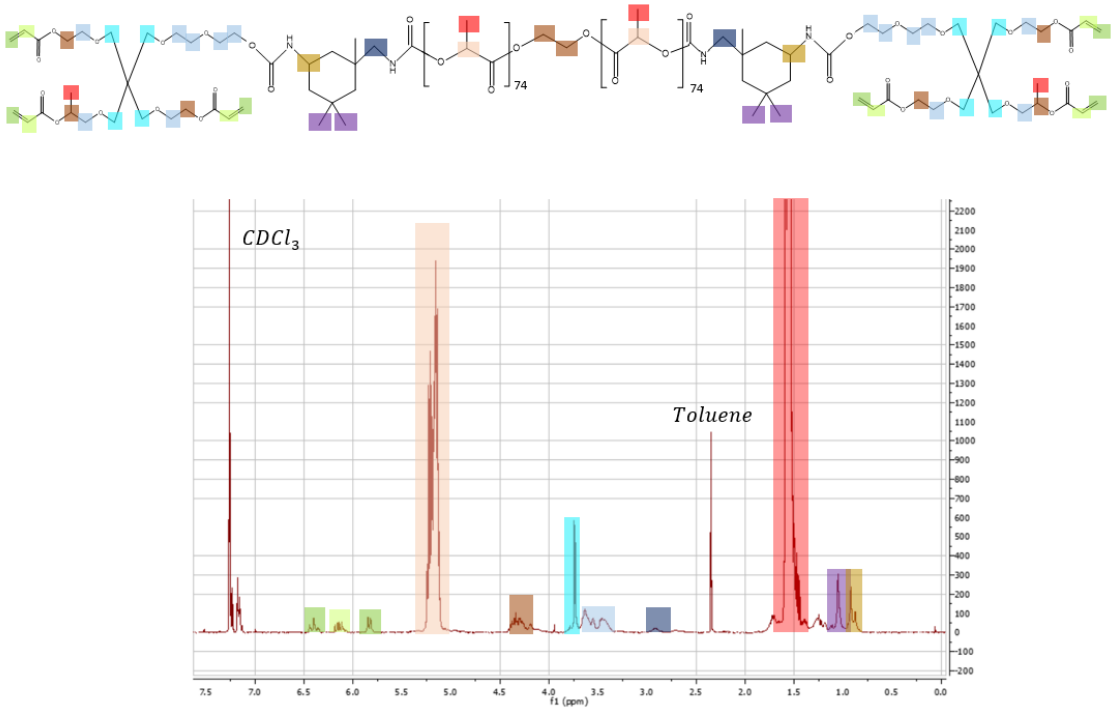

Figure 3.10: H-NMR spectrum of PLA11*AUP(3)

The remaining polymers (PLA6 and PLA13) were also functionalised into both diacrylate and hexaacrylate AUPs. The characteristics for the PDLLA-based AUPs can be found in Table 3.7.
After precipitating PLA11*AUP(3) for a second time in methanol, the acrylate density decreased tremendously, indicating that the EPPETA-based endcap did not react well with the hydroxyl functionalities of the polymer backbone. This might be declared by the 24 hours reaction time of this endcap agent as the optimal reaction time still needed to be determined. This can have resulted in undesired side reactions, such as the formation of amine by the presence of H_2O in air, that caused the low acrylate density and degree of substitution as the isocyanates could not react anymore with the hydroxyl functionalities.
For the other polymer backbones (PLA6 and PLA13), the AUPs with one acrylate functionality at each end showed an inferior acrylate density compared to the theoretical target, which means that the reaction of PDLLA with the bisomer PEA6-based endcap was not successful. We expect that the reactive isocyanate functionalities reacted with H_2O present in air.

Table 3.7: Characteristics of AUPs with PDLLA as starting material

Material	**Precipitation**	**Yield (%)**	**Acrylate density ($\mathbf{mol_{acrylates}/g_{AUP}}$)**	**DS (%)**
PLA6AUP(1)	2x MeOH	76	1.17E-04	36.7
PLA6AUP(3)	2x MeOH	55	5.96E-04	65.2
PLA11*AUP(1)	1x MeOH	37	1.19E-04	69.4
PLA11*AUP(3)	1x/2x MeOH	32	2.95E-04/1.62E-04	47.5/29.4
PLA13AUP(1)	2x MeOH	65	6.04E-05	35.9
PLA13AUP(3)	2x MeOH	52	3.57E-04	79.2

3.1.2.4 Synthesis of TPU-based AUPs

Finally, the obtained TPUs were functionalised into AUPs. TPU1 was converted into a diacrylate AUP by using bisomer PEA6 (TPU1AUP(1)), while TPU2 and TPU3 were converted into both diacrylate AUPs (TPU2AUP(1) and TPU3AUP(1)) and hexaacrylate AUPs (TPU2AUP(3) and TPU2AUP(3)). The H-NMR spectra of TPU2AUP(1) and TPU2AUP(3) are shown in Appendix C and the three peaks between 5.70 ppm and 6.50 ppm clearly indicate the presence of acrylates. The H-NMR spectra of TPU3-based AUPs are similar to the spectra of TPU2AUPs. The characteristics of the obtained AUPs (yield, acrylate density and lower limit of degree of substitution (DS*)) can be found in Table 3.8.

Table 3.8: Characteristics of TPU-based AUPs

Material	**Precipitation**	**Yield (%)**	**Acrylate density ($\mathbf{mol_{acrylates}/g_{AUP}}$)**	**DS* (%)**
TPU1AUP(1)	2x hex	86	4.51E-04	203
TPU2AUP(1)	1x hex, 1x MeOH	42	1.08E-04	60
TPU2AUP(3)	1x hex, 1x MeOH	44	3.03E-04	53.6
TPU3AUP(1)	1x MeOH	70	2.33E-04	119
TPU3AUP(3)	1x MeOH	82	5.50E-04	88

TPU1AUP(1) was precipitated twice in hexane as this non-solvent was also used by researchers at

Syracuse University for the precipitation of the thermoplastic polyurethanes. After precipitating TPU1AUP(1) twice in hexane, it was clear that a precipitation in hexane was insufficient to remove impurities. A lower limit for the degree of substitution (DS*) was estimated by assuming that the TPU chain would consist of only one PDLLA chain and one POSS monomer (approximately 8 and 10 kg/mol in total for TPU1AUP and TPU2AUP/TPU3AUP respectively). The estimated lower limit for TPU1AUP(1) was 203% which indicated that there was still quite a lot of unreacted endcap agent left. Additionally, a too high amount of endcap was left after one precipitation of TPU2AUPs in hexane. From that moment on, precipitations of TPU-based AUPs were performed in methanol. TPU3AUPs still seem to have a high lower limit for the degree of substitution. However, these materials were only precipitated once to keep the yield high as precipitations in methanol resulted in lower yields. A second precipitation in methanol will probably result in a small decrease in the lower limit.

Since the hydroxyl end groups of TPU cannot be quantified by a H-NMR spectrum due to overlap with other signals, the molar mass of the TPU chain, OH-concentration and exact degree of substitution cannot be determined.

3.1.3 Thermal properties of polymer backbones and AUPs

3.1.3.1 Thermal properties of PDLLAs and PDLLA-based AUPs

The glass transition temperature of PDLLA-based polymers was assessed by differential scanning calorimetry. Thermogravimetric analysis was performed to determine the thermal degradation temperature. A summary of the thermal characteristics of PDLLA and the related AUPs can be found in Table 3.9. No melting nor crystallisation temperature are detected as PDLLA is an amorphous polymer.

Table 3.9: Thermal properties of PDLLAs and PDLLA-based AUPs

Material	$\mathbf{T_{onset}}$**(°C)**	$\mathbf{T_g}$**(°C)**
PLA6	198	32
PLA6AUP(1)	221	39
PLA6AUP(3)	209	37
PLA11*	209	36
PLA11*AUP(1)	221	37
PLA11*AUP(3)	221	35
PLA13	202	42
PLA13AUP(1)	220	42
PLA13AUP(3)	204	39

All thermal degradation temperatures are around or above 200°C, which means that the maximum temperature used during DSC measurements should stay below this threshold of 200°C in order to avoid thermal degradation. Literature states that for long PDLLA chains (35 kg/mol), the degradation temperature is around 277°C which is higher than the synthesised polymers with shorter chains. Impurities and lower molar masses may have caused this lower degradation temperature. An overall increase in onset temperature can be seen when the polymer is

functionalised into an AUP. [21]

Figures 3.11 and 3.12 show TGA thermograms of PLA6 and its AUP forms. The curve of the polymer goes directly to zero, whereas the AUPs have an irregular curve when approaching zero weight percentage. One can conclude that endcap only degrades between 250°C and 400°C as the only difference between Figures 3.11 and 3.12 is the functionalisation of the polymer backbone into an AUP. This hypothesis is confirmed by the TGA thermograms of the endcap agents with one (bisomer PEA6) and three (EPPETA) acrylates (Figure E.3 in Appendix E). Endcap containing bisomer PEA6 starts to degrade tremendously around 303°C, while endcap with EPPETA degrades around 355°C. This explains why the thermograms only reach zero weight percentage after 400°C. The thermograms visualised in Figures E.1 and E.2 in Appendix E, show that the degradation of the endcap agents corresponds to the degradation of bisomer PEA6 and EPPETA. IPDI already degrades around 150°C, which is confirmed by literature. [149]

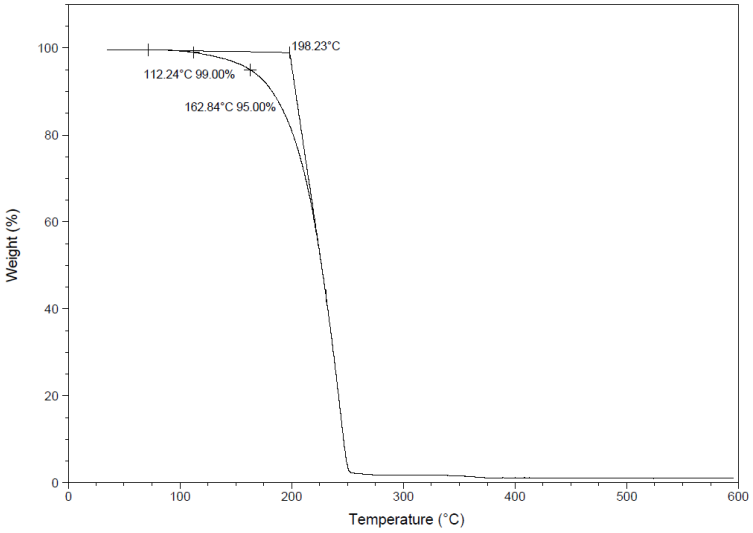

Figure 3.11: TGA thermogram of PLA6

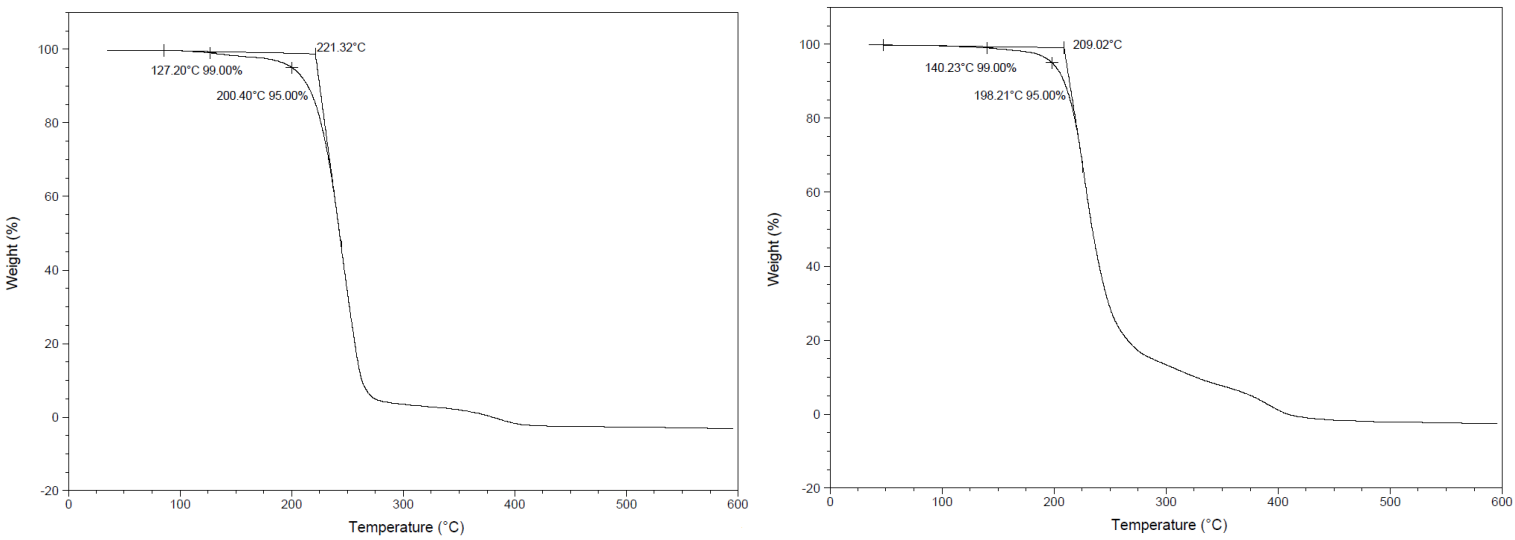

Figure 3.12: TGA thermogram of PLA6AUP(1) (left) and PLA6AUP(3) (right)

The glass transition temperatures are lower than expected as literature states that PDLLA has a T_g around 50°C. [114, 150] These lower glass transition temperatures can be the result of residual solvent like toluene, as well as unreacted monomer or endcap agent. Furthermore, we do expect that the glass transition temperature increases with increasing molar masses. Indeed, PLA6-based materials reach the rubber state at lower temperatures than PLA13-based materials.

3.1.3.2 Thermal properties of PDLLA/PCLs and PDLLA/PCL-based AUPs

The glass transition temperature of pure PDLLA can be decreased to the desired range of 30-35°C by synthesising a copolymer of PDLLA and PCL (T_g = -60°C). [151] Table 3.10 indicates that the degradation temperatures of PDLLA/PCL-based AUPs are above 200°C. Literature shows that the degradation temperatures for PDLLA (with molar mass of 35 kg/mol) and PCL (with molar mass 10 kg/mol) are around 270°C and 280°C respectively. [21, 152] The lower values, compared to literature, can be explained by impurities and lower molar masses. Furthermore, the glass transition temperatures are all close to the targeted range but lower than expected according to the Fox equation that indicated that higher wt% PCL (12-15 wt%) were needed to obtain glass transition temperatures in the desired range. The Fox equation uses high molar masses for which the increase in glass transition temperature with increasing molar mass is not significant anymore. The use of lower molar masses in this master thesis explains why lower weight percentages of PCL resulted in glass transition temperatures between 30 and 35°C.

Unfortunately, no correlation can be seen between the weight percentage of PCL and the glass transition temperature as the materials have various molar masses. The increase in weight percentage of PCL is expected to decrease the glass transition temperature. However, in this work, the copolymers with superior integration of PCL (decreasing the T_g) show the highest molar masses (increasing the T_g), resulting in minor changes in T_g between these copolymers. Additionally, converting the starting materials into AUPs does not give a significant increase or decrease in glass transition temperature.

Table 3.10: Thermal properties of PDLLA/PCLs and PDLLA/PCL-based AUPs

Material	$\mathbf{T_{onset}}$ **(°C)**	$\mathbf{T_g}$ **(°C)**	**Molar mass NMR (kg/mol)**	$\mathbf{wt_{PCL}}$ **(%)**
PLA/PCL11	216	31	11.4	6.24
PLA/PCL11_1AUP(1)	216	29	11.4	6.24
PLA/PCL4	207	30	3.9	4.04 ± 0.04
PLA/PCL4_1AUP(1)	208	34	3.9	4.04 ± 0.04
PLA/PCL11'	213	30	11.0	5.45
PLA/PCL11_1AUP(1)'	212	24	11.0	5.45

3.1.3.3 Thermal properties of TPUs and TPU-based AUPs

Figures 3.13 and 3.14 illustrate the DSC and TGA thermogram of TPU1. The thermal properties of TPUs and TPU-based AUPs can be found in Table 3.11.

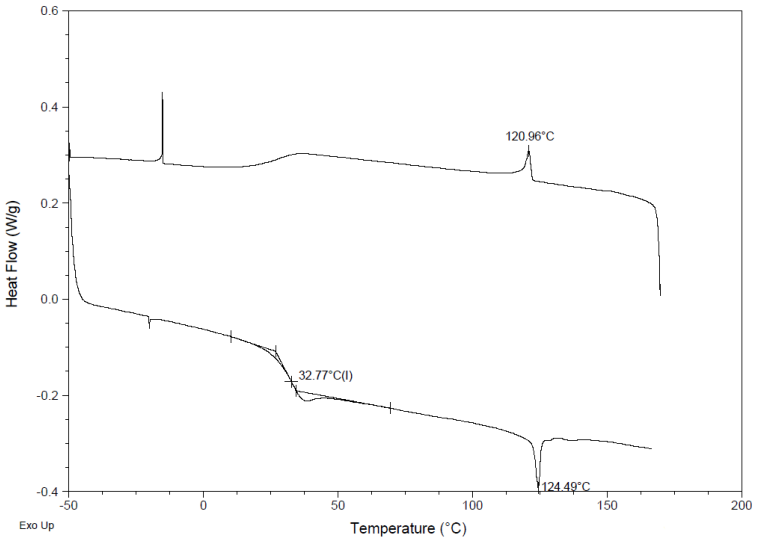

Figure 3.13: DSC thermogram of TPU1

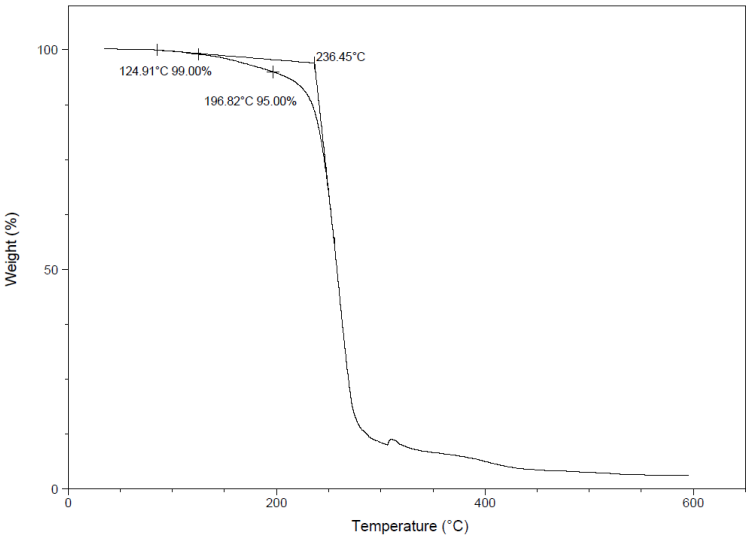

Figure 3.14: TGA thermogram of TPU1

Table 3.11: Thermal properties of TPUs and TPU AUPs

Material	$\mathbf{T_{onset}}$ **(°C)**	$\mathbf{T_g}$ **(°C)**	$\mathbf{T_{melt}}$ **(°C)**	$\mathbf{T_{cryst}}$ **(°C)**
TPU1	236	33	124	121
TPU1AUP(1)	229	47	130	/
TPU2	226	49	122	/
TPU2AUP(1)	238	43	128	/
TPU2AUP(3)	248	48	125	/
TPU3	226	46	125	/
TPU3AUP(1)	240	44	/	/
TPU3AUP(3)	246	42	130	/

Except for TPU1, which contains impurities, the onset temperature increases when the polymer is functionalised into an AUP. The degradation temperatures in Table 3.11 are in line with literature

that states that thermal degradation of TPUs start after 220°C. [153] One can observe that the curves of the TGA thermograms (Figures 3.15 and 3.16) do not go directly to zero after 275°C. This bump is due to the thermal degradation of the POSS structure. Figure 3.17 shows that pure POSS starts to degrade after 278°C and stops around 500°C. Additionally, the endcap has an influence on the degradation profile, as discussed in Section 3.1.3.1.

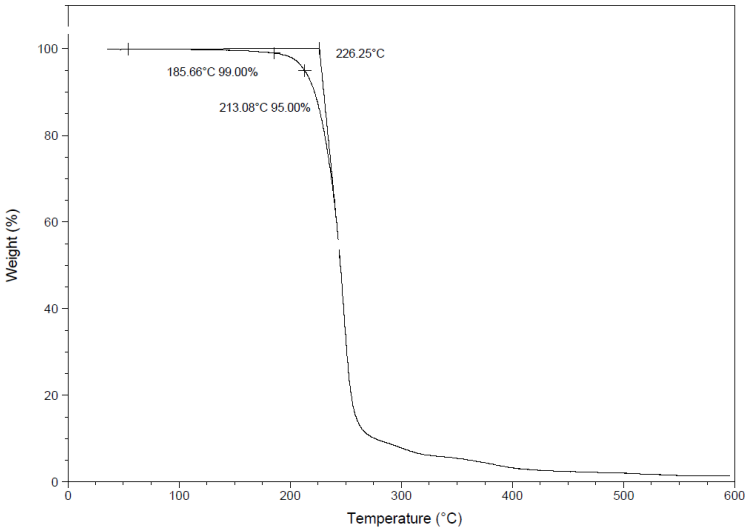

Figure 3.15: TGA thermogram of TPU3

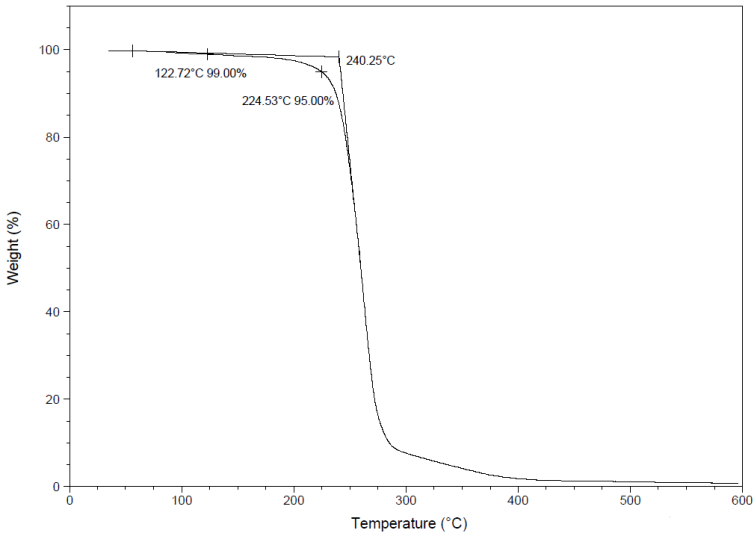

Figure 3.16: TGA thermogram of TPU3AUP(1)

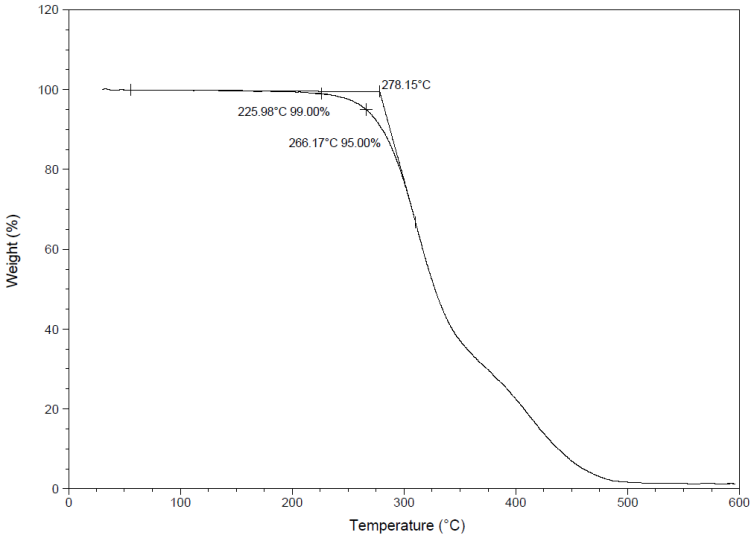

Figure 3.17: TGA thermogram of 1,2-propanediolisobutyl POSS

As TPUs are semi-crystalline materials due to the silicon cages, also melt and crystallisation peaks are visible in the DSC thermograms next to the glass transition. These peaks are clearly present for TPU1 (Figure 3.13). For the other two materials (TPU2 and TPU3) the melt and crystallisation peaks are less visible (see Figures D.1 and D.2 in Appendix D). A hypothesis for this difference is that TPU1 contains shorter PDLLA chains and thus the POSS monomers, which

are responsible for the semi-crystalline behaviour, are closer together which could result in a higher degree of crystallinity. The melt and crystallisation temperatures, respectively around 125°C and 120°C, are in line with literature which states that the melt temperature of 1,2-propanediolisobutyl POSS is around 120°C-130°C. [11, 145]

At last, the glass transition temperature is expected to be around 50°C according to literature. [145] Most TPUs and TPU-based AUPs are close to this expected glass transition temperature. TPU1 however shows a lower glass transition temperature, probably due to the presence of some monomer lactide and POSS. The presence of lactides (5.05 ppm) and POSS monomers (2.60 - 2.80 ppm) are confirmed by the H-NMR spectrum depicted in Figure C.1 in Appendix C. In general, glass transition temperatures are quite susceptible to solvents and impurities, such as residual monomer and unreacted endcap agent, which act as plasticiser and lower the glass transition temperature.

3.1.3.4 Comparison of thermal properties of obtained AUPs

The degradation temperatures of the three different materials, before and after conversion into AUPs, were examined. Comparing the starting materials via one-way ANOVA resulted in a statistically significant difference between the three groups (p-value: 0.04). In order to know which groups differ, t-tests were performed between TPU and PDLLA, TPU and PDLLA/PCL and, PDLLA and PDLLA/PCL. There was no statistical difference between PDLLA and PDLLA/PCL (p-value: 0.25), however TPU compared to PDLLA (p-value: 0.005) and TPU compared to PDLLA/PCL (p-value: 0.009) did show a statistical significance (Figure 3.18). One can conclude that the degradation temperature for TPUs is significantly higher than PDLLA and PDLLA/PCL. This confirms that including POSS results in a better thermal stability. Although more materials should be analysed to confirm this statement, literature describes that TPUs containing POSS contain a stable Si-O-Si network and the formation of microdomains results in an increase in molecular rigidity which is related to an improvement of thermal stability. [154–158]

The same conclusions can be made after conversion into AUPs. The difference in degradation temperature of TPU AUPs and both PDLLA AUPs and PDLLA/PCL AUPs is statistically significant with p-values below 0.0001 (Figure 3.18).

The increase in degradation temperature upon functionalisation into an AUP was significant for both PDLLA (p-value: 0.015) and PDLLA/POSS (p-value: 0.02). The absence of a statistical increase of PDLLA/PCL might be a result of the low degree of substitution.
There is no correlation between the molar mass, type of endcap or weight percentage PCL and the degradation temperature.

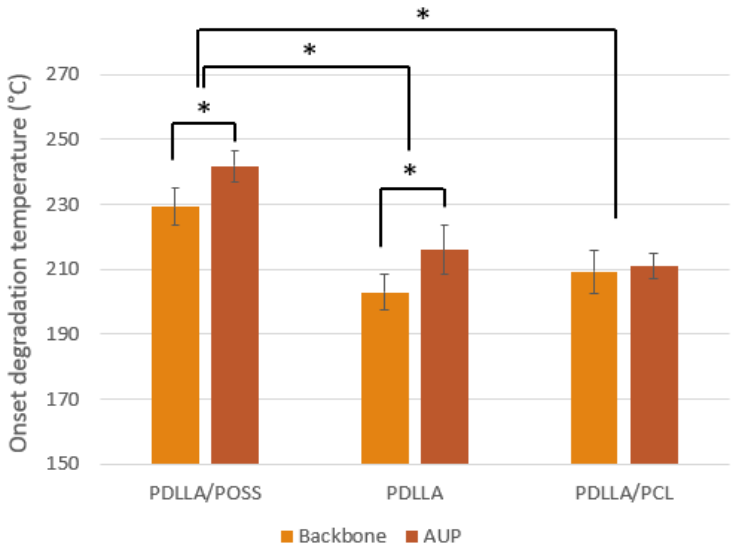

Figure 3.18: Onset degradation temperature of the obtained polymer backbones and AUPs

When investigating the glass transition temperatures of these materials (see Figure 3.19), a statistical difference is seen between PDLLA/PCL and PDLLA (p-value: 0.047), and PDLLA/PCL and TPU (p-value: 0.0038) polymers (TPU1 not included due to the influence of impurities on the glass transition temperature). The same conclusion can be drawn for AUPs. The p-values for PDLLA/PCL AUP vs PDLLA AUP and PDLLA/PCL AUP vs TPU AUP are 0.0016 and 0.0007 respectively (TPU1AUP(1) disregarded due to impurities). This proves that the addition of PCL lowers the glass transition temperature. A significantly higher glass transition temperature for TPU compared to PDLLA was expected as we assume that TPUs have higher molar masses and thus more entanglements. Knight et al. (2008) saw an increase of 6°C when the PDLLA chains were converted into thermoplastic polyurethanes. They state that the addition of POSS would lead to soft block confinement. In this master thesis, a statistical significant difference (p-value: 0.005) was observed between TPU AUPs and PDLLA AUPs (TPU1AUP(1) disregarded due to impurities) which is in line with literature (Figure 3.19). [125, 145, 159]

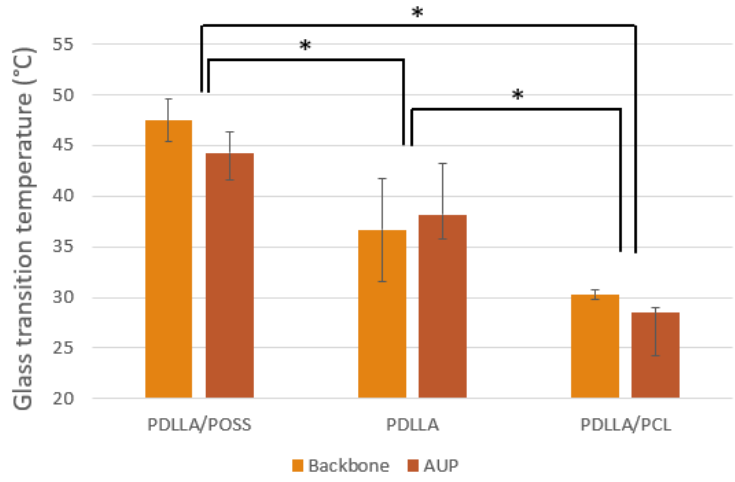

Figure 3.19: Glass transition temperature of the obtained polymer backbones and AUPs

The hypothesis of increased glass transition temperature for higher molar masses was next to the comparison of PDLLA with PDLLA/POSS also visible for PLA6 and PLA13 (see Figure 3.20). The three materials based on PLA13 (polymer backbone, AUP(1) and AUP(3)) have a higher glass transition temperature when compared to the three materials based on PLA6, due to the longer polymer chains and increased entanglements. However, more materials need to be examined before a statistical significance can be demonstrated. The low glass transition temperature for PLA6 is explained by residual toluene left in the polymer, visible in the H-NMR spectrum (Figure C.5 in Appendix C).

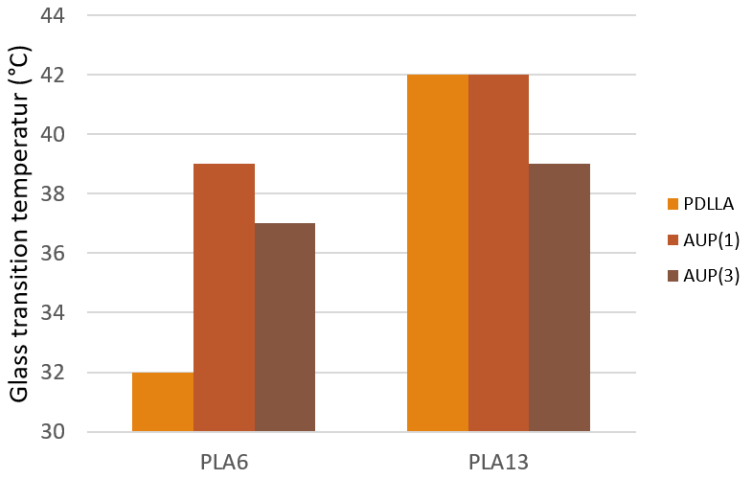

Figure 3.20: Glass transition temperatures for PLA6- and PLA13-based materials

The conversion of a polymer into an AUP does not result in a significant increase or decrease of the glass transition temperature according to the examined materials. Furthermore, no statistical difference was found between the glass transition temperatures of AUPs with bisomer PEA6 vs EPPETA.

3.2 Manufacturing of a scaffold

3.2.1 Components of the resin

The polymer resin consists of four components: the AUP as photocrosslinkable material creating the scaffold, photoinitiator to start the radical polymerisation, photoblocker to absorb the excess of light and to improve printing resolution and a solvent to create a liquid mixture.

3.2.1.1 Solvent

The solvent used for DLP printing should dissolve the different components to create a homogeneous resin and should be non-volatile to avoid evaporation during DLP printing. Four different solvents were tested, being dioxane, dimethylsulfoxide (DMSO), ethyl lactate and NMP. These solvents were chosen based on literature. [160, 161] The solubility of AUPs in these solvents was tested and visually checked. AUPs dissolved best in NMP and worst in DMSO. Additionally,

the solubility of the photoinitiator candidates (Irgacure 2959 and TPO-L) in the solvents was also investigated. Only Irgacure 2959 did not dissolve in ethyl lactate. All other combinations of photoinitiator and solvent did dissolve. The boiling points for the different solvents can be found in Table 3.12 as an indication for the volatile behaviour. In conclusion, NMP was chosen as solvent for the resins as it dissolves AUPs efficiently and has the highest boiling temperature.

Table 3.12: Boiling temperatures of the solvent candidates

Solvent	**Boiling temperature (°C)**
Dioxane	101
DMSO	189
Ethyl lactate	154
NMP	202

3.2.1.2 Photoinitiator

A photoinitiator is a component that splits into radicals when exposed to UV-light. These radicals will initiate the photopolymerisation by attacking the acrylate functionalities of the AUPs resulting in the formation of a 3D polymer network.
The choice of potential photoinitiators was again based on literature. TPO-L and Irgacure 2959 were the two potential photoinitiators that were often used in literature for biomedical applications. [161, 162] The requirements for a suitable photoinitiator in this work are its solubility in NMP (the used solvent) as well as having active absorbance in the range around 405 nm, the wavelength of the DLP printer. Both TPO-L and Irgacure 2959 dissolved in NMP. Therefore, the selection was based on their absorption spectra. These spectra were measured via UV-VIS spectroscopy and are illustrated in Figure 3.21. Different concentrations were used as the absorbance of Irgacure 2959 for lower concentrations was too high around 280 nm to measure via UV-VIS spectroscopy.

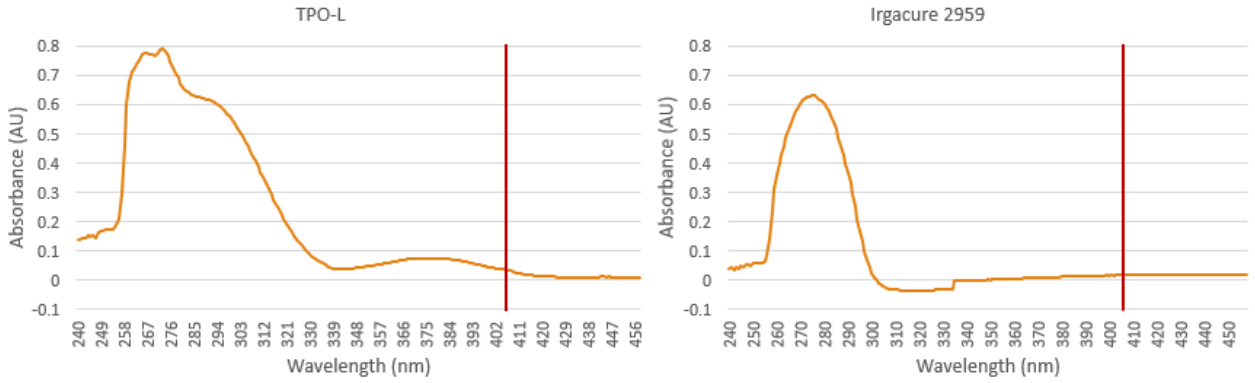

Figure 3.21: Absorption spectra of TPO-L (left, 0.01 $g_{(\mathrm{TPO-L})}/ml_{NMP}$) and Irgacure 2959 (right, 1E-05 $g_{(Irgacure2959)}/ml_{NMP}$)

One can conclude that Irgacure 2959 is active between 250 and 300 nm. This range is too low for the *LumenX* (DLP printer), which operates around 405 nm (red line). TPO-L is also active at lower wavelengths. However, it has a local maximum around 380 nm as well, resulting in an

increased absorption around 405 nm. Therefore, TPO-L was selected as photoinitiator for DLP printing with *LumenX*.

3.2.1.3 Photoblocker

Tartrazine is an active photoblocker in the area around 405 nm (Figure 1.6). [6] The active absorbance of tartrazine was examined by UV-VIS spectroscopy and the result can be seen in Figure 3.22. This spectrum shows that tartrazine is indeed active in the operating area of the *LumenX*. Additionally, tartrazine is used in the food industry as colour dye and is thus a biocompatible photoblocker with a low cytotoxicity. [163]

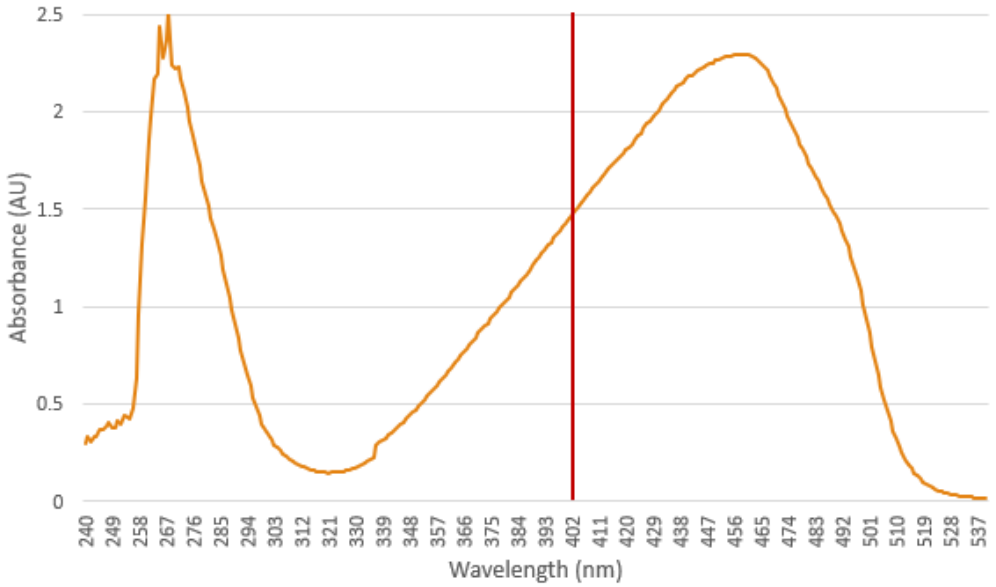

Figure 3.22: Absorption spectrum of tartrazine (1E-04 $g_{(tartrazine)}/ml_{(NMP)}$)

3.2.1.4 Acrylate-endcapped urethane-based polymers

The fourth component of the resin is the synthesised AUP. Thanks to the acrylate functionalities, the materials can be chemically crosslinked into a solid 3D network by radical polymerisation, initiated by a photoinitiator.

Initially, the crosslinking capacities of PDLLA/PCL-based AUPs were tested because of the ability to adjust the glass transition temperature by controlling the weight percentage PCL.

Different resins were made with PLA/PCL11_1AUP(1)' as this material has the highest degree of substitution. Varying weight percentages AUP (40 wt% - 70 wt%) and mole percentages photoinitiator (2, 10 and 20 mol% TPO-L) were used to test the crosslinking capacity of the resin by placing it under UVA-lamps for 30 minutes (photoblocker was not yet used for these experiments). Against all expectations, none of these resins crosslinked, implying that the acrylate density was still too low to create a solid 3D network.

There are two ways to increase the number of acrylates: by decreasing the molar mass of the polymer or by increasing the number of acrylate functionalities per polymer backbone.

PDLLA- and PDLLA/POSS-based AUPs were used for DLP printing as these materials are easier to synthesise and easier to compare due to the absence of batch-to-batch variations regarding the weight percentage of PCL. Even though the glass transition temperatures of these materials are too high, one can decrease these temperatures by adding PCL as proven in the previous section. Lowering the molar masses or using other initiators during the synthesis of the backbones like polyethylene glycol (T_g = -48°C) can also result in a decrease of the glass transition temperature. [145]
Due to the expected lower molar mass of PDLLA compared to PDLLA/POSS, a better crosslinking capacity was predicted for AUPs based on PDLLA. Table 3.7 shows that PLA6AUP(3), PLA11*AUP(1) and PLA13AUP(3) have the highest degrees of substitution and are, as a consequence, good candidates for DLP printing.

3.2.2 Optimisation of the resin

Once the different components were selected, the optimal amounts of AUP, photoinitiator and photoblocker needed to be determined. The maximum weight percentage AUP was defined based on viscosity measurements. The optimal amount of photoinitiator was determined by photorheology measurements. The desired amount of photoblocker was defined by trial-and-error during DLP printing and will be discussed in the next section (Section 3.2.3).

3.2.2.1 Viscosity

During digital light processing, the resin needs sufficient fluidity to flow homogenously over the printing area in order to print the next layer. Therefore, the resin needs to have a viscosity below three Pa.s. Both the concentration of AUP in the resin and molar mass of the polymer backbone determine the fluidity of the resin. Although a low viscosity is required for DLP printing, adding sufficient AUP is necessary to maintain the crosslinking capacity of the material. Therefore, there needs to be a balance between adding sufficient AUP, while keeping the viscosity low. The optimal amount of AUP was determined for the different materials by examining the viscosity, using a rheometer from *Anton Paar*.

Viscosity of PDLLA/POSS-based AUPs
As TPU2 and TPU3 had similar properties, only the viscosities of TPU2-based AUPs were determined by assuming that the optimal concentration AUP would be the same for TPU2 AUPs and TPU3 AUPs. TPU1AUP(1) was not used for DLP printing due to its impurities and therefore, no further research was conducted on this material.

The viscosity as a function of shear rate for TPU2AUPs is shown in Figure 3.23 for different concentrations AUP. This graph shows a decrease in viscosity with increasing shear rate. This behaviour is called shear thinning. The silica cages of POSS tend to form microdomains by self-aggregation. Physical bonds are formed resulting in a high viscosity at low shear rates. At higher shear rates, these bonds break and POSS molecules align instead of forming aggregations,

resulting in a decrease in viscosity. [164] Due to the shear thinning behaviour, it is not possible to define one single viscosity value (see Table 3.13).

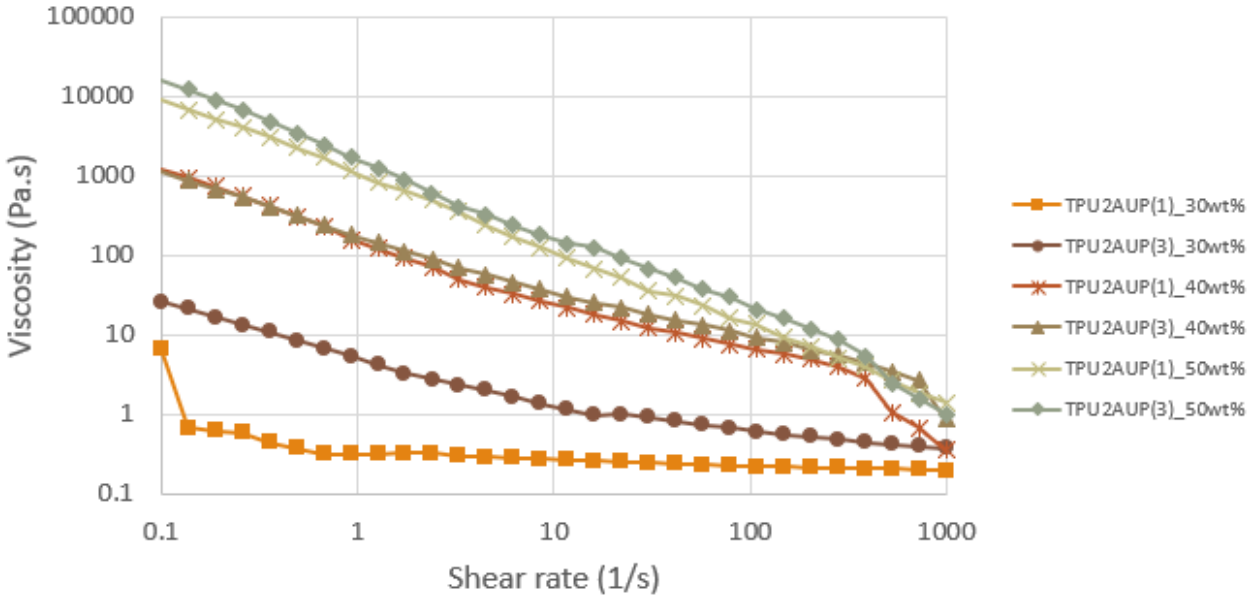

Figure 3.23: Viscosity as a function of shear rate for TPU2AUP(1) and TPU2AUP(3) for different wt% AUP

Higher AUP concentrations lead to increased viscosities as more polymer chains are present, resulting in more entanglements and less mobility. [165] Figure 3.23 shows the viscosity as a function of shear rate for resins of TPU2AUP(1) and TPU2AUP(3) with 30-40-50 wt% AUP. In order to have a good fluidity for DLP printing, resins with a weight percent of 30% need to be used as these do not cross the threshold of three Pa.s (starting from 1 1/s).
Additionally, chain-ends with EPPETA seemed to have higher viscosities compared to chain-ends with bisomer PEA6 as functionalisation of polymer backbones into AUPs with EPPETA results in higher molar masses.
The shear thinning behaviour is less explicit for the resins with 30 weight percentage AUP than for resins with higher AUP concentrations. A possible explanation is the increase in mobility due to the addition of more solvent resulting in less pronounced shear thinning behaviour. [164, 166]

Table 3.13: Viscosity (Pa.s) for different shear rates of PDLLA/POSS-based AUPs

Material	**wt% AUP**	**Viscosity (Pa.s)**			
		[0.1 - 1 (1/s)]	**[1 - 10 (1/s)]**	**[10 - 100 (1/s)]**	**[100 - 1000 (1/s)]**
TPU2AUP(1)	30	1.26	0.30	0.24	0.21
TPU2AUP(1)	40	567	61.9	13.5	3.27
TPU2AUP(1)	50	4150	407	45.2	5.64
TPU2AUP(3)	30	13.6	2.51	0.89	0.47
TPU2AUP(3)	40	547	79.5	19.3	5.06
TPU2AUP(3)	50	7060	557	77.9	8.48

Viscosity of PDLLA-based AUPs

The viscosity of PDLLA-based materials (PLA11*AUP(3)) was examined for different weight percentages of AUP (50-60-70 wt%) and the results are illustrated in Figure 3.24. Only the viscosities of AUPs with EPPETA at the chain-ends were examined as these result in a higher viscosity than their equivalents with bisomer PEA6 for similar concentrations. Therefore, if the hexaacrylate AUP stays under the threshold of three Pa.s, one can expect that the diacrylate AUP will not exceed this threshold either. The expected increase in viscosity for increasing weight percentage was confirmed as shown in the previous section. PDLLA-based AUPs do not show a shear thinning effect. Only for 70 wt% AUP, a small decrease in viscosity was observed at high shear rates. This can be explained by the fact that PLA (not in a resin) shows a shear thinning behaviour as the chains of PLA are highly entangled for low shear rates whereas by increasing the shear rate, the chains will align. [167] The increase at low shear rates for 50 wt% can indicate the presence of a small undissolved part of AUP.

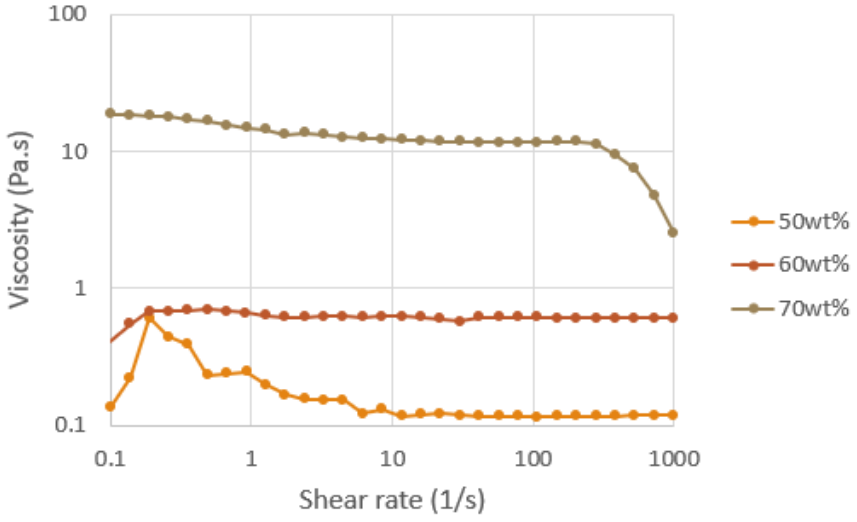

Figure 3.24: Viscosity as a function of shear rate for PLA11*AUP(3) for different weight percentages

The viscosities that can be found in Table 3.14 represent the mean viscosities of the materials between 10 and 1000 1/s as the viscosity becomes constant from a shear rate of 10 1/s onwards, except for 70 wt% AUP. The threshold of three Pa.s, which is the upper limit for DLP printing, was exceeded for 70 wt% AUP. In this respect, 60 weight percentage would be ideal to create a good flow and still have enough material to crosslink. However, by inspecting the resins of 60 weight percentage visually, one could conclude that the resin might not have sufficient fluidity to refill the printing area despite the low viscosity of 0.61 Pa.s. This low viscosity might be the result of an inhomogeneous resin of 60 wt% AUP, for which a too liquid part was used for rheology measurements. Therefore, weight percentages of 50% were chosen for the resin development. Additionally, this lower weight percentage was also chosen to obtain sufficiently low viscosities for other PDLLA AUPs with higher molar masses (such as PLA13AUP).

Table 3.14: Viscosity (Pa.s) for different weight percentages PLA11*AUP(3)

Material	**wt_{AUP} (%)**	**Viscosity (Pa.s)**
PLA11*AUP(3)	50	0.12 ± 0.0016
PLA11*AUP(3)	60	0.61 ± 0.011
PLA11*AUP(3)	70	10.2 ± 2.97

This was confirmed for PLA6AUP(1) and (3) as well as PLA13AUP(1) and (3). These resins show a good fluidity and a sufficiently low viscosity for a concentration of 50 wt%.

Although it's not possible to compare AUPs based on PDLLA and PDLLA/POSS due to the unknown molar mass and shear thinning behaviour of PDLLA/POSS, one can still conclude that the viscosities for PDLLA-based AUPs seem to be lower than PDLLA/POSS-based AUPs. Semi-crystalline materials like PDLLA/POSS have a more organised structure due to the microdomains, which results in stronger intermolecular forces that will decrease the mobility and increase the viscosity. The effective high molar masses for PDLLA/POSS-based AUPs might also declare the increase in viscosity due to more chain entanglements. [159]

3.2.2.2 Crosslinking capacity

The crosslinking capacity was examined by photorheology. The storage and loss moduli of different materials were examined upon UV exposure. As these resins are liquid mixtures, their loss moduli are higher than the storage moduli before exposure to UV-light. Once the light is turned on, the material starts to crosslink and the storage moduli become higher than the loss moduli. The UV-light used during these measurement has a wavelength around 365 nm. Although this light operates at a lower wavelength than the UV-source of the DLP printer (405 nm), photorheology measurements could be performed as the photoinitiator (TPO-L) is also active in this range (see Figure 3.21). The resins used during these measurements did not contain photoblocker.

Photorheology measurements enabled to determine the optimal amount of photoinitiator in the resin. Several TPO-L concentrations were tested, expressed as mol% of the amount of acrylates in the resin. The photoinitiator concentration must be high enough in order to obtain efficient crosslinking but not too high to avoid termination reactions. For efficient DLP printing, crosslinking needs to occur within seconds. On the other hand, high concentrations of photoinitiator are cytotoxic as the photoinitiator forms radicals after being exposed to UV-light and these radicals can cause apoptosis of cells. For these reasons, a threshold needed to be found. [168, 169]

The optimal mol% TPO-L needed for efficient crosslinking was examined by comparing four different resins with 2, 10, 20 and 50 mol% photoinitiator. This was tested for TPU1AUP(1) (70 wt%). For all resins, the storage moduli surpass the loss moduli which indicated that crosslinking did occur. Figure 3.25 illustrates the photocrosslinking and allows to compare the crosslinking speed of the different resins. The slope of the storage modulus curved with increasing amount of TPO-L. This indicated that higher photoinitiator concentrations resulted in faster photopolymerisation. However, the photoinitiator concentration can't be too high due to cytotoxic effects and termination reactions. The moment where the modulus reached approximately 97% of the total increase (plateau value), was determined to enable proper comparison of the resins. For

50 mol% TPO-L, 97% was reached after ten seconds, while resins with 2, 10 and 20 mol% needed respectively 68, 40 and 25 seconds to reach this level. As an increase in initiator concentration from 2 to 10 mol% has the greatest influence on the crosslinking speed, the optimal amount of TPO-L was chosen to be 10 mol%. The storage moduli differ after crosslinking for different TPO-L concentrations. 2 mol% TPO-L might have been insufficient to have adequate crosslinking which resulted in a lower modulus than 10 mol% TPO-L. Additionally, the too high amount of photoinitiator (20 and 50 mol% TPO-L) resulted in more and faster termination reactions due to the presence of a high amount of radicals leading to a lower storage modulus.

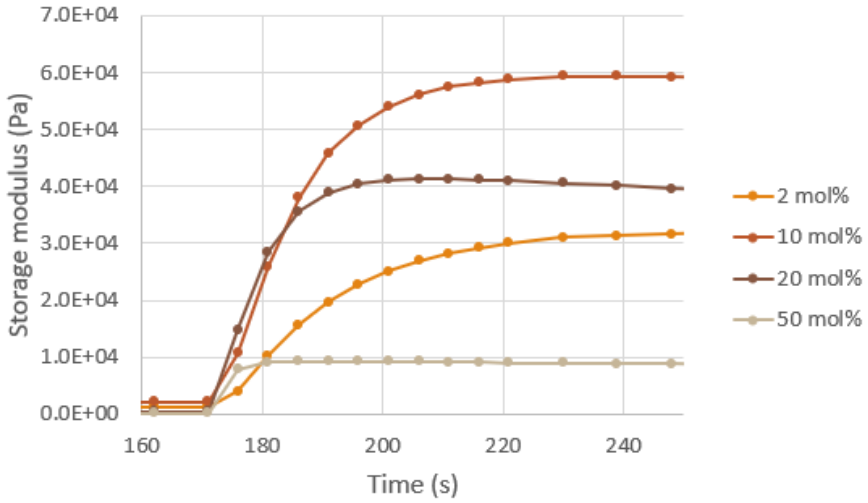

Figure 3.25: Storage modulus for resins with 70 wt% TPU1AUP(1) and different amounts of photoinitiator (2, 10, 20 and 50 mol%) as a function of time upon UV exposure

This optimal amount of TPO-L was also obtained for PLA11*AUP(1). Three resins of this polymer were made with 2, 10 and 20 mol% TPO-L and 60 weight percentage AUP. The photorheology measurement for 2 mol% TPO-L showed no increase in storage modulus and no gel point, so we can conclude that no crosslinking occurred (see Figure F.1 in Appendix F). When the amount of photoinitiator was increased to 10 mol%, crosslinking of the material was obtained. Figure 3.26 shows that the storage modulus increases after UV exposure and surpasses the loss modulus. The small decrease after the peak can be explained by relaxation of the polymer. [139] Finally, resins with PLA11*AUP(3) were tested for different amounts of TPO-L. Unfortunately, no crosslinking behaviour was observed, not even with 50 mol% photoinitiator, due to the low degree of substitution.

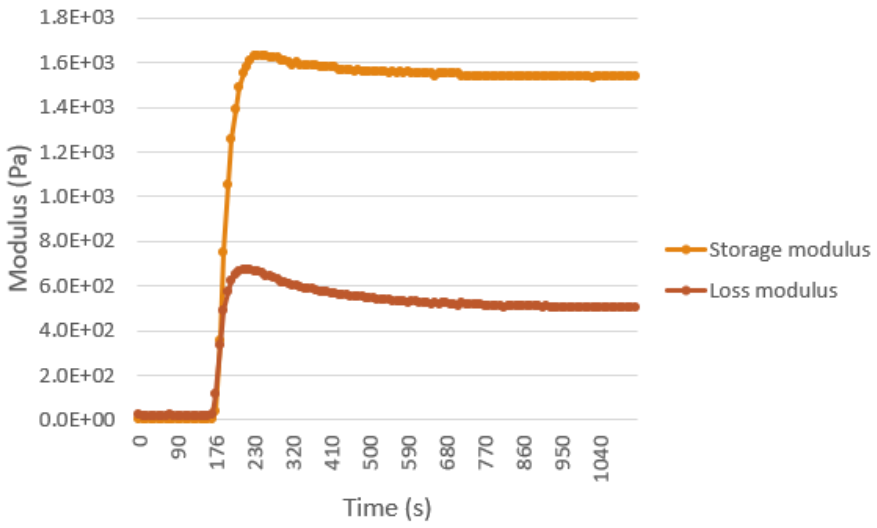

Figure 3.26: Storage (orange) and loss (brown) moduli of a resin with 60 wt% PLA11*AUP(1) and 10 mol% TPO-L as a function of time during UV irradiation

In order to compare different materials (for example in view of cell assays), the amount of initiator was redefined as a weight percentage of AUP. The chosen value was based on previously described findings and on literature. Literature shows that weight percentages of TPO-L between one and two were successfully used for digital light processing. [170–172] For different weight percentages in this range, the corresponding mole percentages were calculated to verify if the minimal mol% is still close to the optimal 10 mol%, found above. Of all materials, PLA6AUP(3) has the highest acrylate density and will therefore have the lowest mol% TPO-L for equal weight percentages. Using 1.5 wt% TPO-L for PLA6AUP(3) resulted in a photocrosslinkable resin with 7.7 mol% TPO-L. The crosslinking capacity was examined and confirmed by photorheology (Figure F.2 in Appendix F). All other materials had a mol% above ten for this constant weight percentage TPO-L. From now on, all resins were made with 1.5 wt% TPO-L.
The crosslinking capacity of other promising materials with 1.5 wt% TPO-L was examined. Photorheology results showed the crosslinking capacity of PLA13AUP(3) (Figure F.3 in Appendix F).
Additionally, TPU3AUP(1) and TPU3AUP(3) were examined and TPU3AUP(1) did not show any crosslinking activity while TPU3AUP(3) did. One can conclude that for this material, the use of endcap with three acrylates is crucial to obtain crosslinking. However, resins with TPU1AUP(1) did form a crosslinked network upon UV exposure. This might be explained by a difference in molar mass or degree of substitution. Unfortunately, these can not be calculated due to overlapping signals on the H-NMR spectra.

3.2.3 Optimisation of the printing conditions

Once the wt% AUP and photoinitiator were found, the optimal conditions for DLP printing were investigated. To this end, the material with the greatest potential for DLP printing purposes was used. PLA6AUP(3) showed the best crosslinking capacity, having the highest acrylate density and degree of substitution, due to the low molar mass and use of EPPETA.

The *LumenX* printer, from the company *Cellink*, was used as DLP printer during this project. *LumenX* has a projection power output between 10 and 40 mW/cm^2 at a wavelength of 405 nm. The printer has a resolution in the XY-direction of 50 µm and a resolution of 5 µm in the Z-direction.

First, resin was made out of 50 wt% PLA6AUP(3), 1.5 wt% TPO-L (compared to the amount of AUP) and a 0.1 molar ratio of photoblocker to photoinitiator. The latter was chosen based on previous experiences in the research group and needed to be optimised further. One droplet of this resin was placed on the petridish of the DLP printer to have an initial idea about the exposure time. For an intensity of 19.51 mW/cm^2, the droplet was fully crosslinked after approximately 15 seconds. Subsequently, a scaffold was printed with an intensity of 19.51 mW/cm^2 and an exposure time of 20 seconds. After printing, the scaffold was washed with acetone to remove residual, uncrosslinked resin. Figure 3.27 (left) shows that it was possible to print a scaffold with this composition. However, the resolution was not optimal due to overcuring so further optimisation steps were needed. The same conditions were used to try to create a scaffold with PLA13AUP(3). These conditions did not result in the formation of a scaffold (see Figure 3.27 (right)). This confirmed that PLA6AUP(3) has a better crosslinking capacity than PLA13AUP(3).

Figure 3.27: DLP printed scaffolds of PLA6AUP(3) (left) and PLA13AUP(3) (right) with an intensity of 19.51 mW/cm^2, exposure time of 20 seconds, 1.5 wt% TPO-L and molar ratio PB/PI of 0.1

Resins with different molar ratios of photoblocker compared to photoinitiator were printed with an intensity of 19.51 mW/cm^2 and exposure time of 20 seconds. Increasing the amount of photoblocker resulted in a better resolution. At the same time, this increase led to incomplete scaffolds (for PB/PI of 0.135 and 0.15). In these cases, we assume that the photoblocker absorbed too much of the UV-light resulting in fewer initiating reactions. This was confirmed by literature. [173] For a molar ratio of 0.2, the amount of photoblocker was so high that no scaffold was formed at all. For this reason, a molar ratio PB/PI of 0.125 was chosen as most optimal amount of photoblocker.

Furthermore, the intensity and exposure time can be adapted in order to obtain optimal printing conditions. Figure 3.28 shows that an exposure time of 20 seconds and intensity of 19.51 mW/cm^2 resulted in overcuring as the struts of the scaffold were not well delineated. Decreasing the exposure time up to five seconds and increasing the intensity to 40 mW/cm^2 resulted in better resolutions. However, further optimisation is still needed as there are still no clear pores in the scaffold.

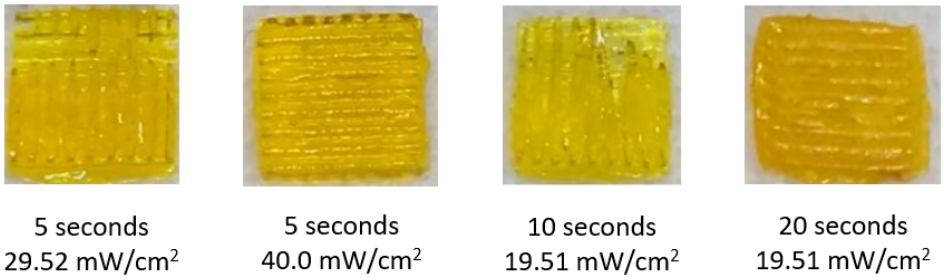

Figure 3.28: DLP printed scaffolds of PLA6AUP(3) with different intensities and exposure times for a molar ratio PB/PI of 0.125

3.2.4 Characterisation of the scaffolds

Different material properties were investigated, considering the fact that these materials will be used (after optimisation) for breast reconstruction purposes. The gel fractions of different materials were determined in order to have an indication about the crosslinking effectiveness. The swelling of the scaffold, when it comes in contact with body fluids, was mimicked by immersing crosslinked discs in DPBS. This characteristic is reported as the swelling ratio. Furthermore, the effect of leaching components on the viability and proliferation of cells was investigated by live/dead staining and MTS assays respectively. Finally, the shape memory behaviour was tested as proof of concept.

3.2.4.1 Gel fraction

From the photorheology measurements of TPU1AUP(1), one decided that 10 mol% photoinitiator was sufficient for efficient crosslinking (see Section 3.2.2.2). The gel fractions of this material were determined for 10 mol% and 20 mol% photoinitiator, to see if an increase in photoinitiator would improve the crosslinking effectiveness. The gel fractions for 10 mol% and 20 mol% TPO-L were respectively 45.6% and 45.2%. This means that there is no significant difference between these two mole percentages photoinitiator in terms of amount of crosslinked material. This supports the previous conclusion that approximately 10 mol% photoinitiator is sufficient for crosslinking. McElroy et al. (2014) concluded that there is an increase in gel fraction for increasing amount of photoinitiator. However, once an efficient amount of photoinitiator is found, the gel fraction remains constant upon further increase. This is in accordance with the results found in this master dissertation. [174]
One should be careful by making conclusions based on these data as small parts of the material have gone lost during this process by sticking to the vials. Therefore, these gel fraction results should be used for relative purposes only, by comparing them amongst each other instead of using the absolute values. These measurements were done in threefold.

The gel fractions of other materials, with sufficient crosslinking capacity, were also calculated (see Figure 3.29). These resins consisted of 1.5 wt% TPO-L.

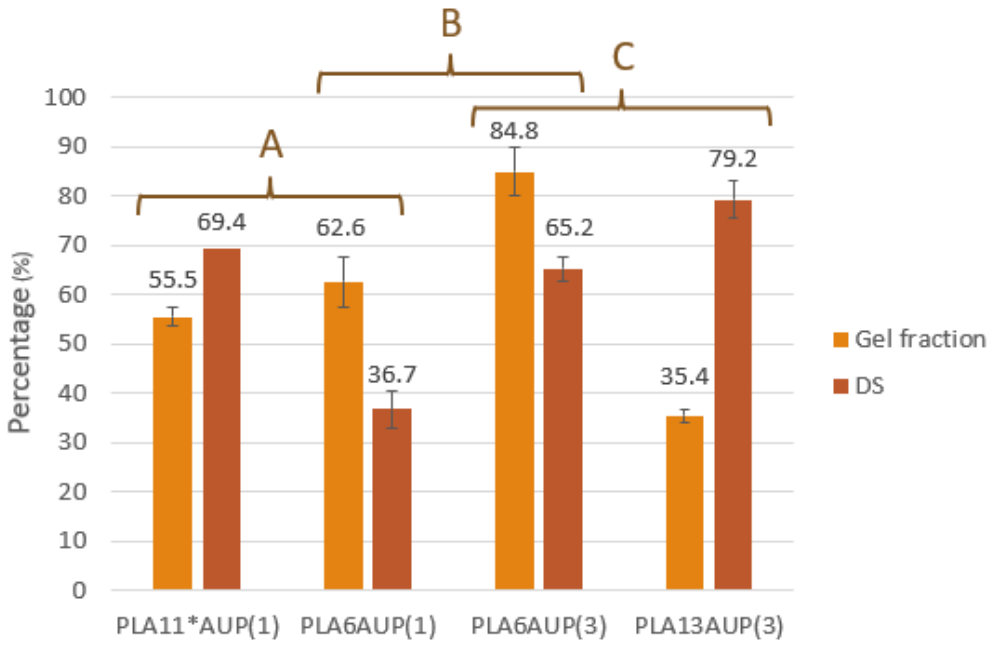

Figure 3.29: Gel fraction (orange) and degree of substitution (brown) of different AUPs based on PDLLA

The gel fraction (orange) is highest for PLA6AUP(3) as this material had the best crosslinking capacity for DLP printing due to the low molar mass and the use of endcap with EPPETA. PLA13AUP(3) has a lower gel fraction for a similar degree of substitution. This can be explained by its lower acrylate density due to the higher molar mass. Radicals will thus have more difficulties with finding an acrylate to react with (C in Figure 3.29). [175]
In case of PLA6AUP(1) more material was leached out during the immersion in THF than PLA6AUP(3), due to its lower degree of substitution and therefore a higher amount of chain-ends without an acrylate functionality was present. Having one acrylate at each end of the chain instead of three results in a decrease in gel fraction of 22% (B in Figure 3.29). Yildiz et al. (2012) confirmed that an increase in acrylate content (for styrenic macroinimers) results in a decrease in gel fraction. [175]
PLA11*AUP(1) has a similar gel fraction as PLA6AUP(1) due to the similar acrylate densities (A in Figure 3.29).

The degree of substitution and molar masses were not known for TPU3AUP(3). We can expect that the molar mass will be higher than PDLLA AUPs as similar TPUs from Syracuse University have molar masses between 20 and 40 kg/mol. [145] This can (partially) explain the lower gel fraction (42.4% $\pm$ 1.76). The gel fraction of TPU3AUP(3) is slightly lower than TPU1AUP(1) (45.6%). The increase in gel fraction due to the use of EPPETA for TPU3AUP(3) was counteracted by the higher molar mass resulting in similar gel fractions for TPU3AUP(3) and TPU1AUP(1).

3.2.4.2 Swelling ratio

The swelling ratio can give a first indication of the swelling behaviour of the scaffold upon implantation into the patient's breast. In case of significant swelling, the size of the scaffold needs to be adapted to avoid excessive pressure on the patient's breast. The results can be found in Figure 3.30.

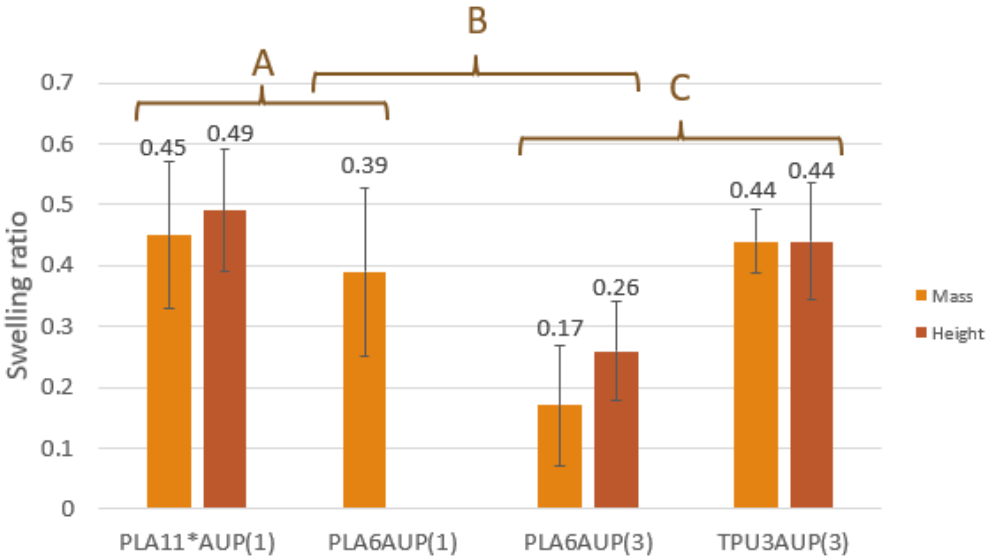

Figure 3.30: Swelling ratio determined by mass (orange) and height (brown) of different AUPs based on PDLLA in DPBS

Next to the gel fraction, the swelling ratio is also related to the acrylate density and thus on the type of endcap agent, the degree of substitution and the molar mass. This dependency on crosslinking density was also found in literature. [175, 176] The swelling ratios were calculated by comparing the mass during the swollen state and the dry state (after swelling). The same was done by comparing the heights and the diameter of the discs. As these discs were not perfectly circular, the swelling ratios, calculated by the diameter, did not give accurate results. Figure 3.30 shows that the swelling ratios calculated by mass and height are quite similar. The swelling ratio by mass is considered as the most accurate measuring method.

The efficient crosslinking of PLA6AUP(3) is confirmed by its low swelling ratio due to the formation of a dense 3D network. Petchsuk et al. (2012) obtained swelling ratios above 0.54 for crosslinked poly(lactic acid-co-glycidyl metacrylate). [177] Aliphatic urethane diacrylate oligomers synthesised by Canak et al. (2016) had swelling ratios above 0.21. [178] These findings confirm the low swelling ratio of PLA6AUP(3) (0.17). Changing the endcap from three to one acrylate (PLA6AUP(1)) resulted in an increase in swelling due to the lower crosslinking density. This increase is reinforced by the lower degree of substitution (B in Figure 3.30). Due to similar reasons as described in the previous section, the swelling ratio of PLA11*AUP(1) is in the same range as PLA6AUP(1). The difference in degree of substitution and molar mass will counteract which leads to similar swelling ratios. (A)
The (expected) high molar mass of TPU3AUP(3) resulted in a higher swelling ratio compared to PLA6AUP(3). The effect of the degree of substitution is not known as the DS of TPU3AUP(3)

cannot be determined. (C)

3.2.4.3 In vitro biological evaluation

The results of the live/dead viability and MTS assays are shown in Figure 3.31 with a tissue culture plate (TCP) as positive control. All materials have a cell viability above 70% which indicates, according to the ISO standard 10993, that they are all biocompatible. The morphology of the ASCs (Figure 3.32) looks normal for all materials except for TPU3AUP(3) (for day three (D3) and day seven (D7)). These morphological changes are correlated with a statistically significant decrease in cell viability (p-values: <0.0001) and in metabolic activity (p-values below 0.01) (Figure 3.31). A possible explanation for this decrease is the low gel fraction (42.4%). Despite the immersion of the material in acetone and an ethanol solution for sterilisation, some residual cytotoxic components might have leached out of the discs into the culture medium as there is still an effect on the metabolic activity. At day seven, a slightly lower metabolic activity was found for PLA13AUP(3), which can be correlated again with a lower gel fraction (35.4%). In general, it seems that materials with lower gel fractions have a decreased metabolic activity.

The biocompatibility of PDLLA-based AUPs is in accordance with literature that states that polylactic acid is biocompatible. Li et al. (2015) demonstrated the biocompatibility of PDLLA films with kidney epithelial cells. [179]

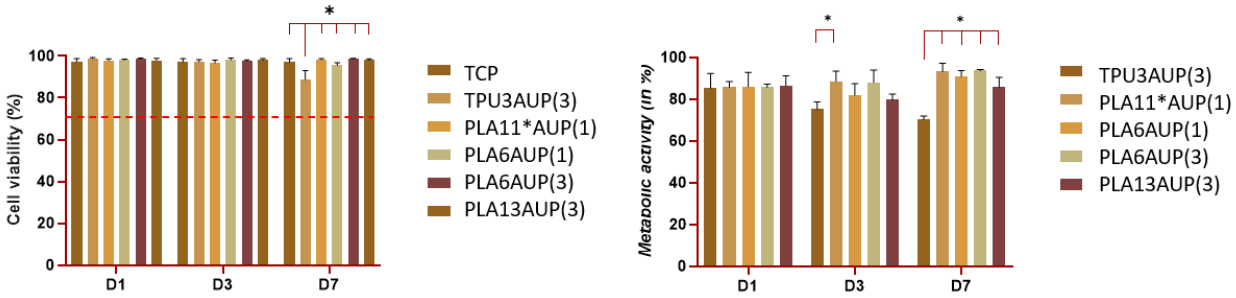

Figure 3.31: Cell viability (left) and metabolic activity (right) obtained via live/dead and MTS assays for different materials

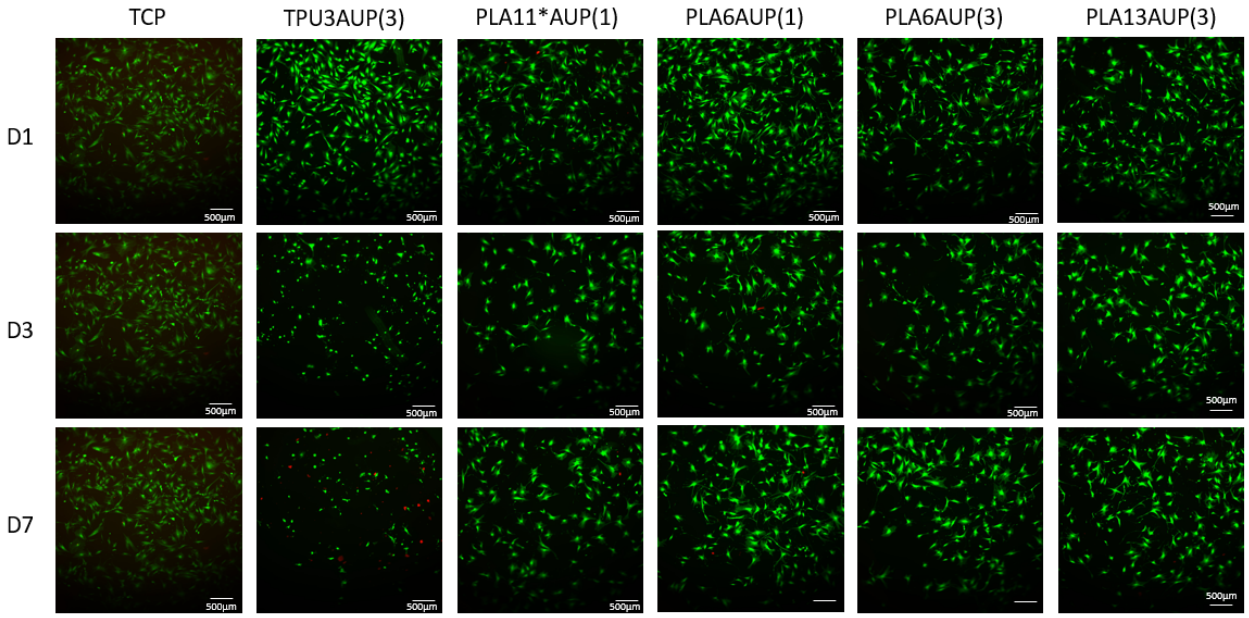

Figure 3.32: Results of live/dead viability assays

3.2.4.4 Shape memory effect

As a proof of concept, the shape memory behaviour of a scaffold (created from a resin with 50 wt% PLA6AUP(3), 1.5 wt% TPOL and a molar ratio PB/PI of 0.125) was investigated. To this end, two scaffolds were heated above the glass transition temperature by immersion in warm water (around 100°C). Next, the scaffolds were deformed into a folded shape and cooled down below their glass transition temperature by placing them in a freezer for a couple of minutes. Then, one scaffold was placed in cold water and the other in water around body temperature. Upon immersion in water, the deformed scaffold in the water at room temperature did barely change in shape, whereas the other scaffold unfolded back into its original shape within seconds. Figures 3.33 and 3.34 show the scaffolds before and after they were put in cold water or water around 37°C. The recovery to the original shape of the scaffold in water around body temperature proves the shape memory effect of the scaffold.

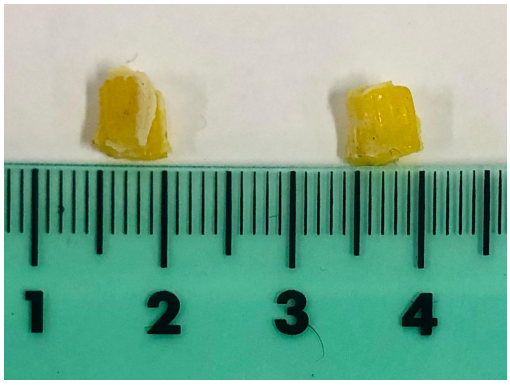

Figure 3.33: Deformed scaffolds before immersion in water

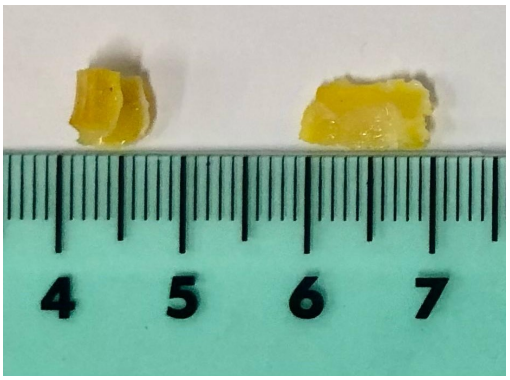

Figure 3.34: Scaffolds after immersion in cold water (left) and water at body temperature (right)

4. Conclusion and future work

In this master dissertation, the development of a scaffold with shape memory effect right below body temperature was examined for the purpose of minimally invasive breast reconstructions. PDLLA/POSS-based AUPs show great potential as material for the scaffold due to the many advantages like thermal stability, expected biodegradability and mechanical properties by combining amorphous, organic PDLLA with semi-crystalline, inorganic POSS. However, the glass transition temperature of this polymer is too high to have a shape memory effect triggered by the body temperature. Studies with PDLLA-and PDLLA/PCL-based AUPs showed that addition of PCL can lower the glass transition temperature towards the targeted range. Additionally, decreasing the molar mass should result in lower glass transition temperatures. This effect was seen in this master dissertation, however, more materials need to be compared to prove the statistical significance. TGA measurements indicated that the addition of POSS enhanced the thermal stability of the AUP. Moreover, conversion of the starting materials into AUPs resulted also in higher degradation temperatures.

Resins for DLP printing consisting of a PDLLA-based AUP with a low molar mass and three acrylates functionalities at the chain-ends resulted in an increased crosslinking capacity. Additionally, this resin also includes TPO-L as photoinitiator, tartrazine as photoblocker and NMP as solvent to form a homogeneous substance. During rheology measurements, the maximum AUP concentration resulting in sufficient fluidity to homogeneously refill the printing area was determined. The concentrations for PDLLA/POSS-based and PDLLA-based AUPs were 30 wt% and 50 wt% respectively. The higher molar masses and the inclusion of POSS monomers, which decreases the mobility, made it inconvenient to use higher concentrations TPU AUPs. Photorheology showed that 10 mol% TPO-L was ideal to initiate the radical photopolymerisation. The optimal amount of photoblocker for PLA6AUP(3) was investigated by trial-and-error during DLP printing and turned out to be a molar ratio of 0.125 PB/PI as higher ratios resulted in incomplete scaffolds. The optimal exposure time and intensity need to be further optimised to create adequate porosity.

For the final application, one should keep in mind that the scaffold might swell in the aqueous environment of the body. This swelling should not cause additional pressure on the surrounding tissues. A first indication of this swelling was obtained by measuring the swelling ratio. Less swelling was observed in materials with better crosslinking capacities. The material with the best crosslinking capacity turned out to be PLA6AUP(3) due to the high acrylate density and low molar mass. This was confirmed by photorheology, gel fraction and DLP printing tests. By conducting in vitro biological evaluations, the biocompatibility of the materials was examined. All materials were biocompatible according to ISO standard 10993. However, TPU3AUP(3) seemed to cause adverse morphological changes, which might be the result of leaching components. Eventually, the shape memory effect of the scaffolds was demonstrated as a proof of concept.

This master dissertation was the beginning of the development of a scaffold for minimally invasive breast reconstruction. Next to the future perspectives that were mentioned in previous sections, further research can still be conducted. An important aspect of the scaffold, that was not yet tested during this project, consists of the mechanical properties. Moreover, quantitative studies on shape memory behaviour should be conducted with dynamic mechanical thermal analysis (DMTA) and biodegradability and direct cell assays should be performed. Furthermore, the possible effect of crosslinking on the glass transition temperature needs to be examined. There is still a lot of research that needs to be conducted before these scaffolds can move to small animal experiments.

Bibliography

[1] University of Iowa Health care, "Breast reconstruction after cancer treatment — University of Iowa Hospitals Clinics," 2019. [Online]. Available: https://uihc.org/health-topics/breast-reconstruction-after-cancer-treatment

[2] A. U. Daniels, "Silicone breast implant materials," jul 2012.

[3] A. Aydiner, A. Igci, and A. Soran, *Breast disease: Diagnosis and pathology.* Springer International Publishing, jan 2015, vol. 1.

[4] C. M. Murphy, F. J. O'Brien, D. G. Little, and A. Schindeler, "Cell-scaffold interactions in the bone tissue engineering triad," pp. 120–132, sep 2013.

[5] M. V. Varma, B. Kandasubramanian, and S. M. Ibrahim, "3D printed scaffolds for biomedical applications," *Materials Chemistry and Physics*, vol. 255, p. 123642, nov 2020.

[6] Y. Yang, Y. Zhou, X. Lin, Q. Yang, and G. Yang, "Printability of external and internal structures based on digital light processing 3D printing technique," *Pharmaceutics*, vol. 12, no. 3, mar 2020.

[7] S. M. Hasan, L. D. Nash, and D. J. Maitland, "Porous Shape Memory Polymers: Design and Applications," *J. Polym. Sci., Part B: Polym. Phys*, vol. 54, pp. 1300–1318, 2016.

[8] C. Liu, H. Qin, and P. T. Mather, "Review of progress in shape-memory polymers," *Journal of Materials Chemistry*, vol. 17, no. 16, pp. 1543–1558, apr 2007.

[9] "Fibers for medical applications," 2011. [Online]. Available: https://nptel.ac.in/content/storage2/courses/116102006/module6/chapter6.1.html

[10] P. VanWouwe, M. Dusselier, E. Vanleeuw, and B. Sels, "Lactide Synthesis and Chirality Control for Polylactic acid Production," *ChemSusChem*, vol. 9, no. 9, pp. 907–921, may 2016. [Online]. Available: http://doi.wiley.com/10.1002/cssc.201501695

[11] "AL0130 - 1,2-Propanediollsobutyl POSS." [Online]. Available: https://hybridplastics.com/product/al0130-12-propanediollsobutyl-poss/

[12] S. Wendels and L. Avérous, "Biobased polyurethanes for biomedical applications," pp. 1083–1106, apr 2021.

[13] Q. Guo, P. T. Knight, and P. T. Mather, "Tailored drug release from biodegradable stent coatings based on hybrid polyurethanes," *Journal of Controlled Release*, vol. 137, no. 3, pp. 224–233, aug 2009. [Online]. Available: https://pubmed.ncbi.nlm.nih.gov/19376173/

[14] A. Houben, P. Roose, H. Van den Bergen, H. Declercq, J. Van Hoorick, P. Gruber, A. Ovsianikov, D. Bontinck, S. Van Vlierberghe, and P. Dubruel, "Flexible oligomer spacers as the key to solid-state photopolymerization of hydrogel precursors," *Materials Today Chemistry*, vol. 4, pp. 84–89, jun 2017.

[15] "Isocyanate Reactions." [Online]. Available: https://polymerdatabase.com/polymerchemistry/Urethanes.html

[16] M. Rezai, M. Darsow, S. Kümmel, and S. Krämer, "Autologous and alloplastic breast reconstruction - Overview of techniques, indications and results," pp. 68–75, apr 2008.

[17] P. G. Cordeiro, "Breast reconstruction after surgery for breast cancer," *New England Journal of Medicine*, vol. 359, no. 15, pp. 1590–1601, oct 2008.

[18] S. Farah, D. G. Anderson, and R. Langer, "Physical and mechanical properties of PLA, and their functions in widespread applications — A comprehensive review," pp. 367–392, dec 2016.

[19] E. Huber, M. Mirzaee, J. Bjorgaard, M. Hoyack, S. Noghanian, and I. Chang, "Dielectric property measurement of PLA," in *IEEE International Conference on Electro Information Technology*, vol. 2016-Augus. IEEE Computer Society, aug 2016, pp. 788–792.

[20] S. Zhang, C. C. Njoku, W. G. Whittow, and J. C. Vardaxoglou, "Novel 3D printed synthetic dielectric substrates," *Microwave and Optical Technology Letters*, vol. 57, no. 10, pp. 2344–2346, oct 2015.

[21] E. Choinska, T. Muroya, W. Swieszkowski, and T. Aoyagi, "Influence of macromolecular structure of novel 2- and 4-armed polylactides on their physicochemical properties and in vitro degradation process," *Journal of Polymer Research*, vol. 23, no. 7, pp. 1–11, jul 2016. [Online]. Available: https://link.springer.com/article/10.1007/s10965-016-1023-4

[22] A. . Gierej, M. . Vagenende, A. . Filipkowski, B. . Siwicki, R. . Buczynski, H. . Thienpont, S. . Van Vlierberghe, T. . Geernaert, P. . Dubruel, F. Berghmans, A. Gierej, M. Vagenende, A. Filipkowski, A. Gierej, M. Vagenende, A. Filipkowski, B. Siwicki, R. Buczynski, H. Thienpont, S. V. Vlierberghe, T. Geernaert, P. Dubruel, . A. Filipkowski, B. Siwicki, R. Buczynski, H. Thienpont, T. Geernaert, and F. Berghmans, "Poly(D, L-Lactic Acid) (PDLLA) Biodegradable and Biocompatible Polymer Optical Fiber," *Journal of Lightwave Technology*, vol. 37, no. 9, pp. 1916–1916, 2019.

[23] World Health Organization, "WHO — Breast cancer," 2018. [Online]. Available: http://www.who.int/cancer/prevention/diagnosis-screening/breast-cancer/en/

[24] "Europa Donna » Breast Cancer Facts." [Online]. Available: https://www.europadonna.org/breast-cancer-facs/

[25] L. R. Mundy, K. Homa, A. F. Klassen, A. L. Pusic, and C. L. Kerrigan, "Breast cancer and reconstruction: Normative data for interpreting the BREAST-Q," *Plastic and Reconstructive Surgery*, vol. 139, no. 5, pp. 1046–1055, may 2017.

[26] C. E. DeSantis, C. C. Lin, A. B. Mariotto, R. L. Siegel, K. D. Stein, J. L. Kramer, R. Alteri, A. S. Robbins, and A. Jemal, "Cancer treatment and survivorship statistics, 2014," *CA: A Cancer Journal for Clinicians*, vol. 64, no. 4, pp. 252–271, jul 2014.

[27] M. Col (Ret) Alvin M. Cotlar, USAF, MC, Capt Joseph J. Dubose, USAF, MC, andMaj D. Michael Rose, USAF, "History of Surgery for Breast Cancer: Radical to the Sublime," 2003.

[28] M. Plesca, C. Bordea, B. El Houcheimi, E. Ichim, and A. Blidaru, "Evolution of radical mastectomy for breast cancer," pp. 183–186, apr 2016.

[29] R. E. Young, "The history of breast cancer surgery: Halsted's radical mastectomy and beyond," 2013.

[30] T. W. Uroskie and L. B. Colen, "History of Breast Reconstruction," *Seminars in Plastic Surgery*, vol. 18, no. 2, pp. 65–69, may 2004.

[31] M. W. A. Warren M. Rozen, Amrish K. S. Rajkomar, Namrata S. Anavekar, "Post-Mastectomy Breast Reconstruction: A History in Evolution," 2009.

[32] T. D. Cronin and R. O. Brauer, "Augmentation mammaplasty." *The Surgical clinics of North America*, vol. 51, no. 2, pp. 441–452, apr 1971.

[33] J. B. Hammond, G. ram Han, P. A. Cronin, H. E. Kosiorek, A. M. Rebecca, W. J. Casey, E. A. Kruger, C. M. Teven, and B. A. Pockaj, "Exploring the Effect of Post-mastectomy complications on 5-year survival," *American Journal of Surgery*, sep 2020.

[34] R. Miseré, S. Schop, E. Heuts, A. P. de Grzymala, and R. van der Hulst, "Psychosocial well-being at time of diagnosis of breast cancer affects the decision whether or not to undergo breast reconstruction," *European Journal of Surgical Oncology*, vol. 46, no. 8, pp. 1441–1445, aug 2020.

[35] M. Charavel, A. Brémond, and I. Courtial, "Psychosocial profile of women seeking breast reconstruction," *European Journal of Obstetrics and Gynecology and Reproductive Biology*, vol. 74, no. 1, pp. 31–35, jul 1997.

[36] M. M. Howard-McNatt, "Patients opting for breast reconstruction following mastectomy: An analysis of uptake rates and benefit," pp. 9–15, feb 2013.

[37] S. K. Al-Ghazal, L. Fallowfield, and R. W. Blamey, "Comparison of psychological aspects and patient satisfaction following breast conserving surgery, simple mastectomy and breast reconstruction," *European Journal of Cancer*, vol. 36, no. 15, pp. 1938–1943, oct 2000.

[38] M. Gardani, N. Bertozzi, M. P. Grieco, M. Pesce, F. Simonacci, P. L. Santi, and E. Raposio, "Breast reconstruction with anatomical implants: A review of indications and techniques based on current literature," *Annals of Medicine and Surgery*, vol. 21, pp. 96–104, 2017.

[39] J. H. Yun, R. Diaz, and A. G. Orman, "Breast Reconstruction and Radiation Therapy," 2018.

[40] P. B. Garvey, M. W. Clemens, A. E. Hoy, B. Smith, H. Zhang, S. J. Kronowitz, and C. E. Butler, "Muscle-sparing TRAM flap does not protect breast reconstruction from postmastectomy radiation damage compared with the DIEP flap," *Plastic and Reconstructive Surgery*, vol. 133, no. 2, pp. 223–233, feb 2014.

[41] M. Brdoder, "Trends in Breast Reconstruction After Mastectomy," 2017. [Online]. Available: https://www.medpagetoday.com/resource-centers/breast-cancer-advances/trends-breast-reconstruction-after-mastectomy/

[42] C. Radovan, "Breast reconstruction after mastectomy using the temporary expander," *Plastic and Reconstructive Surgery*, vol. 69, no. 2, pp. 195–206, 1982.

[43] A. L. Pusic and P. G. Cordeiro, "Breast Reconstruction with Tissue Expanders and Implants: A Practical Guide to Immediate and Delayed Reconstruction," *Seminars in Plastic Surgery*, vol. 18, no. 2, pp. 71–77, may 2004.

[44] C. Dr. Constance, "Immediate vs Delayed Breast Reconstruction: What is Right for You?" 2020.

[45] P. M. Chevray, "Timing of Breast Reconstruction: Immediate versus Delayed," Tech. Rep., 2008.

[46] A. A. Patel, S. A. Martin, J. E. Cheesborough, G. K. Lee, and R. S. Nazerali, ""The Safety and Efficacy of Autologous Fat Grafting During Second Stage Breast Reconstruction"," *Journal of Plastic, Reconstructive Aesthetic Surgery*, oct 2020.

[47] A. W. Brown, M. Kabir, K. A. Sherman, F. Meybodi, J. R. French, and E. B. Elder, "Patient reported outcomes of autologous fat grafting after breast cancer surgery," *The Breast*, vol. 35, pp. 14–20, oct 2017.

[48] F. E. Thiessen, T. Tondu, B. Cloostermans, Y. A. Dirkx, D. Auman, S. Cox, V. Verhoeven, G. Hubens, G. Steenackers, and W. A. Tjalma, "Dynamic InfraRed Thermography (DIRT) in DIEP-flap breast reconstruction: A review of the literature," *European Journal of Obstetrics Gynecology and Reproductive Biology*, vol. 242, pp. 47–55, nov 2019.

[49] S. Fracon, N. Renzi, and M. Manara, "Patient satisfaction after breast reconstruction: Implants vs. autologous tissues," 2018.

[50] O. Pirro, O. Mestak, V. Vindigni, A. Sukop, V. Hromadkova, A. Nguyenova, L. Vitova, and F. Bassetto, "Comparison of patient-reported outcomes after implant versus autologous tissue breast reconstruction using the BREAST-Q," *Plastic and Reconstructive Surgery*, vol. 5, no. 1, jul 2017.

[51] M. Charalambous, R. Daoud, and I. Karat, "Technological advances in breast implants," in *Advances in Medical and Surgical Engineering*. Elsevier, 2020, pp. 141–147.

[52] J. P. Mayesh and A. R. Vicari, "Legal Aspects of Biomaterials," in *Biomaterials Science: An Introduction to Materials: Third Edition*. Elsevier Inc., jan 2013, pp. 1431–1443.

[53] S. L. Spear and M. R. Jespersen, "Breast implants: Saline or silicone?" pp. 557–570, aug 2010.

[54] G. P. Maxwell and A. Gabriel, "Possible Future Development of Implants and Breast Augmentation," *Clinics in Plastic Surgery*, vol. 36, no. 1, pp. 167–172, jan 2009.

[55] A. J. Spiegel, K. Kania, and K. L. Hamilton, "2020 special issue: Twenty years of breast reconstruction: Past, present, and future," *The Breast Journal*, vol. 26, no. 1, pp. 39–41, jan 2020.

[56] C. Conci, L. Bennati, C. Bregoli, F. Buccino, F. Danielli, M. Gallan, E. Gjini, and M. T. Raimondi, "Tissue engineering and regenerative medicine strategies for the female breast," pp. 369–387, feb 2020.

[57] M. Boháč, Danišovič, J. Koller, J. Dragúňová, and I. Varga, "What happens to an acellular dermal matrix after implantation in the human body? A histological and electron microscopic study," *European Journal of Histochemistry*, vol. 62, no. 1, pp. 1–11, jan 2018.

[58] J. M. Smith, J. M. Broyles, Y. Guo, S. H. Tuffaha, D. Mathes, and J. M. Sacks, "Human acellular dermis increases surgical site infection and overall complication profile when compared with submuscular breast reconstruction: An updated meta-analysis incorporating new products," *Journal of Plastic, Reconstructive and Aesthetic Surgery*, vol. 71, no. 11, pp. 1547–1556, nov 2018.

[59] G. Berna, S. J. Cawthorn, G. Papaccio, and N. Balestrieri, "Evaluation of a novel breast reconstruction technique using the Braxon® acellular dermal matrix: a new muscle-sparing breast reconstruction," *ANZ Journal of Surgery*, vol. 87, no. 6, pp. 493–498, jun 2017.

[60] H. Hallberg, S. Rafnsdottir, G. Selvaggi, A. Strandell, O. Samuelsson, I. Stadig, T. Svanberg, E. Hansson, and R. Lewin, "Benefits and risks with acellular dermal matrix (ADM) and mesh support in immediate breast reconstruction: a systematic review and meta-analysis," pp. 130–147, may 2018.

[61] K. J. Burg, B. Inskeep, and T. c. Burg, "Breast Tissue Engineering: Reconstruction Implants and Three-Dimensional Tissue Test Systems," 2014.

[62] A. Mira, "A biomechanical breast model for the evaluation of the compression and the discomfort perception in mammography," 2018.

[63] PDQ Adult Treatment Editorial Board, *Breast Cancer Treatment During Pregnancy*. National Cancer Institute (US), oct 2002. [Online]. Available: http://www.ncbi.nlm.nih.gov/pubmed/26389161

[64] E. Marieb and K. Hoehn, *Human anatomy and physiology*, 11th ed., 2019.

[65] N. Sarvazyan, "Tissue Engineering: Principles, Protocols, and Practical Exercises Learning Materials in Biosciences[1] N. Sarvazyan, "Tissue Engineering: Principles, Protocols, and Practical Exercises Learning Materials in Biosciences," 2020." Tech. Rep., 2020.

[66] A. A. Khalili and M. R. Ahmad, "A Review of cell adhesion studies for biomedical and biological applications," pp. 18 149–18 184, aug 2015. [Online]. Available: https://www.ncbi.nlm.nih.gov/pmc/articles/PMC4581240/

[67] J. H. Choi, J. M. Gimble, K. Lee, K. G. Marra, J. P. Rubin, J. J. Yoo, G. Vunjak-Novakovic, and D. L. Kaplan, "Adipose tissue engineering for soft tissue regeneration," pp. 413–426, aug 2010.

[68] M. Cheng, M. Chhaya, M. Hintz, S. Piper, L. Visscher, J. T. Schantz, C. Wong, O. Ung, M. Wagels, and D. W. Hutmacher, "Breast tissue engineering," in *Comprehensive Biomaterials II*. Elsevier, jan 2017, pp. 435–454.

[69] E. Donnely, M. Griffin, and P. E. Butler, "Breast Reconstruction with a Tissue Engineering and Regenerative Medicine Approach (Systematic Review)," pp. 9–25, jan 2020.

[70] L. Bacakova, J. Zarubova, M. Travnickova, J. Musilkova, J. Pajorova, P. Slepicka, N. S. Kasalkova, V. Svorcik, Z. Kolska, H. Motarjemi, and M. Molitor, "Stem cells: their source, potency and use in regenerative therapies with focus on adipose-derived stem cells – a review," pp. 1111–1126, jul 2018.

[71] C. T. Gomillion and K. J. Burg, "Stem cells and adipose tissue engineering," pp. 6052–6063, dec 2006.

[72] A. C. Volz, B. Huber, and P. J. Kluger, "Adipose-derived stem cell differentiation as a basic tool for vascularized adipose tissue engineering," pp. 52–64, jul 2016.

[73] A. Samani, J. Zubovits, and D. Plewes, "Elastic moduli of normal and pathological human breast tissues: An inversion-technique-based investigation of 169 samples," *Physics in Medicine and Biology*, vol. 52, no. 6, pp. 1565–1576, mar 2007.

[74] N. G. Ramião, P. S. Martins, R. Rynkevic, A. A. Fernandes, M. Barroso, and D. C. Santos, "Biomechanical properties of breast tissue, a state-of-the-art review," *Biomechanics and Modeling in Mechanobiology*, vol. 15, no. 5, pp. 1307–1323, oct 2016.

[75] L. Tytgat, L. Van Damme, J. Van Hoorick, H. Declercq, H. Thienpont, H. Ottevaere, P. Blondeel, P. Dubruel, and S. Van Vlierberghe, "Additive manufacturing of photo-crosslinked gelatin scaffolds for adipose tissue engineering," *Acta Biomaterialia*, vol. 94, pp. 340–350, aug 2019.

[76] A. M. Behrens, J. Kim, N. Hotaling, J. E. Seppala, P. Kofinas, and W. Tutak, "Rapid fabrication of poly(DL-lactide) nanofiber scaffolds with tunable degradation for tissue engineering applications by air-brushing," *Biomedical Materials (Bristol)*, vol. 11, no. 3, apr 2016.

[77] H. Zhang, L. Zhou, and W. Zhang, "Control of scaffold degradation in tissue engineering: A review," pp. 492–502, oct 2014.

[78] I. Van Nieuwenhove, L. Tytgat, M. Ryx, P. Blondeel, F. Stillaert, H. Thienpont, H. Ottevaere, P. Dubruel, and S. Van Vlierberghe, "Soft tissue fillers for adipose tissue regeneration: From hydrogel development toward clinical applications," pp. 37–49, nov 2017.

[79] M. P. Chae, D. J. Hunter-Smith, S. V. Murphy, and M. W. Findlay, "3D bioprinting adipose tissue for breast reconstruction," in *3D Bioprinting for Reconstructive Surgery: Techniques and Applications*. Elsevier Inc., jan 2018, pp. 305–353.

[80] P. Szymczyk-Ziółkowska, M. B. Łabowska, J. Detyna, I. Michalak, and P. Gruber, "A review of fabrication polymer scaffolds for biomedical applications using additive manufacturing techniques," pp. 624–638, apr 2020.

[81] A. Bagheri Saed, A. H. Behravesh, S. Hasannia, S. A. Alavinasab Ardebili, B. Akhoundi, and M. Pourghayoumi, "Functionalized poly L-lactic acid synthesis and optimization of process parameters for 3D printing of porous scaffolds via digital light processing (DLP) method," *Journal of Manufacturing Processes*, vol. 56, pp. 550–561, aug 2020.

[82] Z. Gu, J. Fu, H. Lin, and Y. He, "Development of 3D bioprinting: From printing methods to biomedical applications," dec 2020.

[83] H. Quan, T. Zhang, H. Xu, S. Luo, J. Nie, and X. Zhu, "Photo-curing 3D printing technique and its challenges," pp. 110–115, mar 2020.

[84] S. Barone, P. Neri, A. Paoli, A. V. Razionale, and F. Tamburrino, "Development of a DLP 3D printer for orthodontic applications," in *Procedia Manufacturing*, vol. 38. Elsevier B.V., jan 2019, pp. 1017–1025.

[85] J. Zhang, Q. Hu, S. Wang, J. Tao, and M. Gou, "Digital light processing based three-dimensional printing for medical applications," *International Journal of Bioprinting*, vol. 6, no. 1, pp. 12–27, 2020.

[86] J. Van Hoorick, L. Tytgat, A. Dobos, H. Ottevaere, J. Van Erps, H. Thienpont, A. Ovsianikov, P. Dubruel, and S. Van Vlierberghe, "(Photo-)crosslinkable gelatin derivatives for biofabrication applications," pp. 46–73, oct 2019.

[87] H. Kadry, S. Wadnap, C. Xu, and F. Ahsan, "Digital light processing (DLP)3D-printing technology and photoreactive polymers in fabrication of modified-release tablets," *European Journal of Pharmaceutical Sciences*, vol. 135, pp. 60–67, jul 2019.

[88] M. Schönberger and M. Hoffstetter, "Generative Manufacturing Technologies—The Future?" in *Emerging Trends in Medical Plastic Engineering and Manufacturing*. Elsevier, jan 2016, pp. 107–174.

[89] M. Olchanowski, "How to Make Resin 3D Printing 8x Faster and 9x More Precise — Zortrax," 2018. [Online]. Available: https://zortrax.com/blog/resin-3d-printing-faster-and-more-precise/

[90] H. Kondo, "SLA vs FDM: Is Resin 3D Printing Faster? — All3DP," 2020. [Online]. Available: https://all3dp.com/2/sla-vs-fdm-is-resin-3d-printing-faster/

[91] A. Chen, "Detail comparison of 3D printing methods: SLS vs FDM SLA vs DLP," 2019. [Online]. Available: https://www.cmac.com.au/blog/3d-printing-methods-side-by-side-comparison-sls-vs-fdm-sla-vs-dlp

[92] CELLINK, "LumenX: construct microscopic features with speed, fidelity and precision," Tech. Rep.

[93] M. Krkobabić, D. Medarević, N. Pešić, D. Vasiljević, B. Ivković, and S. Ibrić, "Digital light processing (DLP) 3D printing of atomoxetine hydrochloride tablets using photoreactive suspensions," *Pharmaceutics*, vol. 12, no. 9, pp. 1–17, sep 2020. [Online]. Available: https://pubmed.ncbi.nlm.nih.gov/32878260/

[94] D. A. Komissarenko, P. S. Sokolov, A. D. Evstigneeva, I. A. Shmeleva, and A. E. Dosovitsky, "Rheological and curing behavior of acrylate-based suspensions for the DLP 3D printing of complex zirconia parts," *Materials*, vol. 11, no. 12, nov 2018. [Online]. Available: https://www.ncbi.nlm.nih.gov/pmc/articles/PMC6316993/

[95] C. Kolb, N. Lindemann, H. Wolter, and G. Sextl, "3D-printing of highly translucent ORMOCER®-based resin using light absorber for high dimensional accuracy," *Journal of Applied Polymer Science*, vol. 138, no. 3, jan 2021.

[96] J. Delaey, P. Dubruel, and S. Van Vlierberghe, "Shape-Memory Polymers for Biomedical Applications," *Advanced Functional Materials*, vol. 30, no. 44, oct 2020.

[97] C. C. Hornat and M. W. Urban, "Shape memory effects in self-healing polymers," p. 101208, mar 2020.

[98] W. Zhao, L. Liu, F. Zhang, J. Leng, and Y. Liu, "Shape memory polymers and their composites in biomedical applications," pp. 864–883, apr 2019.

[99] L. F. Tseng, P. T. Mather, and J. H. Henderson, "Shape-memory-actuated change in scaffold fiber alignment directs stem cell morphology," *Acta Biomaterialia*, vol. 9, no. 11, pp. 8790–8801, nov 2013.

[100] S. Neuss, I. Blomenkamp, R. Stainforth, D. Boltersdorf, M. Jansen, N. Butz, A. Perez-Bouza, and R. Knüchel, "The use of a shape-memory poly(ϵlunate-caprolactone)dimethacrylate network as a tissue engineering scaffold," *Biomaterials*, vol. 30, no. 9, pp. 1697–1705, mar 2009.

[101] C. M. Yakacki, R. Shandas, C. Lanning, B. Rech, A. Eckstein, and K. Gall, "Unconstrained recovery characterization of shape-memory polymer networks for cardiovascular applications," *Biomaterials*, vol. 28, no. 14, pp. 2255–2263, may 2007.

[102] H. Wu, P. Chen, C. Yan, C. Cai, and Y. Shi, "Four-dimensional printing of a novel acrylate-based shape memory polymer using digital light processing," *Materials and Design*, vol. 171, p. 107704, jun 2019.

[103] H. Meng and G. Li, "Shape-memory and self-reinforcing polymers as sutures," in *Shape Memory Polymers for Biomedical Applications*. Elsevier Ltd, mar 2015, pp. 282–300.

[104] A. Subash and B. Kandasubramanian, "4D printing of shape memory polymers," p. 109771, jul 2020.

[105] W. Zhang, K. Zhang, G. Li, S. Yan, L. Cui, and J. Yin, "Effects of large dimensional deformation of a porous structure on stem cell fate activated by poly(l-glutamic acid)-based shape memory scaffolds," *Biomaterials Science*, vol. 6, no. 10, pp. 2738–2749, oct 2018.

[106] J. Wang, M. E. Brasch, R. M. Baker, L. F. Tseng, A. N. Peña, and J. H. Henderson, "Shape memory activation can affect cell seeding of shape memory polymer scaffolds designed for tissue engineering and regenerative medicine," *Journal of Materials Science: Materials in Medicine*, vol. 28, no. 10, pp. 1–9, oct 2017.

[107] S. Ertan, M. Kaya, and A. Cihaner, "Polyhedral oligomeric silsesquioxane cage integrated soluble and fluorescent poly(3,4-propylenedioxythiophene) dye," *Polymer*, p. 123127, oct 2020.

[108] X. Lu, Z. Sun, W. Cai -, J. Hu, Y. Han, X. Zhuang, A. , P. Thu Ha, T. Minh Nguyet Tran, and H. Duong Pham, "Effect of initiators on synthesis of poly(L-lactide) by ring opening polymerization," 2017.

[109] A. B. Kremer and P. Mehrkhodavandi, "Dinuclear catalysts for the ring opening polymerization of lactide," 2018.

[110] M. Jalabert, C. Fraschini, and R. E. Prud'Homme, "Synthesis and characterization of poly(L-lactide)s and poly(D-lactide)s of controlled molecular weight," *Journal of Polymer Science, Part A: Polymer Chemistry*, vol. 45, no. 10, pp. 1944–1955, may 2007.

[111] Z. Liu, D. Hu, L. Huang, W. Li, J. Tian, L. Lu, and C. Zhou, "Simultaneous improvement in toughness, strength and biocompatibility of poly(lactic acid) with polyhedral oligomeric silsesquioxane," *Chemical Engineering Journal*, vol. 346, pp. 649–661, aug 2018.

[112] O. M. Sanusi, A. Benelfellah, D. N. Bikiaris, and N. Aït Hocine, "Effect of rigid nanoparticles and preparation techniques on the performances of poly(lactic acid) nanocomposites: A review," p. pat.5104, oct 2020.

[113] L. Huang, J. Tan, W. Li, L. Zhou, Z. Liu, B. Luo, L. Lu, and C. Zhou, "Functional polyhedral oligomeric silsesquioxane reinforced poly(lactic acid) nanocomposites for biomedical applications," *Journal of the Mechanical Behavior of Biomedical Materials*, vol. 90, pp. 604–614, feb 2019.

[114] C. L. Sungyeap Hong, "An Overview of the Synthesis and Synthetic Mechanism of Poly (Lactic acid)," *Modern Chemistry Applications*, vol. 02, no. 04, p. 144, 2014.

[115] L. P. Icart, E. Fernandes, L. Agüero, M. Z. Cuesta, D. Z. Silva, D. E. Rodríguez-Fernández, F. G. Souza, L. Maurício, T. R. Lima, and M. L. Dias, "End Functionalization by Ring Opening Polymerization: Influence of Reaction Conditions on the Synthesis of End Functionalized Poly(lactic Acid)," *Article J. Braz. Chem. Soc*, vol. 29, no. 1, pp. 99–108, 2018.

[116] Z. Guo, C. Yang, Z. Zhou, S. Chen, and F. Li, "Characterization of biodegradable poly(lactic acid) porous scaffolds prepared using selective enzymatic degradation for tissue engineering," 2017.

[117] K. N. Raftopoulos, B. Janowski, L. Apekis, P. Pissis, and K. Pielichowski, "Direct and indirect effects of POSS on the molecular mobility of polyurethanes with varying segment Mw," *Polymer*, vol. 54, no. 11, pp. 2745–2754, may 2013.

[118] J. Wu and P. T. Mather, "POSS polymers: Physical properties and biomaterials applications," *Polymer Reviews*, vol. 49, no. 1, pp. 25–63, jan 2009.

[119] B. Zhao, S. Xu, M. Adeel, and S. Zheng, "Formation of POSS-POSS interactions in polyurethanes: From synthesis, morphologies to shape memory properties of materials," *Polymer*, vol. 160, pp. 82–92, jan 2019.

[120] J. D. Lichtenhan, K. Pielichowski, and I. Blanco, "POSS-Based Polymers," oct 2019.

[121] S. H. Phillips, R. L. Blanski, S. A. Svejda, T. S. Haddad, A. Lee, J. D. Lichtenhan, H. Plastics, F. J. Feher, P. T. Mather, and B. S. Hsiao, "New Insightl into the Structure-Property Relationships of Hybrid (Inorganic/Organic) Poss™ Thermoplastics," *MRS Proceedings*, vol. 628, p. CC4.6, feb 2000.

[122] L. V. Karabanova, L. A. Honcharova, N. V. Babkina, V. I. Sapsay, and D. O. Klymchuk, "Poss-containing nanocomposites based on polyurethane/poly(hydroxypropyl methacrylate) polymer matrix: dynamic mechanical properties and morphology," *Polymer Testing*, vol. 69, pp. 556–562, aug 2018.

[123] Ł. John, M. Malik, M. Janeta, and S. Szafert, "First step towards a model system of the drug delivery network based on amide-POSS nanocarriers," 2017.

[124] Mather, "Shape memory polymers based on semicrystalline thermoplastic polyurethanes bearing nanostructured hard segments," Tech. Rep. 12, mar 2009.

[125] P. T. Knight, K. M. Lee, H. Qin, and P. T. Mather, "Biodegradable thermoplastic polyurethanes incorporating polyhedral oligosilsesquioxane," *Biomacromolecules*, vol. 9, no. 9, pp. 2458–2467, sep 2008.

[126] P. T. Knight, J. T. Kirk, J. M. Anderson, and P. T. Mather, "In vivo kinetic degradation analysis and biocompatibility of aliphatic polyester polyurethanes," in *Journal of Biomedical Materials Research - Part A*, vol. 94, no. 2. John Wiley and Sons Inc., 2010, pp. 333–343.

[127] E. Mcmullin, H. T. Rebar, and P. T. Mather, "Biodegradable Thermoplastic Elastomers Incorporating POSS: Synthesis, Microstructure, and Mechanical Properties," 2016.

[128] M. Villani, R. Consonni, M. Canetti, F. Bertoglio, S. Iervese, G. Bruni, L. Visai, S. Iannace, and F. Bertini, "Polyurethane-Based Composites: Effects of Antibacterial Fillers on the Physical-Mechanical Behavior of Thermoplastic Polyurethanes," *Polymers*, vol. 12, no. 2, p. 362, 2020. [Online]. Available: https://www.mdpi.com/2073-4360/12/2/362

[129] A. Houben, N. Pien, X. Lu, F. Bisi, J. Van Hoorick, M. N. Boone, P. Roose, H. Van den Bergen, D. Bontinck, T. Bowden, P. Dubruel, and S. Van Vlierberghe, "Indirect Solid Freeform Fabrication of an Initiator-Free Photocrosslinkable Hydrogel Precursor for the Creation of Porous Scaffolds," *Macromolecular Bioscience*, vol. 16, no. 12, pp. 1883–1894, dec 2016.

[130] P. Roose, E. Vermoesen, and S. Van Vlierberghe, "Non-steady scaling model for the kinetics of the photo-induced free radical polymerization of crosslinking networks," *Polymer Chemistry*, vol. 11, no. 14, pp. 2475–2484, apr 2020.

[131] H. Annemie, R. Patrice, V. D. B. Hugues, B. Francesca, D. Heidi, C. Maria, B. Dirk, V. V. Sandra, and D. Peter, "First ever solid state crosslinking of hydrogel precursors: opening up unprecedented hydrogel processing avenues in the biomedical field." *Frontiers in Bioengineering and Biotechnology*, vol. 4, 2016.

[132] N. Pien, I. Peeters, L. Deconinck, L. Van Damme, L. De Wilde, A. Martens, S. Van Vlierberghe, P. Dubruel, and A. Mignon, "Design and development of a reinforced tubular electrospun construct for the repair of ruptures of deep flexor tendons," *Materials Science and Engineering C*, vol. 119, p. 111504, feb 2021.

[133] Q. D. Shen, "Preparation, structure and properties of fluorine-containing polymers," in *Dielectric Polymer Materials for High-Density Energy Storage*. Elsevier, jan 2018, pp. 59–102.

[134] S. Zhu and A. Hamielec, "Polymerization Kinetic Modeling and Macromolecular Reaction Engineering," in *Polymer Science: A Comprehensive Reference, 10 Volume Set*. Elsevier, jan 2012, vol. 4, pp. 779–831.

[135] C. Magee, Y. Sugihara, P. B. Zetterlund, and F. Aldabbagh, "Chain transfer to solvent in the radical polymerization of structurally diverse acrylamide monomers using straight-chain and branched alcohols as solvents," *Polymer Chemistry*, vol. 5, no. 7, pp. 2259–2265, apr 2014.

[136] R. M. Slattery, A. E. Stahl, K. R. Brereton, A. L. Rheingold, D. B. Green, and J. M. Fritsch, "Ring opening polymerization and copolymerization of L-lactide and -caprolactone by bis-ligated magnesium complexes," *Journal of Polymer Science, Part A: Polymer Chemistry*, vol. 57, no. 1, pp. 48–59, jan 2019.

[137] "TETRAHYDROFURAN — CAMEO Chemicals — NOAA." [Online]. Available: https://cameochemicals.noaa.gov/chemical/1582

[138] H. Park, X. Guo, J. S. Temenoff, Y. Tabata, A. I. Caplan, F. K. Kasper, and A. G. Mikos, "Effect of swelling ratio of injectable hydrogel composites on chondrogenic differentiation of encapsulated rabbit marrow mesenchymal stem cells in vitro," *Biomacromolecules*, vol. 10, no. 3, pp. 541–546, mar 2009. [Online]. Available: https://www.ncbi.nlm.nih.gov/pmc/articles/PMC2765566/

[139] A. Arslan, "Design and development of photo-crosslinkable urethane-based polymers for unprecedented scaffold manufacturing," 2020. [Online]. Available: http://hdl.handle.net/1854/LU-8684278

[140] X. Li, B.-J. Yang, P. Wu, and G.-M. Zeng, "New Titanium Complex bearing O, N, N, O-tetradentate Ligands: Synthesis, Characterization and Catalysis on the Ring-opening Polymerization of D, L-lactide." Atlantis Press, feb 2018, pp. 182–189.

[141] X. Lu, Z. Sun, W. Cai -, J. Hu, Y. Han, X. Zhuang, A. , P. Thu Ha, T. Minh Nguyet Tran, and H. Duong Pham, "Effect of initiators on synthesis of poly(L-lactide) by ring opening polymerization," 2017.

[142] A. Cação, "Development of new L-lactic acid copolymers: studies on the structure/properties relationship," 2019.

[143] C. Hagiopol, "Copolymers," in *Encyclopedia of Condensed Matter Physics*. Elsevier Inc., jan 2005, pp. 235–240.

[144] S. Harrisson, "The downside of dispersity: Why the standard deviation is a better measure of dispersion in precision polymerization," pp. 1366–1370, mar 2018.

[145] P. T. Knight, "Polyester-based Biodegradable Systems Incorporating POSS," 2010.

[146] "IR Spectrum Table Chart — Sigma-Aldrich." [Online]. Available: https://www.sigmaaldrich.com/technical-documents/articles/biology/ir-spectrum-table.html

[147] N. Nomura, A. Akita, R. Ishii, and M. Mizuno, "Random Copolymerization of ϵ-Caprolactone with Lactide Using a Homosalen-Al Complex." [Online]. Available: http://pubs.acs.org.

[148] L. Mezzasalma, S. Harrisson, S. Saba, P. Loyer, O. Coulembier, and D. Taton, "Bulk Organocatalytic Synthetic Access to Statistical Copolyesters from l-Lactide and -Caprolactone Using Benzoic Acid," vol. 20, no. 5, pp. 1965–1974, 2019.

[149] M. Attaei, M. V. Loureiro, M. do Vale, J. A. Condeço, I. Pinho, J. C. Bordado, and A. C. Marques, "Isophorone diisocyanate (IPDI) microencapsulation for mono-component adhesives: Effect of the active H and NCO sources," *Polymers*, vol. 10, no. 8, jul 2018. [Online]. Available: https://www.ncbi.nlm.nih.gov/pmc/articles/PMC6403942/

[150] I. Armentano, M. Gigli, F. Morena, C. Argentati, L. Torre, and S. Martino, "Recent advances in nanocomposites based on aliphatic polyesters: Design, synthesis, and applications in regenerative medicine," aug 2018.

[151] T. P. Gumede, A. S. Luyt, and A. J. Müller, "Review on PCL, PBS, AND PCL/PBS blends containing carbon nanotubes," pp. 505–529, jun 2018.

[152] M. Unger, C. Vogel, and H. W. Siesler, "Molecular weight dependence of the thermal degradation of poly(ϵ-caprolactone): A thermogravimetric differential thermal fourier transform infrared spectroscopy study," *Applied Spectroscopy*, vol. 64, no. 7, pp. 805–809, jul 2010.

[153] M. Mohamed Zamzam and M. Mohamed, "A Study on the Thermal Degradation Resistance of Thermoplastic Polyurethane Coatings Recommended Citation," Tech. Rep., 2005.

[154] V. Pistor, B. G. Soares, and R. S. Mauler, "Influence of the polyhedral oligomeric silsesquioxane n-phenylaminopropyl - POSS in the thermal stability and the glass transition temperature of epoxy resin," *Polimeros*, vol. 23, no. 3, pp. 331–338, 2013.

[155] K. Tanaka and Y. Chujo, "Unique properties of amphiphilic POSS and their applications," *Polymer Journal*, vol. 45, pp. 247–254, 2013. [Online]. Available: www.nature.com/pj

[156] X. Li, J. Wang, Y. Sun, D. Zhang, N. Zhu, and L. Jing, "The effect of thermal treatment on the decomposition of phthalonitrile polymer and phthalonitrile-polyhedral oligomeric silsesquioxane (POSS) copolymer," *Polymer Degradation and Stability*, vol. 156, pp. 279–291, oct 2018.

[157] H. Sirin, M. Kodal, and G. Ozkoc, "The influence of POSS type on the properties of PLA," *Polymer Composites*, vol. 37, no. 5, pp. 1497–1506, may 2016.

[158] D. K. Chattopadhyay and D. C. Webster, "Thermal stability and flame retardancy of polyurethanes," pp. 1068–1133, oct 2009.

[159] Q. Fang and M. A. Hanna, "Rheological properties of amorphous and semicrystalline polylactic acid polymers," *Industrial Crops and Products*, vol. 10, no. 1, pp. 47–53, jun 1999.

[160] A. J. Guerra, H. Lara-Padilla, M. L. Becker, C. A. Rodriguez, and D. Dean, "Photopolymerizable Resins for 3D-Printing Solid-Cured Tissue Engineered Implants," *Current Drug Targets*, vol. 20, no. 8, pp. 823–838, jan 2019.

[161] F. P. Melchels, K. Bertoldi, R. Gabbrielli, A. H. Velders, J. Feijen, and D. W. Grijpma, "Mathematically defined tissue engineering scaffold architectures prepared by stereolithography," *Biomaterials*, vol. 31, no. 27, pp. 6909–6916, sep 2010.

[162] M. Rajabi, M. McConnell, J. Cabral, and M. A. Ali, "Chitosan hydrogels in 3D printing for biomedical applications," may 2021.

[163] B. Grigoryan, S. J. Paulsen, D. C. Corbett, D. W. Sazer, C. L. Fortin, A. J. Zaita, P. T. Greenfield, N. J. Calafat, J. P. Gounley, A. H. Ta, F. Johansson, A. Randles, J. E. Rosenkrantz, J. D. Louis-Rosenberg, P. A. Galie, K. R. Stevens, and J. S. Miller, "Multivascular networks and functional intravascular topologies within biocompatible hydrogels," *Science*, vol. 364, no. 6439, pp. 458–464, may 2019.

[164] Z. Qin, B. Qu, L. Yuan, X. Yu, J. Li, J. Wang, H. Lv, and X. Yang, "Injectable shear-thinning hydrogels with enhanced strength and temperature stability based on polyhedral oligomeric silsesquioxane end-group aggregation," *Polymer Chemistry*, vol. 8, no. 10, pp. 1607–1610, mar 2017.

[165] Y. Hong, "Electrospun Fibrous Polyurethane Scaffolds in Tissue Engineering," in *Advances in Polyurethane Biomaterials*. Elsevier Inc., feb 2016, pp. 543–559.

[166] S.-C. Jeng, S.-J. Hwang, Y.-H. Hung, and S.-C. Chen, "Cholesteric liquid crystal devices with nanoparticle aggregation," *Optics Express*, vol. 18, no. 21, p. 22572, oct 2010.

[167] K. Hamad, M. Kaseem, H. W. Yang, F. Deri, and Y. G. Ko, "Properties and medical applications of polylactic acid: A review," *Express Polymer Letters*, vol. 9, no. 5, pp. 435–455, 2015.

[168] A. Beil, F. A. Steudel, C. Bräuchle, H. Grützmacher, and . L. Möckl, "Bisacylphosphane oxides as photo-latent cytotoxic agents and potential photo-latent anticancer drugs."

[169] M. Popal, J. Volk, G. Leyhausen, and W. Geurtsen, "Cytotoxic and genotoxic potential of the type I photoinitiators BAPO and TPO on human oral keratinocytes and V79 fibroblasts," *Dental Materials*, vol. 34, no. 12, pp. 1783–1796, dec 2018.

[170] E. Skliutas, M. Lebedevaite, S. Kasetaite, S. Rekštytė, S. Lileikis, J. Ostrauskaite, and M. Malinauskas, "A Bio-Based Resin for a Multi-Scale Optical 3D Printing," *Scientific Reports*, vol. 10, no. 1, pp. 1–9, dec 2020.

[171] B. Steyrer, P. Neubauer, R. Liska, and J. Stampfl, "Visible light photoinitiator for 3D-printing of tough methacrylate resins," *Materials*, vol. 10, no. 12, dec 2017. [Online]. Available: https://pubmed.ncbi.nlm.nih.gov/29257107/

[172] T. Femmer, "Rapid Prototyping of Membranes and Membrane Devices," Tech. Rep., 2015.

[173] H. Seo, S. G. Heo, H. Lee, and H. Yoon, "Preparation of PEG materials for constructing complex structures by stereolithographic 3D printing," *RSC Advances*, vol. 7, no. 46, pp. 28 684–28 688, 2017.

[174] D. M. McElroy, L. M. Geever, C. L. Higginbotham, and S. M. Devery, "The effect of photoinitiator concentration on the physicochemical properties of hydrogel contact lenses," in *Applied Mechanics and Materials*, vol. 679. Trans Tech Publications Ltd, 2014, pp. 118–127.

[175] U. Yildiz, B. Hazer, and K. Tauer, "Tailoring polymer architectures with macromonomer azoinitiators," pp. 1107–1118, 2012.

[176] Y. Xue, H. Chen, C. Xu, D. Yu, H. Xu, and Y. Hu, "Synthesis of hyaluronic acid hydrogels by crosslinking the mixture of high-molecular-weight hyaluronic acid and low-molecular-weight hyaluronic acid with 1,4-butanediol diglycidyl ether †," 2020.

[177] A. Petchsuk, W. Submark, and P. Opaprakasit, "Development of crosslinkable poly(lactic acid-co-glycidyl methacrylate) copolymers and their curing behaviors," *Polymer Journal*, vol. 45, pp. 406–412, 2013.

[178] K. Fen and M. Derg, "Preparation and Application of Urethane Acrylate Coatings for Enhanching Mechanical Properties of Coagulated Surfaces," Tech. Rep. 2, 2016.

[179] R. Y. Li, Z. G. Liu, H. Q. Liu, L. Chen, J. F. Liu, and Y. H. Pan, "Evaluation of biocompatibility and toxicity of biodegradable poly (DL-lactic acid) films," *American Journal of Translational Research*, vol. 7, no. 8, pp. 1357–1370, sep 2015.

A. Ethical considerations

A.1 Reflection about the potential impact of the study

The results of this master thesis are a first step towards minimally invasive breast reconstruction. It can change the procedure for breast reconstruction after mastectomy. The scaffold with shape memory effect is an alternative for silicone and saline breast implants. Therefore, scandals like the PIP breast implant scandal, can be avoided. The new breast implant will be biodegradable and will help the patient's body to regenerate adipose tissue. So eventually, the patient will not have any human-foreign material left in her body. Due to these changes, compared to conventional treatments, doctors can use smaller incisions for implantation. After implantation, the hospital staff will need to pay attention to the enlarging of the scaffold due to the shape memory effect and the swelling due to contact with body fluids. It is important that the scaffold will not enlarge too much as this can cause pressure on and damage to the adipose tissue.

The distribution of the implants will be a challenge as the temperature of the scaffold may not exceed the glass transition temperature to keep the scaffold in its temporary shape until it is implanted into the patient's breast. Therefore, the distribution will be more challenging in warm countries. After exceeding the glass transition temperature and the enlarging of the scaffold before implantation, the scaffold will not be operable again as hospitals don't have the tools to compress the scaffold into the temporary state. Additionally, the extra shape memory cycle may have an influence on the properties of the scaffold. This still needs to be investigated.

A.2 Scientific integrity

Information from literature was often verified by consulting multiple sources. Every source of information, including images, was added to the bibliography.

Mostly existing protocols were used. Sometimes, these protocols were optimised like for the synthesis of polymers based on PDLLA/PCL, the synthesis of endcap with EPPETA and the method for DSC that needed to be adapted for PDLLA/POSS-based materials due to the high melting temperature. Data which gave no additional information or was not accurate enough to draw conclusions from, was not added in this master thesis report.
Still, more research needs to be performed about these materials as for most experiments, there are still many parameters that have an influence on the results. For example, comparing the gel fractions of different materials while the degree of substitution differs is difficult. Additionally, experiments need to be repeated in order to verify and confirm the reproducibility.

B. Calculations of characteristics via H-NMR spectra

B.1 Molar masses of starting materials

B.1.1 Molar mass of PDLLA

The molar mass of PDLLA was calculated by a H-NMR spectrum. At first, the peak that represents the lactide groups at the end of a PDLLA chain (4.25 ppm - 4.45 ppm) was integrated and the integral was normalised to six (two protons from both ends and four protons from the initiator). Subsequently, the PDLLA backbone peak (5.05 ppm - 5.40 ppm) was integrated. Every lactide (LA) monomer in the chain will have two protons that give a signal in this region. Summing up the molar mass of the backbone, the end groups and initiator results in the total molar mass of PDLLA (Equation B.1).

$$MM_{PDLLA} = MM_{initiator} + MM_{LA} * (1 + \frac{I_{backbonePDLLA}}{2}) \tag{B.1}$$

The molar mass of PDLLA, incorporated in thermoplastic polyurethanes, was calculated in a similar way. Another initiator was used during the polymerisation of PDLLA for TPUs that does not result in a signal between 4.25 ppm and 4.45 ppm. Therefore, the integration of this region was normalised by two instead of six.
The molar mass of PDLLA in TPU can also be determined by a H-NMR spectrum of the TPU itself. Therefore, the peak that comes from the initiator was integrated and the integral was set to four. Subsequently, the PDLLA backbone peak was also integrated and Equation B.1 was used to eventually calculate the molar mass.
The total molar mass of thermoplastic polyurethanes cannot be determined by H-NMR spectroscopy as the end group signals cannot be integrated due to overlap with other signals.

B.1.2 Molar mass of PDLLA/PCL

The calculation of the molar mass of PDLLA/PCL was more challenging as there are two different monomers in the polymer chain. First, the ratio of the signals coming from the backbone of PDLLA (5.05 ppm - 5.40 ppm) and PCL (4.0 ppm - 4.2 ppm) was determined. This ratio was used to calculate the signal that one chain would give between 4.25 ppm and 4.45 ppm, which represents lactide monomers at the end of a polymer chain (see Equation B.2). The integral of this region was then normalised to the calculated value. This calculation is based on the assumption that the ratio of lactide and ϵ-caprolactone molecules located in the backbone is equal

to the ratio of the two monomers located at the end of the chains.

$$I_{endgroupLA} = 4 + 2 * (1 - \frac{I_{backbonePDLLA}}{I_{backbonePCL}}) \tag{B.2}$$

Afterwards, the peaks representing the backbone of PDLLA (5.05 ppm - 5.40 ppm), the backbone of PCL (4.0 ppm - 4.2 ppm) and the end group ϵ-caprolactone (CL, around 3.64 ppm) were integrated. Next, these integrals were used to calculate the molar mass with Equation B.3.

$$\begin{aligned} MM_{PDLLA/PCL} = & \frac{I_{backbonePDLLA}}{2} * MM_{LA} + \frac{I_{backbonePCL}}{2} * MM_{CL} \\ & + MM_{LA} * (1 - \frac{I_{endgroupCL}}{I_{endgroupCL} + I_{endgroupLA} - 4}) \\ & + 2MM_{LA} * (\frac{I_{endgroupCL}}{I_{endgroupCL} + I_{endgroupLA} - 4}) \end{aligned} \tag{B.3}$$

B.2 Weight percentage ϵ-caprolactone in PDLLA/PCL

The weight percentage of ϵ-caprolactone in PDLLA/PCL was calculated by using the same integrals as in the previous section. The weight percentage ϵ-caprolactone in PDLLA/PCL is given by Equation B.4.

$$wt_{PCL}\% = \frac{(\frac{I_{backbonePCL}}{2} + \frac{I_{endgroupCL}}{2}) * MM_{CL}}{(\frac{I_{backbonePCL}}{2} + \frac{I_{endgroupCL}}{2}) * MM_{CL} + (\frac{I_{backbonePDLLA}}{2} + \frac{(I_{endgroupLA} - 4)}{2}) * MM_{LA}} \tag{B.4}$$

B.3 Estimation of OH-concentration

By preparing a sample for H-NMR with a known mass of PDLLA and dimethyl terephthalate (DMT), the OH-concentrations of PDLLA and PDLLA/PCL were measured. The peak that is correlated with DMT (around 8 ppm; four protons) was set to 1000. Afterwards, the hydroxyl groups at the end of the chains (between 4.25 ppm and 4.45 ppm for lactide; three protons for one chain-end and around 3.64 ppm for ϵ-caprolactone; two protons for one chain-end) were also integrated. In order to calculate the OH-concentration, the fraction of ϵ-caprolactone end groups relative to the total number of end groups needed to be defined (Equation B.5).

$$F = \frac{\frac{I_{endgroupCL}}{2}}{I_{endgroupLA} + \frac{I_{endgroupCL}}{2}} \tag{B.5}$$

By using this fraction, the OH-concentration for PDLLA/PCL was estimated by Equation B.6. This equation can also be used for PDLLA by setting the fraction to zero.

$$\frac{n_{OH}}{m_{polymer}} = \frac{(I_{endgroupLA} + I_{endgroupCL})}{I_{DMT}} * \frac{4}{3(1-F)+2F} * \frac{m_{DMT}}{MM_{DMT} * m_{polymer}} \tag{B.6}$$

Determining the OH-concentration for TPUs was unfeasible. The signals from the hydroxyl end groups overlap with other signals and were hard to integrate correctly on H-NMR spectra.

B.4 Molar ratio POSS/PDLLA for thermoplastic polyurethanes

The average ratio of POSS monomers and PDLLA chains in a TPU chain can be calculated by a H-NMR spectrum of TPU. Therefore, the peak of backbone PDLLA (5.05 ppm - 5.4 ppm; two protons) and the peak that refers to POSS monomers in the chain (around 0.9 ppm; 42 protons) were integrated. The integral of both signals and the molar mass of PDLLA were used to estimate the molar ratio of POSS/PDLLA of TPUs (Equation B.7).

$$\frac{n_{POSS}}{n_{PDLLA}} = \frac{I_{backbonePOSS}}{I_{backbonePDLLA}} * \frac{MM_{PDLLA}}{MM_{LA}} * \frac{2}{42} \tag{B.7}$$

B.5 Hard segment weight percentage of TPU

The weight percentage of the hard segment (HDI and POSS) in the thermoplastic polyurethane can be determined by Equation B.8 where the molar ratio of POSS/PDLLA, described above, is presented by x.

$$wt_H\% = \frac{xMM_{POSS} + (x+1)MM_{HDI}}{xMM_{POSS} + (x+1)MM_{HDI} + MM_{PDLLA}} \tag{B.8}$$

B.6 Estimation of the degree of substitution

After functionalisation of the starting materials into AUPs, the degree of substitution (DS) was determined to calculate the number of hydroxyl end groups that was converted into acrylate functionalities. This was done in two ways.

The first approach to determine the DS uses a H-NMR spectrum of the AUP with DMT. The peak of DMT (around 8 ppm) was integrated and set to 1000. Afterwards the three acrylate peaks (between 5.80 and 6.50 ppm) were integrated and summed up. This sum was used to determine the number of acrylates (mole) per gram AUP via Equation B.9.

$$\frac{n_{acrylates}}{m_{AUP}} = \frac{4}{3} * \frac{I_{acrylates}}{I_{DMT}} * \frac{m_{DMT}}{MM_{DMT} * m_{AUP}} \tag{B.9}$$

Multiplying this ratio with the molar mass results in the molar ratio of acrylates over AUP. In theory, this ratio should be equal to two for single endcap agent, and to six for triacrylate endcap agent. Dividing the molar ratio by the ideal molar ratio gives the degree of substitution (see Equation B.10). This approach can be used for PDLLA and PDLLA/PCL and assumes that the mean molar mass is equal to the molar mass of an AUP. This is an assumption as not every end of the polymer chains will have reacted with endcap in practice.

$$DS = \frac{\frac{n_{acrylates}}{m_{AUP}} * MM_{AUP}}{(\frac{n_{acrylates}}{n_{AUP}})_{ideal}} \tag{B.10}$$

The second approach uses the H-NMR spectra of both the starting material and the AUP. First, the peak on the H-NMR spectrum of the starting material that represents the chain-ends (between 4.25 and 4.45 ppm for PDLLA) was integrated and normalised by half of the expected signal for one chain (see Equation B.2). Afterwards, the PDLLA backbone peak (5.05 - 5.40 ppm) was integrated. The same peak was also integrated on the H-NMR spectrum of the AUP and was normalised by the integral of the PDLLA peak obtained from the H-NMR spectrum of the starting material. At last, the acrylate peaks (between 5.8 and 6.5 ppm) were integrated and divided by three for endcap with one acrylate and nine for endcap with three acrylates.
This approach cannot be used for AUPs with a TPU backbone as the hydroxyl end group signals cannot be integrated due to overlap with other signals.

C. H-NMR spectra

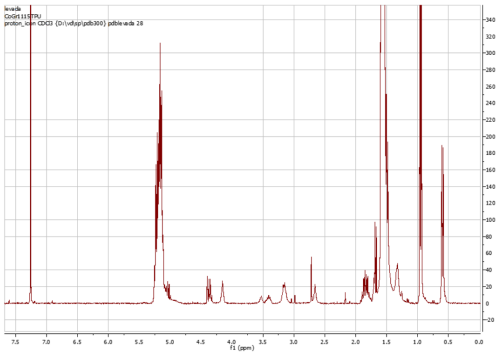

Figure C.1: H-NMR spectrum of TPU1

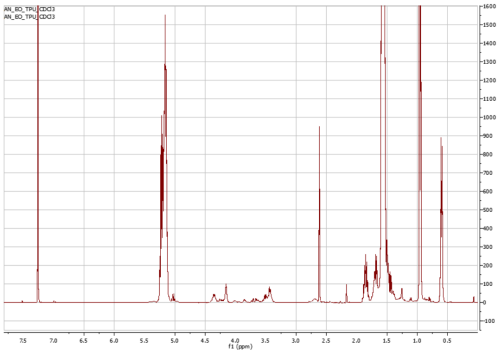

Figure C.2: H-NMR spectrum of TPU3

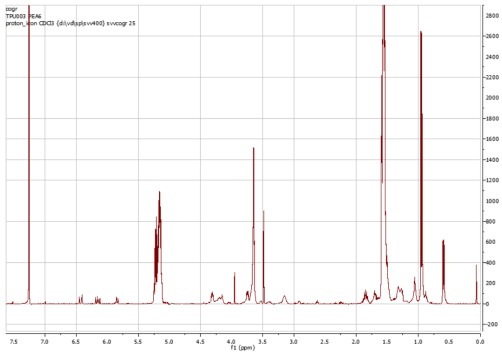

Figure C.3: H-NMR spectrum of TPU2AUP(1)

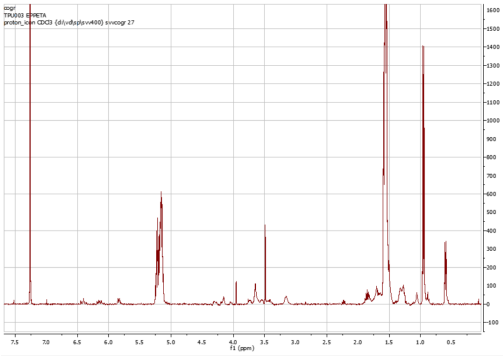

Figure C.4: H-NMR spectrum of TPU2AUP(3)

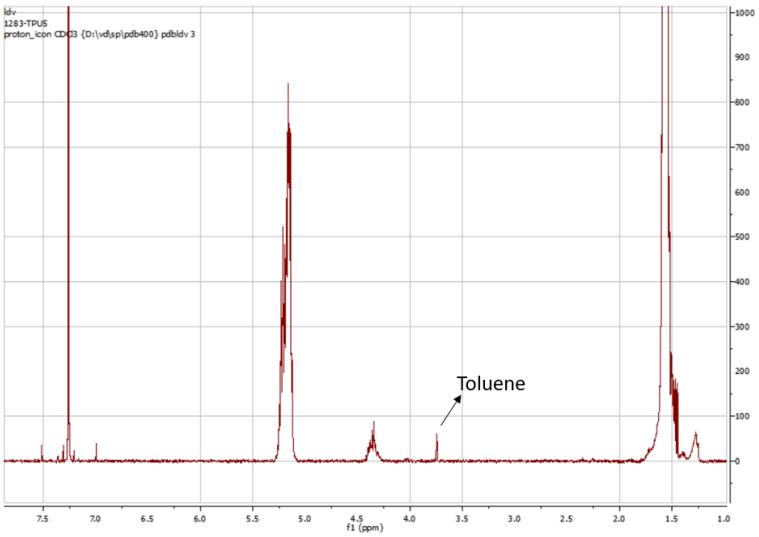

Figure C.5: H-NMR spectrum of PLA6

D. DSC thermograms

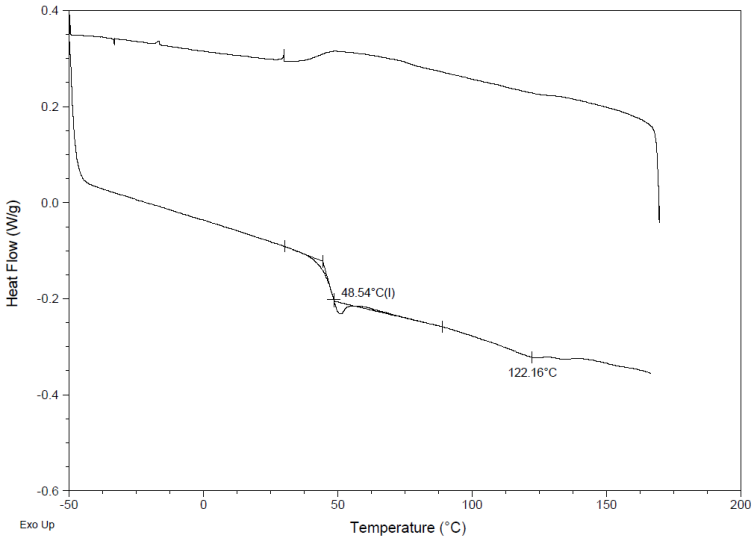

Figure D.1: DSC thermogram of TPU2

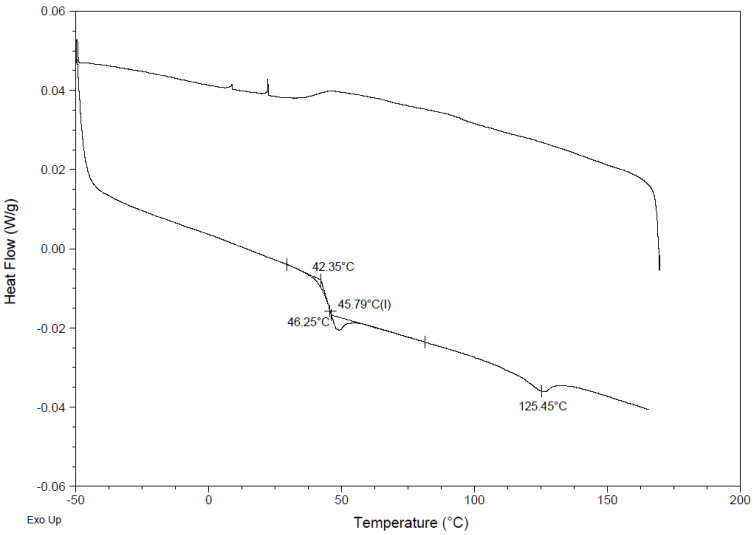

Figure D.2: DSC thermogram of TPU3

E. TGA thermograms

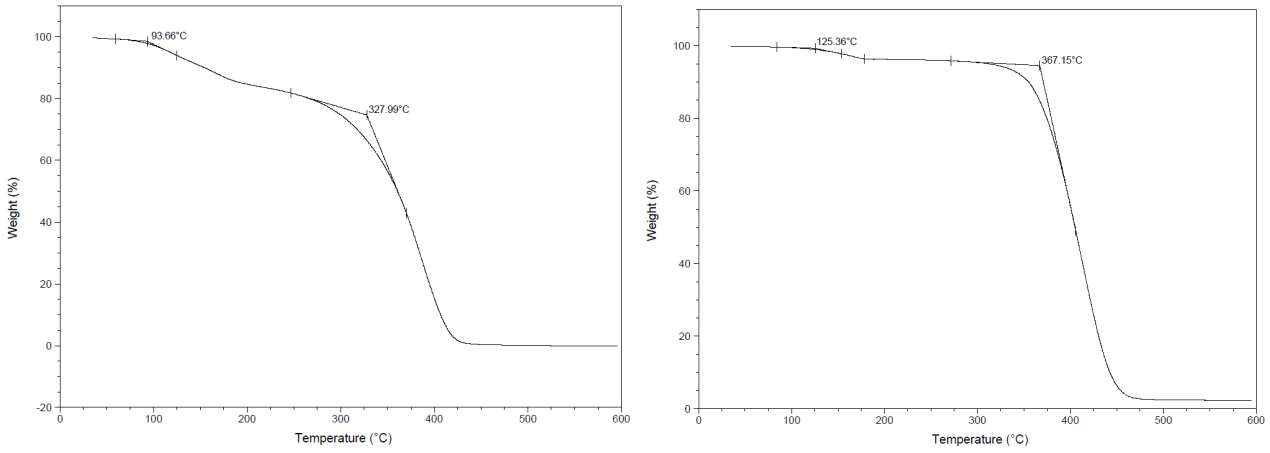

Figure E.1: TGA thermograms of bisomer PEA6 (left) and EPPETA (right)

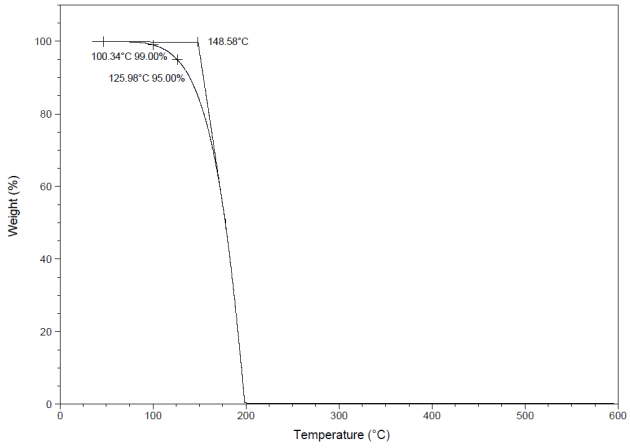

Figure E.2: TGA thermogram of IPDI

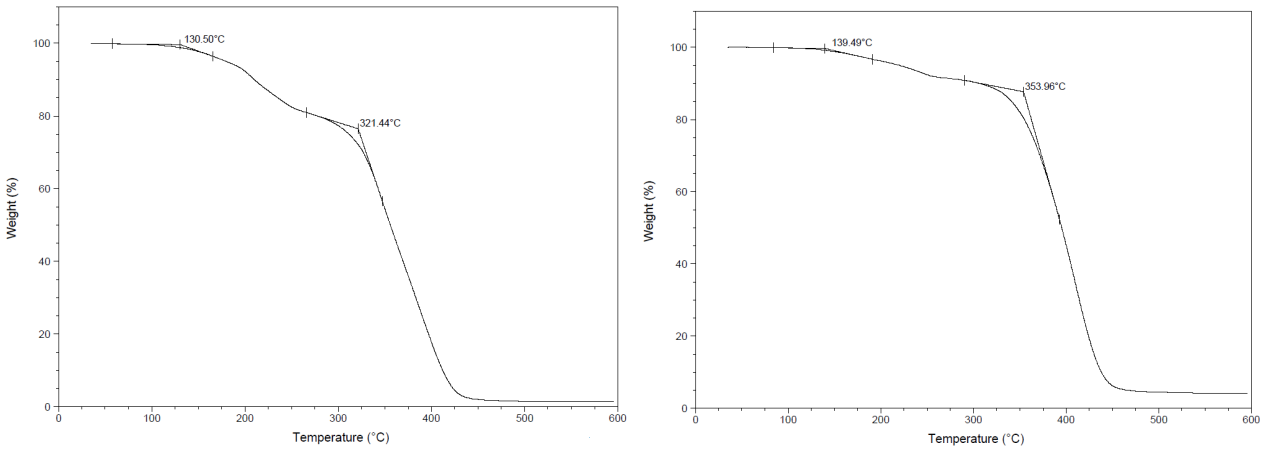

Figure E.3: TGA thermograms of endcap with bisomer PEA6 (left) and EPPETA (right)

F. Photorheology results

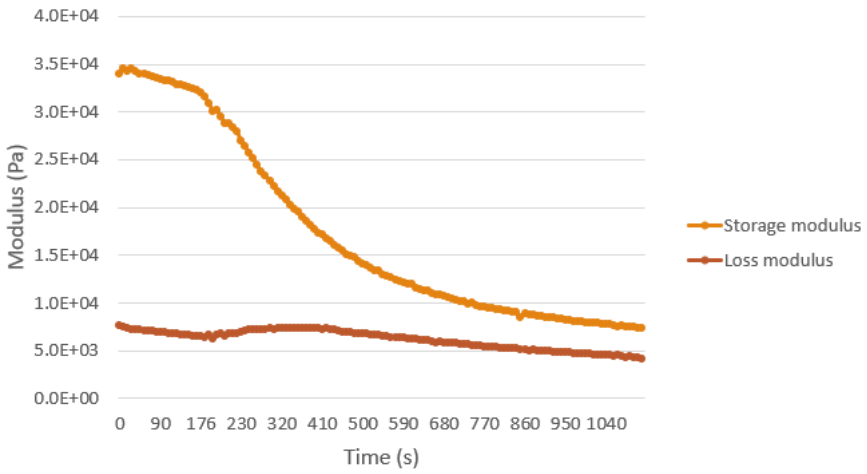

Figure F.1: Storage (orange) and loss (brown) moduli of a resin with 60 wt% PLA11*AUP(1) and 2 mol% TPO-L in function of time during UV irradiation

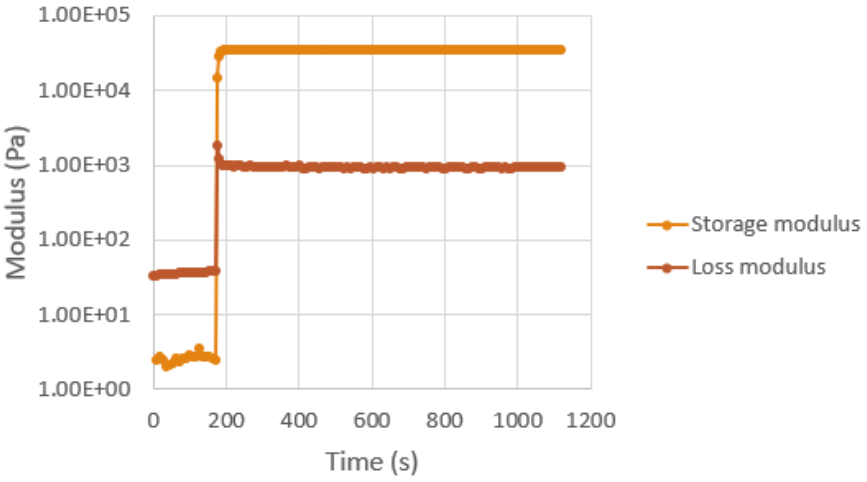

Figure F.2: Storage (orange) and loss (brown) moduli of a resin with 60 wt% PLA6AUP(3) and 1.5 wt% TPO-L as a function of time during UV irradiation

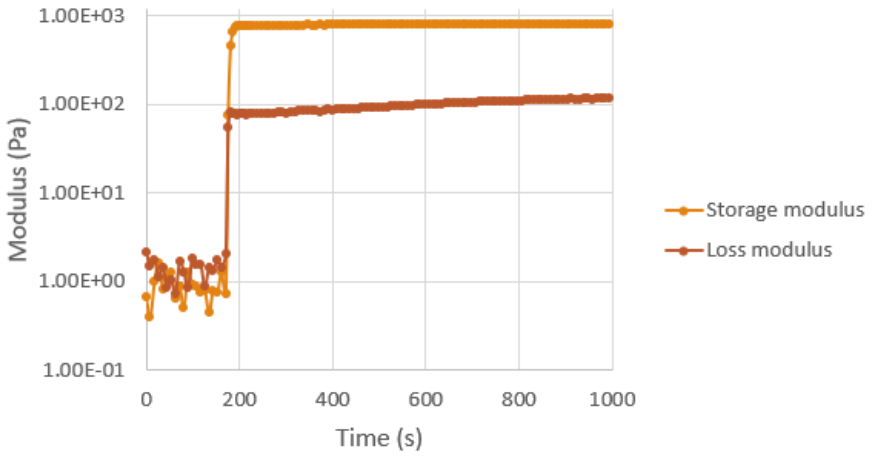

Figure F.3: Storage (orange) and loss (brown) moduli of a resin with 60 wt% PLA13AUP(3) and 1.5 wt% TPO-L as a function of time during UV irradiation

FACULTY OF ENGINEERING AND ARCHITECTURE

Development of acrylate-endcapped urethane-based POSS/PLA scaffolds towards breast reconstruction

Karen De Man
Student number: 01602451

Supervisors: Prof. dr. Sandra Van Vlierberghe, Prof. Ruslan Dmitriev
Counsellor: Ir. Coralie Gréant

Master's dissertation submitted in order to obtain the academic degree of
Master of Science in Biomedical Engineering

Academic year 2020-2021

GHENT UNIVERSITY

VUB VRIJE UNIVERSITEIT BRUSSEL